Bridges with Premature Concrete Deterioration:

Field Observations and Large-Scale Testing

by

Anna Boenig, BCE

Thesis

Presented to the Faculty of the Graduate School of

The University of Texas at Austin

in Partial Fulfillment

of the Requirements

for the Degree of

Master of Science in Engineering

The University of Texas at Austin

May 2000

Bridges with Premature Concrete Deterioration:

Field Observations and Large-Scale Testing

Approved by
Supervising Committee:

_____

_____

Dedication

For my parents, Brenda and Heinrich Boenig.

Acknowledgements

May 2000

Abstract

Bridges with Premature Concrete Deterioration:
Field Observations and Large-Scale Testing

Anna Boenig, MSE

The University of Texas at Austin, 2000

Supervisor: Richard E. Klingner

This thesis describes part of the work associated with TxDOT Study 1857 ("Structural Assessment of In-Service Bridges with Premature Concrete Deterioration"). The focus of this thesis is the use of observations from in-service structures and laboratory specimens with premature concrete deterioration, along with core tests and large-scale tests of laboratory specimens, to predict the capacity of a large element with premature deterioration. The theoretical background of premature concrete deterioration, while not the focus of this thesis, is reviewed. Large-scale tests to failure were conducted on 3 flexure-dominated and 3 shear-dominated specimens. Results from those tests were compared with tested compressive strength and elastic modulus of cores removed from the specimens, and with visual damage indices. Results were also evaluated in the light of observed damage to in-service structures, obtained over two years of field observation of 5 large TxDOT structures in different parts of Texas. These

comparisons are used to propose approaches for evaluating the structural integrity

of in-service structures with premature concrete deterioration.

Table of Contents

List of Tables

List of Figures

Chapter 1: Introduction

1.1   INFORMATION ON TxDOT STUDY 1857

In late 1995 the Texas Department of Transportation (TxDOT) became aware of premature concrete deterioration in several in-service structures around the state (Appendix A). Most affected structures are prestressed beams, though substructures (abutments, columns and bents) at some bridge sites are also damaged. Typical damage to prestressed beams is described as horizontal cracking on the bottom flanges, longitudinal cracks underneath, and distributed "map cracking," concentrated at but not limited to the ends. This premature concrete deterioration has been attributed to two expansive distress mechanisms: Alkali-Silica Reaction (ASR) and Delayed Ettringite Formation (DEF). TxDOT is now deciding what actions to take with respect to this damage. In past instances, structures have been removed from service or repaired after only several years of service (TxDOT 1998). As statewide inspection of in-service concrete structures progresses, more structures with this problem are being identified. The cost for replacing and repairing these structures is already significant, and will continue to increase. This situation was the motivation for TxDOT Study 1857 "Structural Assessment of In-Service Bridges with Premature Concrete Deterioration". This thesis reviews and reports on specific portions of Study 1857.

1.2 **SCOPE AND OBJECTIVES OF STUDY 1857**

TxDOT Study 1857, "Structural Assessment of In-service Bridges with Premature Concrete Deterioration," focuses on five specific tasks:

1) Conduct field investigation to confirm and monitor existing premature concrete deterioration and the rate of increase of such deterioration. Also, determine typical development of damage in laboratory specimens and prepare histograms of crack widths (or other damage indices) at different ages. Correlate results from the observations of the laboratory beams with field observations, with the objective of predicting the distribution of crack widths in a field girder over time, based on its most obvious cracks at a particular age.

2) Conduct laboratory investigations of local effects of premature concrete deterioration. Perform tests on cores and slices removed from several beams with some to large amounts of deterioration, to acquire data on the compressive strength and modulus of elasticity. Conduct push-off tests to determine interface shear strength. From the results, develop damage indices to be used in engineering and finite element models for predicting the capacity of damaged elements as governed by decrease in compression, tension, interface shear and bond.

3) Develop nondestructive evaluation techniques for determining damage indices that will be correlated with physical damage indices.

4) Develop petrographic techniques for identifying Delayed Ettringite Formation (DEF), alone and in combination with Alkali-Silica Reaction

(ASR). TxDOT personnel will perform this task, using cores that will be extracted from the laboratory specimens.

5)   Using the damage indices developed in Tasks 2 and 3, predict the capacity of large elements as a function of DEF-related damage. Present final recommended actions to TxDOT for handling any given case of premature concrete deterioration (Klingner 1998,).

1.3   SCOPE OF THIS THESIS

The parts of Study 1857 reported here concern Tasks (1) and (2). The work consisted of monitoring field and laboratory specimens for two years to measure crack widths and observe crack patterns, and of laboratory testing to determine structural effects of premature damage.

1.3.1   Crack Monitoring

Crack patterns and crack widths were documented for prestressed I-beams in four TxDOT bridge structures, and for prestressed box girders in the laboratory. In the following chapters, histograms are presented showing distributions of crack widths at different ages for each girder studied (Fúnez 1999). Comparison of crack widths and changes in crack widths will relate levels of damage over time of girders in the laboratory to beams in the field. Each girder is classified according to severity of damage and of exposure. Beams close to the lower limit of observed damage are considered to represent specimens with low inherent problems and mild exposure. Beams close to the upper limit of observed damage

are considered to represent specimens with severe inherent problems and severe exposure.

Different techniques for crack monitoring in the field are described, and the most effective is recommended. This monitoring will continue throughout the duration of Study 1857.

1.3.2 Laboratory Tests

The testing program for this part of the study was developed to show how different levels of damage from premature deterioration affect the strength of concrete elements. A series of laboratory tests was conducted on prestressed box girders, each of which displayed a different level of premature concrete deterioration. The ultimate capacity of each specimen is compared to that calculated using current code equations. Compressive strength tests as well as modulus of elasticity tests were performed on cores taken from the same girders.

1.4   OBJECTIVES OF THIS THESIS

Results from the crack monitoring will provide a basis for damage indices to describe a damaged element and predict the crack-width distribution of a girder over time, based on its most obvious cracks at a particular age. By relating the damage indices developed from field and laboratory specimens to material properties and strength data from laboratory tests, the capacity of an element and its remaining service life shall be predicted.

1.5 COMPLEMENTARY WORK

Parallel with the research done for this thesis is work by several other students on the same laboratory specimens and field structures. Brian Tinkey investigated the use of nondestructive test methods (Task 3), including acoustic emission, impact echo and short pulse radar, to assess the degree of distributed damage in the laboratory specimens discussed in this thesis. Luz Fúnez presented the background and field work in a report in December 1999. Yong-Mook Kim conducted similar laboratory tests as those described herein on prestressed I-beams, and is developing finite element models to predict structural capacity of similar I-beams given a level of deterioration (Task 5). Joe Roche is performing fatigue tests on large scale specimens and push-off tests on slices removed from the laboratory specimens (Task 2). Piya Chotickai is developing nondestructive testing procedures for use in the field.

Chapter 2: Premature Concrete Deterioration – A Literature Overview of Damage from Delayed Ettringite Formation (DEF) and Alkali-Silica Reaction (ASR)

This chapter presents background information on ASR and DEF, and their role in premature concrete deterioration. Pertinent information ensuing from a literature search performed by contributors to Project 1857 is included (Funez 1999, Klingner 2000). The presently known impact of premature deterioration on concrete structures in Texas is discussed. Gaps in knowledge of the influence of premature deterioration on concrete structures are introduced, as well as how this research has attempted to fill those gaps.

2.1   INTRODUCTION

Premature concrete deterioration can result from a number of mechanisms. A previous TxDOT investigation of damage to 56 precast, prestressed concrete box beams (Lawrence et al. 1998), identified two possible expansive mechanisms, Alkali-Silica Reaction (ASR) and Delayed Ettringite Formation (DEF).

Premature concrete damage from ASR and DEF, either alone or in combination, typically shows itself through distributed internal and external cracking of the concrete, and a progressive loss of member function with time. This distributed damage also increases a concrete element's susceptibility to corrosion of reinforcement and other types of deterioration due to environmental exposure.

2.2 ALKALI-SILICA REACTION (ASR)

ASR, discussed at length in ACI 221.1 (1998), is caused by a chemical reaction between hydroxyl (OH^-) ions present in the pore-water solution, and various forms of silica present in many aggregates. The silica enters into solution and forms an alkali-silica gel, which absorbs water and increases in volume. This increase in volume produces expansive forces within the concrete, leading to distributed cracking. When the alkalis are present in the fresh concrete, ASR begins at the interface between the aggregate and the paste. It requires three conditions: highly alkaline pore water; high humidity; and reactive silica.

ASR in new structures can be controlled by limiting the total alkalinity in the concrete, by controlling the composition of the cement, and by eliminating combinations of cement and aggregates that are known to be reactive. These measures can be applied alone or in combination. ASR in existing structures can be mitigated only by controlling the humidity of the concrete: below about 80 percent relative humidity, ASR stops. In hardened concrete, relative humidity is controlled by the hydration of the cement, and by controlling the ingress of water from external sources.

2.3 DELAYED ETTRINGITE FORMATION (DEF)

2.3.1 Background of Normal Ettringite Formation

Ettringite is calcium aluminum sulfate ($3CaO \cdot Al_2O_3 \cdot 3CaSO_4 \cdot 32H_2O$). It is a normal hydration product of the tricalcium aluminate (C_3A) component of portland cement. Upon contact with water, the C_3A reacts immediately, forming crystalline hydrates such as C_3AH_6, C_4AH_{19} and C_2AH_8, and liberating substantial

heat. To reduce the rate of this reaction and the associated heat and loss of workability, small quantities of gypsum (calcium sulfate, $CaSO_4 \cdot 2H_2O$) are added to the cement. The sulfate in the gypsum reacts with C_3A and water to form crystals of "primary ettringite," which bind to the C_3A, impeding the access of water to the C_3A particles. Later in the hydration process, when the pore water is depleted of sulfate and richer in aluminate, this primary ettringite becomes unstable, and is gradually converted to monosulfate ($3CaO_4 \cdot A_{12}O_3 \cdot SO_3 \cdot 18H_2O$), a stable hydration product.

2.3.2 Historical Background of DEF

DEF was first noticed in the early 1980's in Germany, and later in the United States, when prestressed concrete railway ties on the east coast began to show distress just a few years after installation. Studies, made using petrographic microscopy, scanning electron microscopy (SEM) and energy-dispersive x-ray elemental analysis, led to the conclusion that although some alkali-silica reaction (ASR) had occurred, the distress was largely or completely due to DEF (Mielenz et al. 1995).

DEF has also been encountered in Canada, South Africa, Australia and Europe. Distress, found mainly in prestressed elements, begins to appear after several years of exterior exposure. The deterioration is often reported because of the appearance of map cracking on the surface of the element (Kesner 1997).

A major question has arisen: was DEF not noticed before 1980? Researchers have identified two possible answers:

1) it did occur, but was not recognized; and

8

2)   composition of portland cements has changed radically during the last few

        decades.

        The first answer relates to the fact that the ettringite present from DEF is

often hard to detect. Ettringite crystals normally have a needle-shaped structure

that allows easy recognition under microscopy. In DEF, however, the crystals

may be so fine as to be resolvable only using SEM at magnifications of 5,000 to

25,000. In several such cases, DEF has been misdiagnosed as ASR.

        The second answer relates to the fact that maximum SO_3 levels in

portland cement clinker have increased from about 2% in the 1940's to more than

4% now (Hime 1996).

2.3.3   Latest Theories on DEF

        The most recent research on DEF and its causes have been compiled and

interpreted by Hime (1996) and Collepardi (1999). According to Hime,

1)   DEF almost certainly will occur only if the concrete is frequently exposed

        to substantial amounts of water.

2)   Destructive DEF will probably not occur, or its effect will be lessened, if

        the concrete is well air-entrained.

3)   If precast concrete is not air-entrained, and exposure to water is frequent,

        then DEF may occur if either:

        - the concrete temperature during curing or in service becomes high

          enough to decompose primary ettringite. Depending on cement

          composition, this temperature may be as low as 140 F (60 C).

- the clinker contains a substantial amount of slowly soluble sulfate. Sulfate levels as low as 1.5% in normal cement, and 2% in high-alkali cements have caused DEF.

4)   Tests of cement by ASTM C 265 or of concrete by the Dugan procedure (1989) may reveal a potential DEF problem for non-air-entrained concrete that will be exposed to substantial amounts of water.

According to Collepardi (1999), the following factors cause DEF:

1)   Microcracks formed during manufacturing, either from Alkali-Silica Reactivity (ASR) or from other causes including those related to steam curing;

2)   Exposure to cycles of wetting and drying;

3)   Late release of sulfate from the cement clinker or other sources;

4)   Migration of reactant ions (SO_4^{-2}, Al^{+3}, Ca^{+2}) through the pore-water solution of concrete exposed to water or saturated air; and

5)   Ettringite deposits inside existing microcracks, and subsequent crack opening by ettringite swelling or crystal growth.

Collepardi proposes a holistic approach to understanding DEF-induced damage, based on the interaction of three essential elements (Figure 2.1):

1)   microcracking,

2)   exposure to water or saturated air, and

3)   late sulfate release.
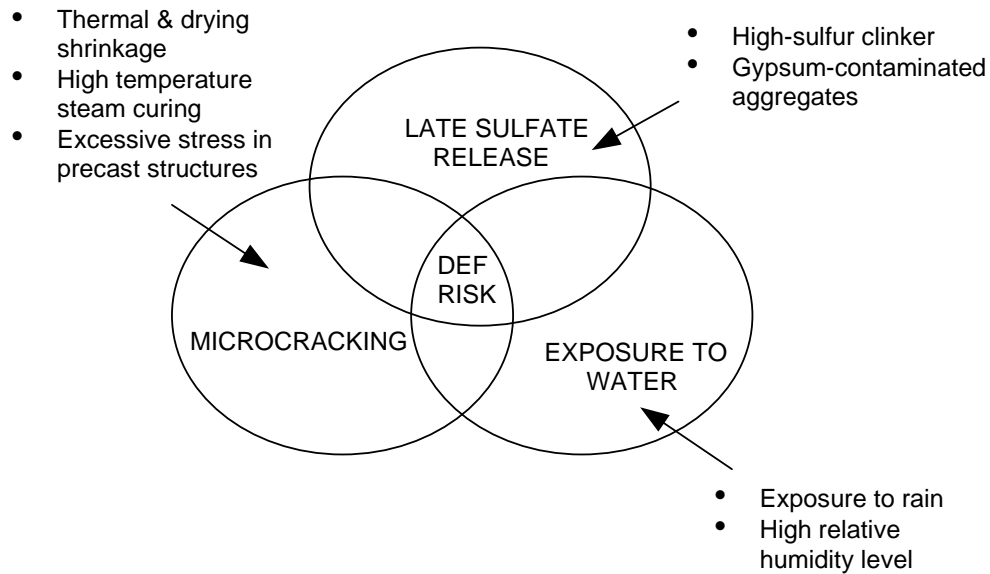
Figure 2.1 A holistic model showing DEF-damage as a function of late sulfate release, microcracking and exposure to water, (Collepardi 1999)

In the absence of any one of these elements, Collepardi states, DEF-related deterioration cannot occur.

2.4   GAPS IN KNOWLEDGE REGARDING DEF

Previous research on DEF damage has concentrated on its chemistry, possible causes, and prevention. As noted in the previous section, however, there is no consensus regarding its causes. Measures to prevent it must be taken before fabricating the concrete elements (for example, reducing the sulfate in the clinker, or using low-temperature steam curing).

Four important areas of research on premature concrete deterioration are as yet unexplored:

1)   the long-term growth or shrinkage of DEF-induced cracking;

2)   whether ASR/DEF-related deterioration can be stopped;

3)   the effect of ASR/DEF on structural integrity; and

4)   the effectiveness of repair techniques for structures damaged by ASR,
        DEF, or both.

2.5   HOW TxDOT STUDY 1857 WILL FILL THOSE GAPS

The objective of TxDOT Study 1857 has been to assess the structural adequacy of in-service structures that are prematurely deteriorated, and to determine the degree to which that deterioration will continue. Information on how DEF affects a structure through time will be used to predict the remaining service life of a concrete element with DEF. Researchers trying to find the causes of DEF may use this information to develop better models of the problem. Researchers trying to find methods of repairing in-service structures might use this information to tell them at which moment in time their solution could be applicable.

Chapter 3: Development of Test Program

3.1 OBJECTIVES AND PLAN

The testing program was designed to investigate variations in structural performance among a set of girders with premature deterioration and to relate strength and failure modes to the level of apparent damage. Cracks in the girders were monitored over time as a basis for classifying levels of damage.

3.1.1 Specimens

Fifty-six prestressed concrete box girders, fabricated at Heldenfels Brothers, Inc. plant in San Marcos, TX, in June through September 1991, displayed premature concrete deterioration while still in the storage yard, and were never installed in TxDOT bridges. Four of those girders, representing typical ranges of damage, were brought to Ferguson Structural Engineering Laboratory (FSEL) at the University of Texas at Austin (UT Austin) for examination (Figure 3.1). The laboratory tests were performed on portions of these girders.

The box girders had a nominal length of 69.83 ft (21.29 m), with solid end blocks 2.17 ft (0.66 m) long. A 1 ft long (0.30 m) intermediate stiffener was cast at 23.33 ft (7.11 m) from each end. Styrofoam was used to form interior voids. Thirty ½-inch diameter, 270 ksi (1862 MPa) strands were distributed in the bottom of the girder. Reinforcing steel was ASTM A615 Grade 60 (420 MPa), and the design compressive strength of the concrete was 6000 lb/in.^{2} (41 MPa).

Figure 3.1 shows the cross-sectional dimensions of these girders. Fabrication details are included in Appendix B.
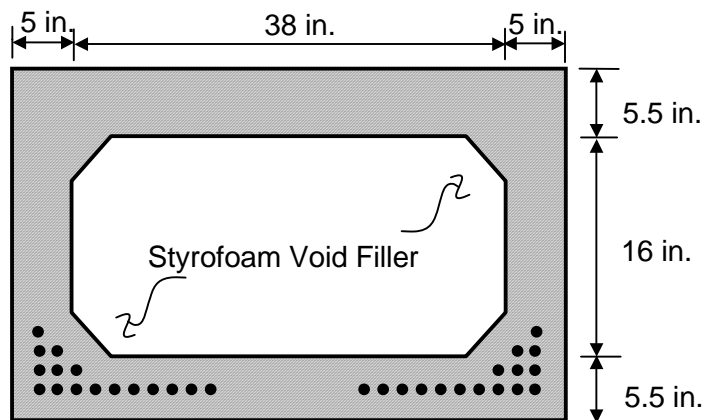
Figure 3.1 Cross-section of box girders from Heldenfels Brothers, Inc. (San Marcos)

The box girders were designated BG1, BG2, BG3, and BG4 ("Box Girder 1," etc.). BG1 and BG2 were immediately moved inside the laboratory (Figure 3.2), while BG3 and BG4 were left outside and uncovered. BG4 was subjected to random periods of wetting and drying in an effort to accelerate damage. Figure 3.3 shows BG3 and BG4 stored outside FSEL.

14

Figure 3.2 Maneuvering BG1 into FSEL

Figure 3.3 BG3 and BG4 (wetted) outside of FSEL

The condition of each girder was documented. Table 3.1 outlines the general appearance of each, and is followed by sections containing detailed descriptions.

Table 3.1 Condition of box girders

Girder	Condition
BG1	Good
BG2	Severe end damage
BG3	Less severe end damage
BG4	Extensive damage over entire length

3.1.1.1 BG1

BG1 was cast on September 20, 1991. Its TxDOT identification number is A5-F37. The materials used are presented in Table 3.2. Its 7-day compressive cylinder strength was 8320 lb/in.^{2} (57.4 MPa).

Table 3.2 Materials used for BG1

Material	Description	Producer
Cement	Type III	Alamo Cement Co., San Antonio, TX
Fine Aggregate	Siliceous sand	Heldenfels Brothers, Inc., Victoria Pit
Coarse Aggregate	Limestone	Gifford-Hill, Yelverton Pit

The condition of BG1 was documented upon arrival at FSEL. Damage was primarily at the ends of the girder, and included many well-distributed cracks

from 0.002 in. (0.05 mm) to 0.06 in. (1.5 mm) wide. The north and south faces, as labeled by researchers, and the 5 ft (1.5 m) of the top surface at the ends were more cracked and had wider cracks than the east and west faces. There was a 0.002 in. (0.05 mm) wide longitudinal crack, 5.5 in. (0.14 m) from the bottom, on the east and west faces of both ends of the girder. This level corresponds to the bottom of the void. A gray line, darker than the typical concrete, suggested that the crack did extend the entire length. Another horizontal crack 0.002 in. (0.05 mm) wide was apparent on the east and west faces, 17 in. (0.43 m) from the bottom. This crack was intermittent along the length. Excepting the end material, the concrete seemed in good condition. Sketches of the cracks are included in Appendix C.

3.1.1.2 BG2

BG2 was cast on June 18, 1991. Its TxDOT identification number is A2-F41. The materials used are presented in Table 3.3. Its 7-day compressive cylinder strength was 9020 lb/in.^{2} (62.2 MPa).

Table 3.3 Materials used for BG2

Material	Description	Producer
Cement	Type III	Alamo Cement Co., San Antonio, TX
Fine Aggregate	Siliceous sand	Centex Materials, Sheppard Pit
Coarse Aggregate	Limestone	Colorado Materials Co., Hunter Pit

BG2 exhibited acute cracking, particularly at its ends. Several cracks were as wide as 0.375 to 0.5 in. (9.5 to 13 mm), and as long as 10 to 20 in. (0.25

to 0.51 m). Distributed cracks from 0.002 in. to 0.06 in. (0.05 to 1.5 mm) wide were obvious on all faces at both ends. The largest cracks at the ends led to corners where concrete had spalled off. Transverse reinforcement was exposed in the east web at both the northeast and southeast corners. The north and south faces, as labeled by researchers, and 10 ft (3 m) of the top surface nearest the ends, were more cracked and had wider cracks than the east and west faces. A horizontal crack 0.06 to ¼ in. (1.5 to 6.4 mm) wide was apparent at the level of the bottom layer of strand, 2 in. (0.051 m) from the bottom, on the east side of the south end face. Expansion of the concrete was evident at the ends. The cross section was 49 in. (1.24 m) wide at mid-depth (1 in. or 25 mm) wider than its original dimension). A longitudinal crack 0.002 to 0.01 in. (0.05 to 0.25 mm) wide extended the entire length, 5.5 in. (0.14 m) from the bottom – at the level of the bottom of the void. On the east and west faces, a horizontal crack 0.003 in. (0.08 mm) wide and 17 in. (0.43 m) from the bottom was intermittent along the length. Away from the ends, the concrete was in better condition. Sketches of the cracks are included in Appendix C.

3.1.1.3 BG3

BG3 was cast on September 11, 1991. Its TxDOT identification number is A3-F37. The materials used are presented in Table 3.4. Its 7-day compressive cylinder strength was 8180 lb/in.^{2} (56.4 MPa).

Table 3.4 Materials used for BG3

Material	Description	Producer
Cement	Type III	Alamo Cement Co., San Antonio, TX
Fine Aggregate	Siliceous sand	Heldenfels Brothers, Inc., Victoria Pit
Coarse Aggregate	Limestone	Gifford-Hill, Yelverton Pit

The ends of BG3 were more damaged than those of BG1, but less damaged than those of BG2. Cracks 0.125 to 0.313 in (3.2 to 7.9 mm) wide had developed on the end faces and at the end 1.5 ft (0.46 m) on the east and west faces. Two horizontal cracks extended the entire length of the east and west sides of the girder. One was 5.5 in. (0.14 m) from the bottom and 0.007 to 0.02 in. (0.18 to 0.51 mm) wide; the other was 17 in. (0.43 m) from the bottom and 0.01 to 0.013 in. (0.25 to 0.33 mm) wide.

3.1.1.4 BG4

BG4 was cast on June 10, 1991. Its TxDOT identification number is A3-F7. The materials used are presented in Table 3.5. Its 7-day compressive cylinder strength was 8720 lb/in.^{2} (60.1 MPa).

Table 3.5 Materials used for BG4

Material	Description	Producer
Cement	Type III	Alamo Cement Co., San Antonio, TX
Fine Aggregate	Siliceous sand	Heldenfels Brothers, Inc., Victoria Pit
Coarse Aggregate	Limestone	Colorado Materials Co., Hunter Pit

BG4 was significantly more damaged than BG1, BG2 and BG3 based on visual inspection. A crack 0.007 in. (0.18 mm) and 5.5 in. (0.14 m) from the bottom was visible for limited distances at the ends. A horizontal crack 0.009 to 0.025 in. (0.23 to 0.64 mm) wide and 17 in. (0.43 m) from the bottom extended the entire length on each side. The webs on the south end, extending 140 in. (3.6 m) north, had many horizontal cracks roughly 0.05 in. (1.3 mm) wide and 100 in. (2.5 m) long, spaced about 4 in. (0.10 m) apart. The webs at the north end had similar damage. The worst cracking in the webs, near the solid blockouts, was accompanied by cracks across the top of the girder at 286 in. (7.3 m) from the north and south ends. A horizontal crack 0.06 to 0.25 in. (1.5 to 6.4 mm) was apparent at the level of the bottom layer of strand, 2 in. (0.051 m) from the bottom, on the east side of the south end face. The concrete in the middle third of the girder was in better condition.

3.1.2 Types of Tests

Two types of tests were conducted on the box girders: flexure-dominated and shear-dominated. Tests for compressive strength and modulus of elasticity were performed on cores taken from the girders. Table 3.6 describes the girders and locations from which each specimen came. Table 3.7 shows the tests performed and the parameters monitored.

Table 3.6 Sources of laboratory specimens

Girder	Flexure-dominated Specimens	Other Specimens
BG1	BG1F	North end used for BG1S
		South end used for cores
BG2	BG2F	South end used for BG2S
		North end used for cores
BG3		Reserved for fatigue testing
BG4	BG4F	South end used for BG4S
		North end used for cores

Table 3.7 Summary of tests and parameters monitored

Test	Parameters Monitored
Flexure-dominated BG1F BG2F BG4F	Load Midspan deflection Deflection at supports Strand slip Widening of existing cracks Crack initiation and propagation Strain profile at midspan Acoustic emission
Shear-dominated BG1S BG2S BG4S	Load Deflection under loading head Deflection at supports Strand slip Deformation of webs Acoustic emission
Compression BG1E-X BG1W-X BG2E-X BG2W-X BG4E-X BG4W-X	Load Longitudinal strain

3.1.2 Nomenclature

Individual test specimens are categorized by the box girder from which the specimen came, and by the type of test. The suffixes "F" and "S" denote flexure-dominated and shear-dominated respectively. For example, the flexure-dominated test performed on BG1 is called BG1F. Compression specimens were labeled according to the location on the box girder where the cores were taken. The letters "E" and "W" denote end-block and web respectively. For example, BG1E-1 designates a core taken from the end-block of BG1.

Chapter 4: Test Results

This chapter presents the data gathered and the observations made during the tests described in Chapter 3.

4.1   EXPLANATION OF DATA MANIPULATION

Positive displacement of the linear potentiometers used for vertical displacement indicates compression of the instrument or downward deflection of the girder. Strand-slip data are presented so that positive deflection represents strand retraction. Strains shown correspond to the first time a given load was attained. Positive displacement of the linear potentiometers used to monitor web deformation in the shear-dominated tests indicates extension of the instrument.

Very small positive and negative displacements (<0.005 in. or 0.1 mm) were recorded by the linear potentiometers during all the tests. These irregular displacements did not apparently correspond to actual events, and might be considered instrument error or explained by movements other than strand slip: the tip of the linear potentiometer sliding against the end of the strand which was not cut perfectly flush; shifting of the anchor bolts that secured the metal instrumentation frame to the end of the girder (since the concrete was not sound); twisting of the metal frame; or movement of the clamps holding the instruments. Readings less than 0.005 in. (0.1 mm) in the linear potentiometers measuring strand slip, crack growth, and extension or shortening of chords in the webs were considered insignificant. Information at this small scale is not presented in this

chapter because that would have implied more precision than is available with the instruments used.

Though most linear potentiometers showed a drastic change at the end of the test, many of those indicated displacements did not actually represent a sudden change in the behavior of the specimen. Failure of the specimen caused many potentiometers to shift off the ends of the strands, and many wires used to monitor shear deformation to break. Only those displacements actually corresponding to strand slip (confirmed by visual inspection after the test) or to deformation of the web (confirmed by inspecting the wires after the test) are presented in this chapter. Appendices E, F and G include all data collected during the flexure-dominated, shear-dominated and core tests respectively.

Chapter 5: Significance of Test Results

This chapter discusses the significance of test results presented in Chapter 4. Results from the core tests and crack monitoring are used to relate material properties and degree of damage to the behavior of the larger test specimens. Behavior of the three flexure-dominated specimens and the three shear-dominated specimens is compared to each other, and to a proposed theoretical framework. The consistency of the test results with that theoretical framework is reviewed.

5.1   PROPOSED THEORETICAL FRAMEWORK

As a tentative working hypothesis, the essential differences between the behavior of undamaged and damaged girders can be described in terms of strut-and-tie models (Figure 5.1).
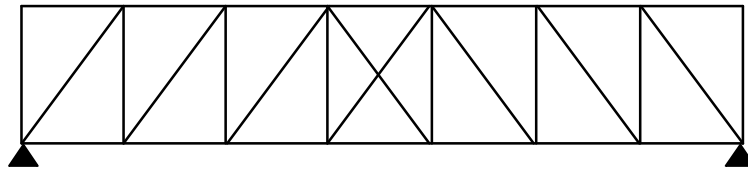
Figure 5.1 Strut-and-tie-model of girder

In flexure-dominated tests, the compression struts are assumed to carry relatively little load, and to remain elastic; the top chord carries all compression, and the bottom chord (prestressing strand) carries all tension (Figure 5.2). Thus flexure-dominated, under-reinforced beams are governed by the compressive strength of concrete in the top chord in the region of maximum moment.
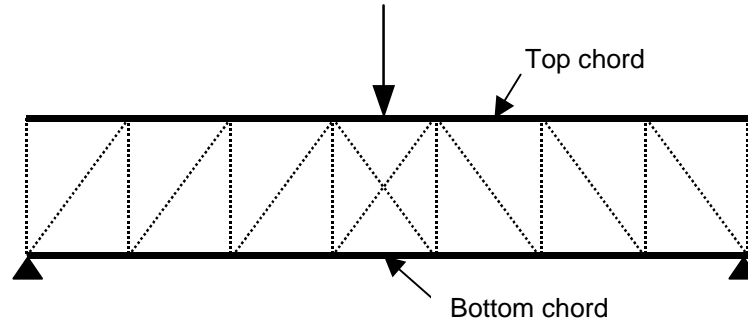
Figure 5.2 Load-carrying chords of strut-and-tie model for flexure-dominated
tests

Shear-dominated tests are governed by concrete compressive strength in the diagonal compression struts, by the concrete tensile strength in the bottom chord, and by the bond strength between the prestressing strand and the concrete (Figure 5.3).
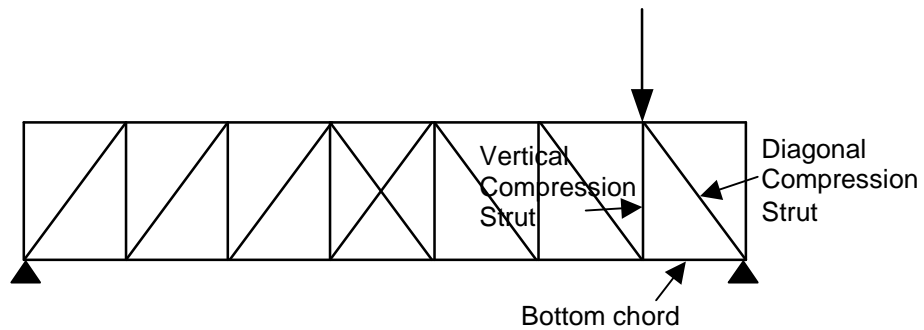
Figure 5.3 Governing load-carrying members of strut-and-tie model for shear-
dominated tests

5.2   SIGNIFICANCE OF CORE TESTS

The compressive strength and modulus of elasticity of concrete cores taken from the box girders are shown in Table 5.1. For girders BG1, BG2, and BG4 respectively, compressive strength of cores from the end-blocks, where damage was more pronounced, was 60%, 38% and 42% of the compressive strength of cores from the webs, where damage was less pronounced. Thus the local effect of deterioration is obvious. Results from core tests show that internal damage in the end-blocks of BG1, though superficially undetectable, made those end-blocks significantly weaker than the webs.

Table 5.1 Concrete compressive strength and modulus of elasticity of box girders

Girder	Location	Number of Cores Averaged	Average f_c lb/in.^{2} (MPa)	Average E kips/in.^{2} (MPa)
BG1	End-block	6	6310 (43.5)	3100 (21400)
	Web	3	10550 (72.7)	----
BG2	End-block	2	2870 (19.8)	1050 (7100)
	Web	2	7550 (52.1)	3300 (22500)
BG4	End-block	3	3520 (24.3)	1750 (12000)
	Web	3	8300 (57.2)	4100 (28300)

As would be expected, concrete compressive strength and modulus of elasticity vary inversely with the degree of deterioration (Figures 5.4 and 5.5). BG1, with the least deterioration, had the highest compressive strength and

modulus; BG2, with the most deterioration, had the lowest compressive strength and modulus.

The specified compressive strength of the girders was 6000 lb/in.^{2} (41.4 MPa). Cores from the end-blocks of BG2 and BG4 have already deteriorated to the point that their compressive strength is below that value, and compressive strengths of cores from the end-block of BG1 are only 5% above it (Figure 5.4).
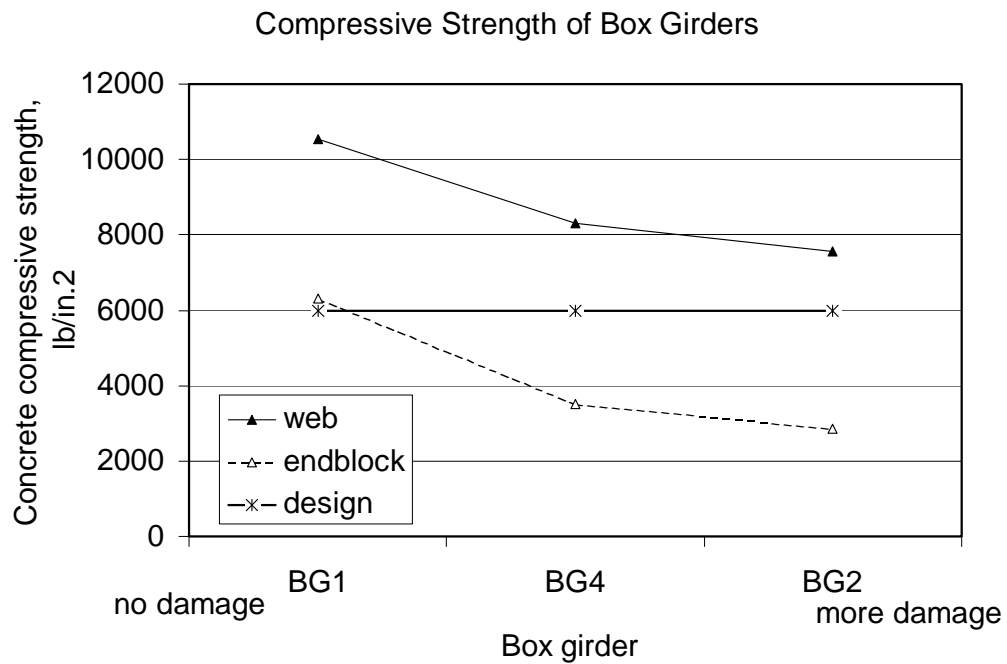
Figure 5.4 Concrete compressive strength of cores from box girders

Modulus of Elasticity of Box Girders
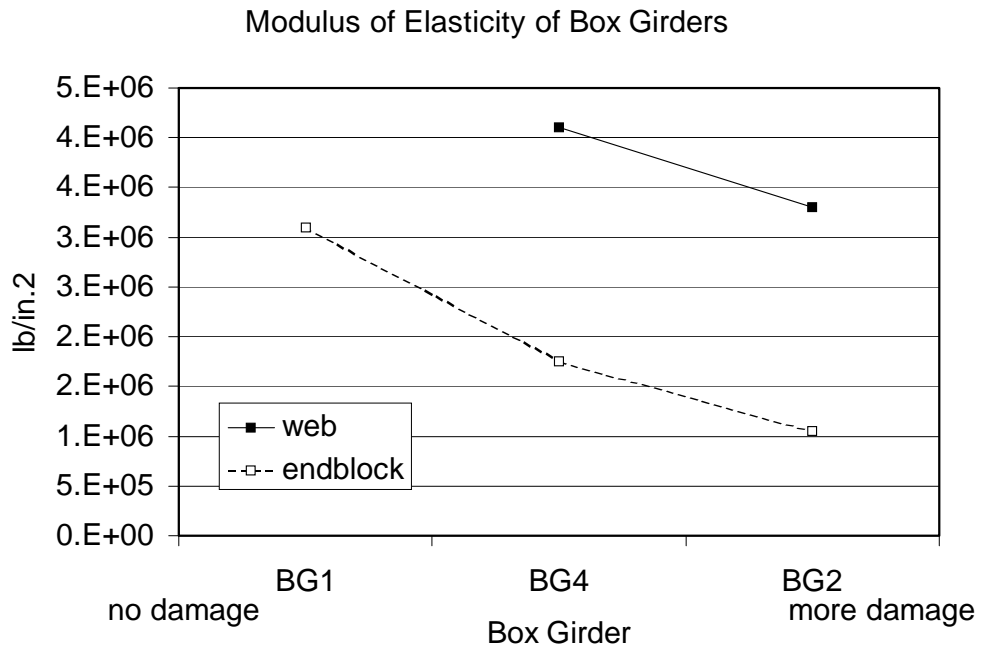
Figure 5.5 Modulus of elasticity of cores from box girders

In Figure 5.6 is shown the relationship between modulus of elasticity and compressive strength of cores from box girders. A parabolic curve fit to the test values, and the ACI 318-99 equation for modulus of elasticity, $E_c = 57,000(f_c)^{0.5}$ (US customary units), are also plotted.

Modulus of Elasticity versus Core Compressive Strength
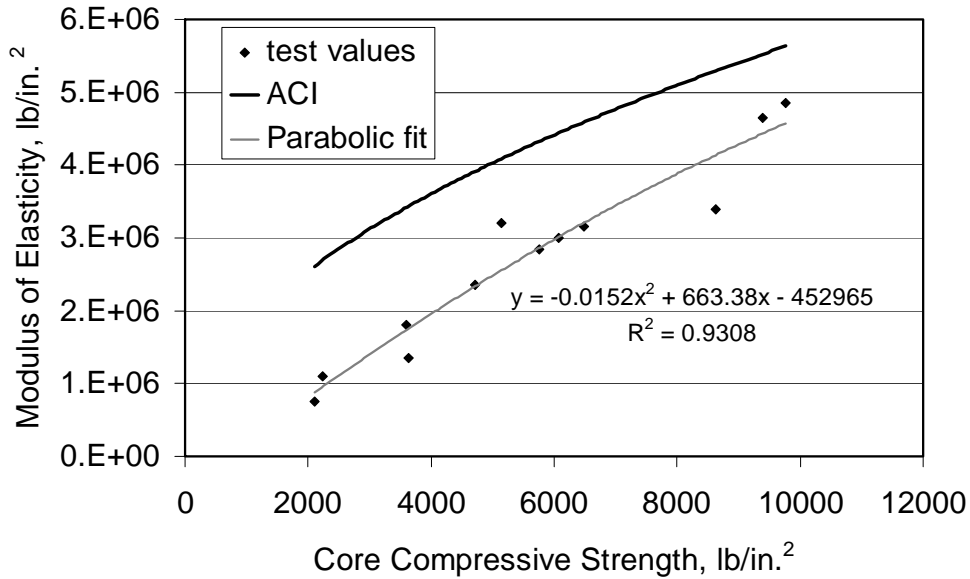
Figure 5.6 Modulus of elasticity versus concrete compressive strength of cores
from box girders

According to the ACI 318-99 Commentary, Section R8.5.1, "measured values range typically from 120 to 80 percent of the specified value." The parabolic curve fit to measured values from the box girder cores ranges from 81 to 33 percent of the specified value. The premature damage seems to not only reduce the compressive strength of cores, but also disproportionately reduce the modulus of elasticity relative to that compressive strength.

5.3   SIGNIFICANCE OF CRACK MONITORING

The maximum crack widths of the girders monitored are displayed in Figure 5.7, in terms of the age of the girders. The effect of a more severe

environment (exposure to water) is evident. BG4 (wetted) showed a drastic
increase over time in maximum crack width. BG3 is considered to have severe
inherent problems because of its constant, large maximum crack width.

Maximum Crack Width of Box Girders
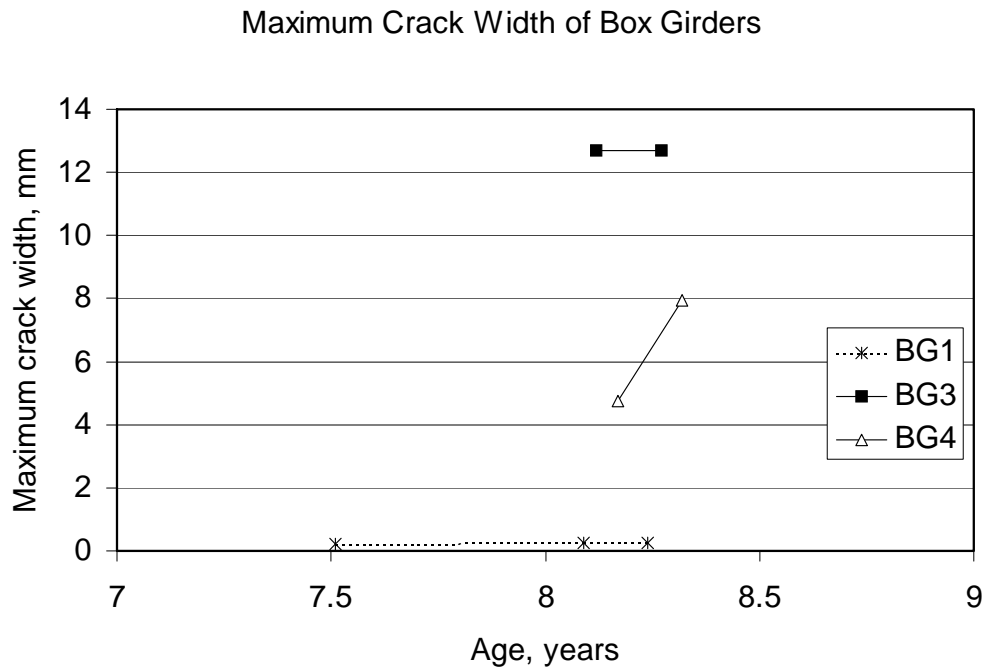
Figure 5.7 Maximum crack width versus age for box girders

Plots of damage index versus age for the representative squares, and of the
average damage index for the box girders, are shown in Figures 5.8 and 5.9. Ages
were determined by averaging the ages of the three box girders monitored based
on their casting dates.
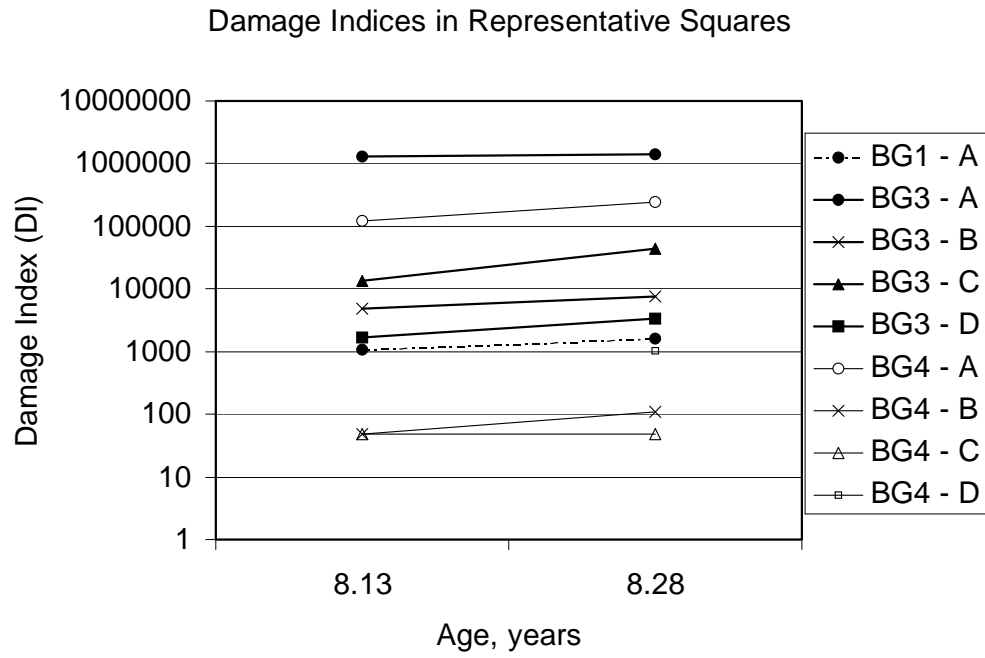
Figure 5.8 Damage Indices versus age for representative squares

Average Damage Indices of Box Girders
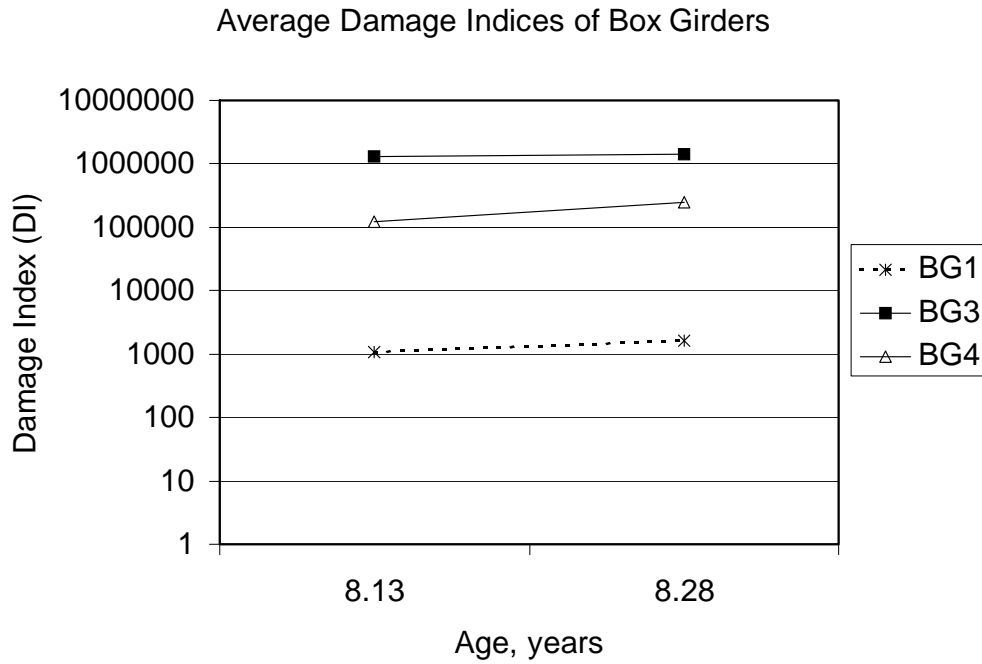
Figure 5.9 Average damage indices versus age for box girders

High damage indices correlate well with high levels of visually observed damage. All three girders monitored showed an increase in damage index over time. The slopes of the lines suggest that the damage index is increasing by 3500 per year for BG1, 815,100 per year for BG3 and 839,200 per year for BG4. The percentage increases in damage index for the representative squares and box girders from 8.13 years to 8.28 years are shown in Table 5.2.

Table 5.2 Percentage increase in DI for representative squares and box girders

Girder	Square	% Increase in DI	% Increase in Total DI
BG1	A	49	49
BG3 (dry)	A	7	9
	B	56	
	C	227	
	D	98	
BG4 (wetted)	A	104	104
	B	125	
	C	0	

The comparative percentage increases in Total DI for the box girders also suggest that exposure to water accelerates the damage process.

A correlation is seen between maximum crack width and damage index (Figure 5.10). The best-fit curve shows that damage index increases exponentially as maximum crack width increases.

Damage Index vs. Maximum Crack Width of Box Girders

$$y = 2022.6e^{0.5462x}$$

Legend:
- ✳ BG1
- ■ BG3
- △ BG4
- — curve fit

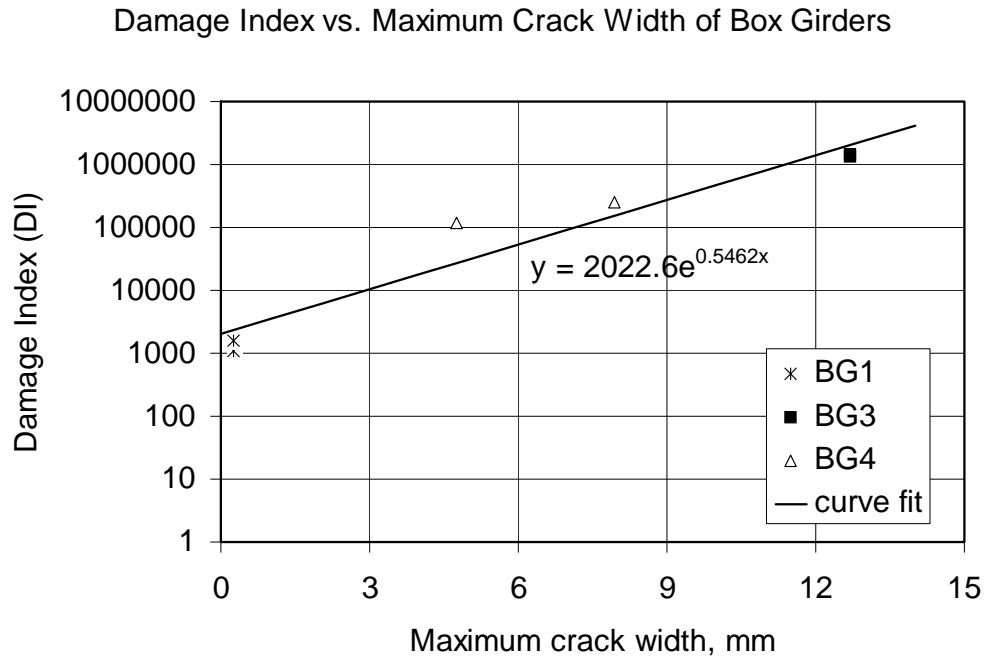Axes: Damage Index (DI) vs. Maximum crack width, mm

Figure 5.10 Damage index versus maximum crack width of box girders

As would be expected, cores taken from areas with greater Damage Indices have lower compressive strengths. Figure 5.11 shows this relationship; a logarithmic fit to the data is also plotted. The points plotted are from cores of BG1 (representing girders with slight inherent problems and mild exposure) and BG4 (representing girders with severe inherent problems and severe exposure). The damage indices used are those that correspond most closely to the test date of the core in question. The damage index from Square A was used to represent end-block damage, and the damage index from Square B was used to represent web damage, since those locations corresponded most closely to the areas from which cores were taken.

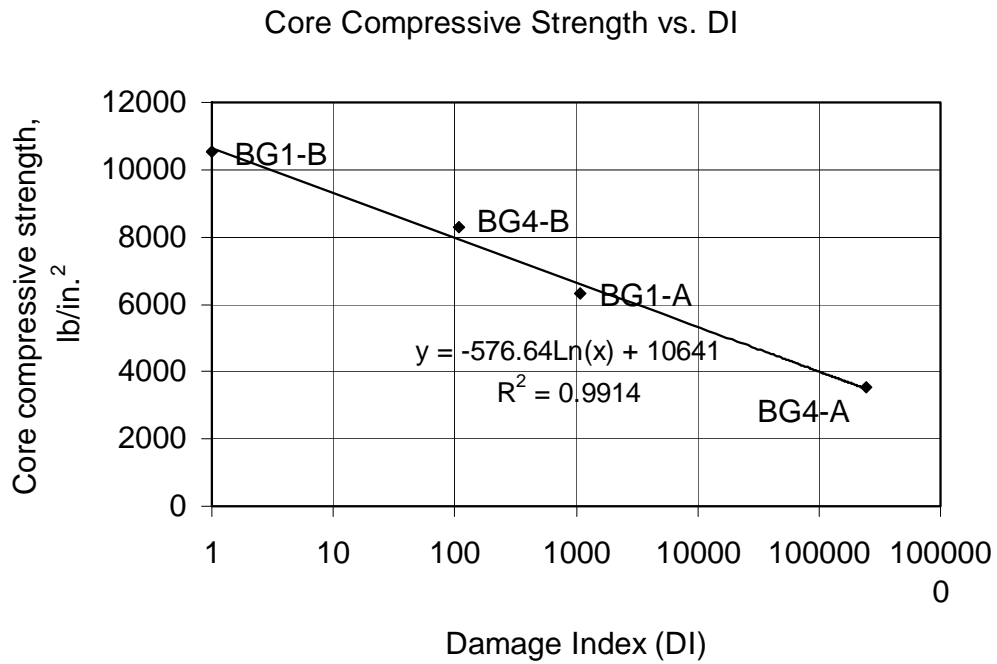Core Compressive Strength vs. DI

Figure 5.11 Concrete compressive strength of cores from box girders versus damage index

5.4 SIGNIFICANCE OF FLEXURE-DOMINATED TESTS

Figure 5.12 shows the load-deflection curves for the flexure-dominated specimens as well as the predicted response and maximum load expected according to ACI 318-99.

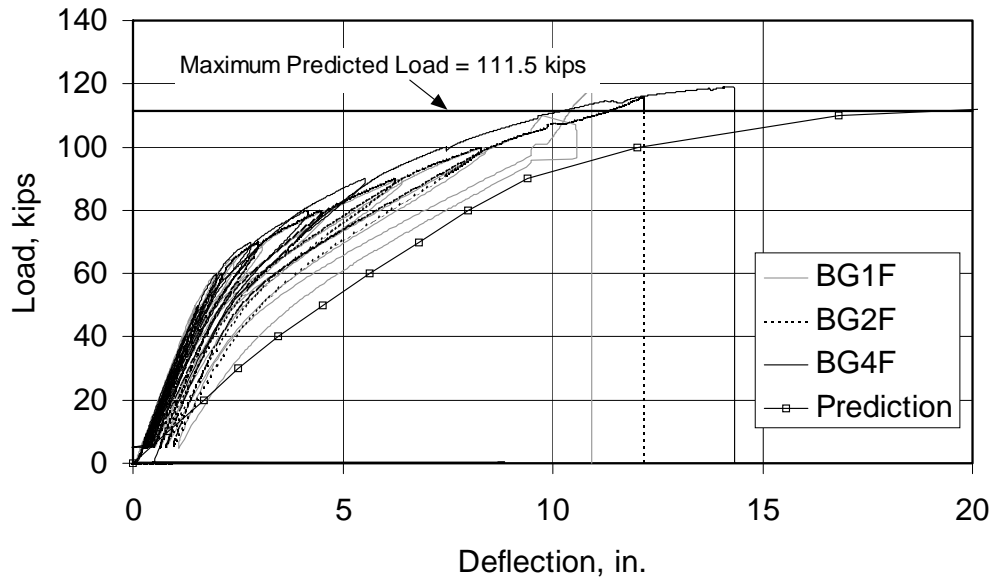Load vs. Deflection for Flexure-Dominated Specimens

Figure 5.12 Load-deflection curves and predicted behavior for flexure-dominated specimens

The ultimate capacity of the three flexure-dominated specimens varied by only 2.7 kips (12 kN), or 2% of the lowest capacity, while the final deflection varied by 3.44 inches (87 mm), or 32% of the lowest deflection. Actual deflection of BG1 may have been greater than recorded; due to the limitation of the deflection-measuring instrument; the actual variation in final deflection may be less than 32%. The similar capacity of the three specimens may be explained by their comparable damage in the critical flexural area.

All three specimens carried more than the predicted maximum load of 111.5 kips (496 kN). The ratios of tested to calculated flexural strength were 1.06, 1.04, and 1.07 for BG1F, BG2F and BG4F respectively. These values are at

least as high as the value of 1.03 found by Mattock (1961) for prestressed beams with well-bonded tendons tested in simple bending. Therefore it appears that the minimal pre-existing damage in the critical flexural area of these beams did not reduce their flexural capacity.

Since the girders were under-reinforced, their flexural capacity was governed by the available force in the tension chord (the prestressing strand), provided that the compressive strength of the concrete in the compression chords was not excessively reduced by premature deterioration. Because all three specimens had no visible damage in their top flanges, their flexural capacities should have been almost equal. This is consistent with the theoretical model introduced in Section 5.1.

If the cores taken from the webs of the girders are representative of the concrete near the mid-span of the girders, then BG1 had a higher modulus of elasticity than BG2 and BG4, and was therefore stiffer than BG2 and BG4. Consistent with the model of elastic behavior, BG1 had a smaller ultimate displacement than BG2 and BG4.

Table 5.3 shows the maximum compressive strains recorded during the flexure-dominated tests.

Table 5.3 Maximum compressive strains recorded during flexure-dominated tests

Specimen	Maximum Compressive Strain, $\mu\varepsilon$	Maximum Strain Normalized by Maximum Strain of BG1F
BG1F	2582	1
BG2F	2889	1.12
BG4F	1911	0.74

Since the three specimens had similar capacities, little variation among the maximum strains would be expected. This was not observed, possibly because of the difference in failure patterns of the specimens. The length longitudinally of crushed concrete in the top flange was shortest for BG2 – about 1 ft (0.30 m), and longest for BG4 – about 2 ft (0.61 m). Also, the gages may not have been placed at the location of maximum strain.

BG1 and BG2, both of which had an intermittent crack at 5.5 in. (0.14 m) from the bottom, showed a maximum average increase of 0.016 in. (0.39 mm) in the width of that crack at failure. In comparison with BG4, which did not have a pre-existing crack at that level in the critical flexural area, the presence and growth of a pre-existing crack of such width and at that location did not affect their ultimate strength.

Flexural capacity is plotted against damage index in Figure 5.13. The damage indices and specimens plotted were chosen as described in Section 5.3.
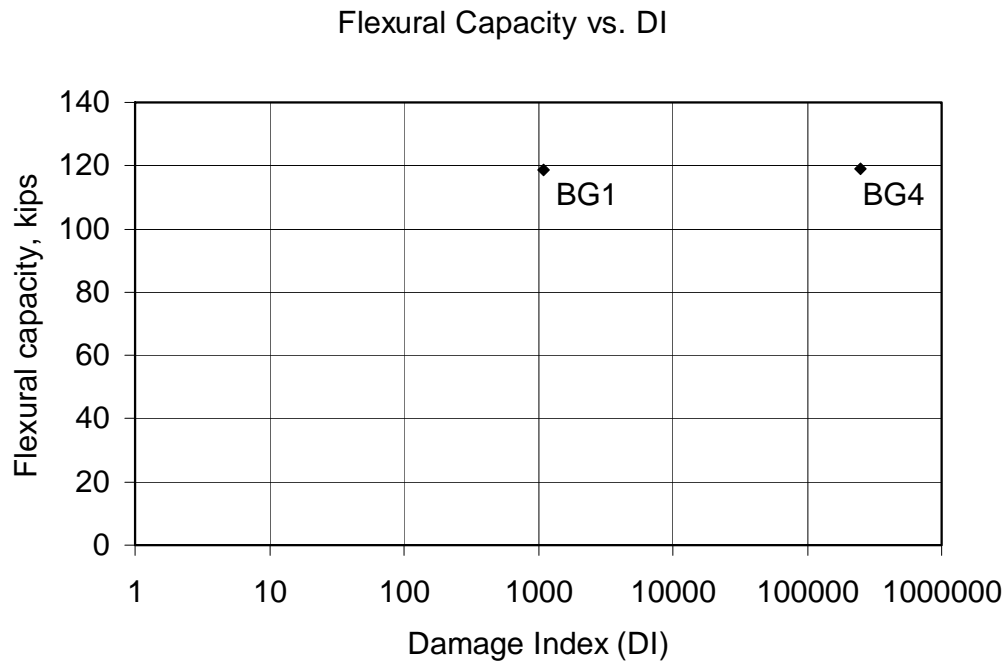
Flexural Capacity vs. DI

Figure 5.13 Flexural capacity versus damage index

5.5   SIGNIFICANCE OF SHEAR-DOMINATED TESTS

Figure 5.14 shows the load-deflection curves for the shear-dominated specimens as well as the maximum expected load calculated according to ACI 318-99, assuming a specified concrete compressive strength of 6,000 lb/in.[2] (41.4 MPa).
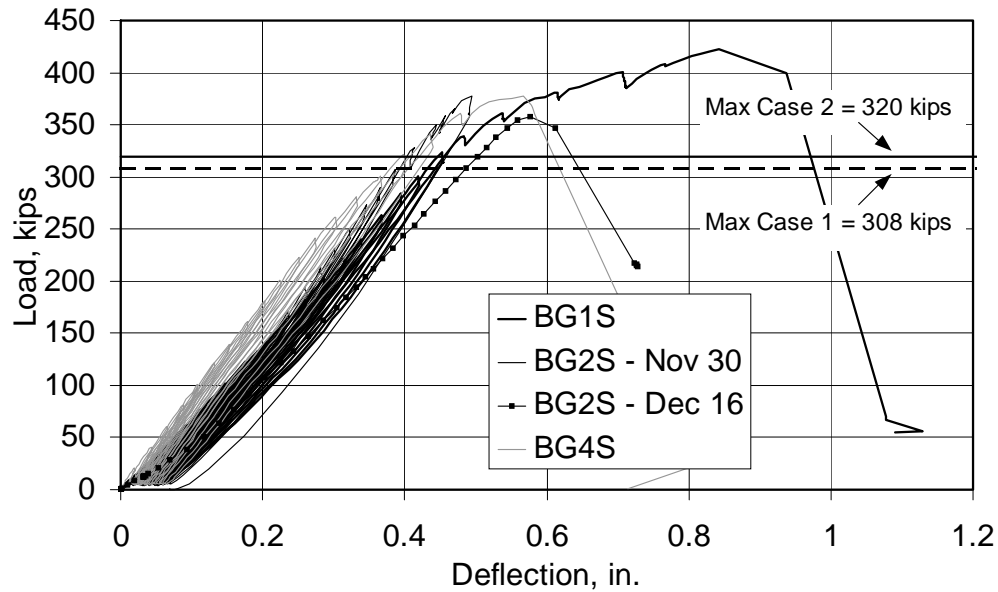
Figure 5.14 Load-deflection curves and predicted maximum loads for shear-
dominated specimens

BG2S and BG4S had ultimate capacities of 377.1 kips (1680 kN) and
377.8 kips (1681 kN) respectively, while BG1S had an ultimate capacity of 422.6
kips (1880 kN). BG2S and BG4S had final deflections of 0.73 in. (19 mm) and
0.88 in. (22 mm) respectively; BG1S had a final deflection of 1.13 in. (29 mm).
Thus the less damaged girder, BG1S, carried 12% more load and deflected 40%
more than the severely damaged girders, BG2S and BG4S.

The ratios of tested to calculated ultimate strength were 1.32, 1.18, and
1.18 for BG1S, BG2S and BG4S respectively. Though these ratios exceed 1.0,
they fall below the average ratio of 1.368 found by Hognestad et al. (1967) - even

114

for BG1S, which had the least damage. The more-damaged specimens are almost 14% below the average expected for specimens with normal concrete.

Shear behavior, using the theoretical framework of Section 5.1, is governed by the concrete compressive strength of the diagonal compression struts, by the tensile strength of the prestressing strand comprising the bottom chord, and by the compressive strength of the concrete comprising the top chord. Because shear capacity was not governed by strand slip, it was governed by concrete compressive strength. Looking at the core strengths, BG1S would be expected to have the highest capacity, BG4S a lower capacity, and BG2S the lowest. This is consistent with the test results.

Figure 5.15 shows the relationship between shear at the critical section at failure and the compressive strength of concrete cores. Also plotted in that figure are the best straight-line fit to the test data, and ACI Equation 11-2 for nominal shear strength (V_c plus V_s) of prestressed-concrete beams. The shear at the critical section at failure is the end reaction minus the self-weight between the support and the end of the void. An average core strength was used because cores were not taken from the critical shear area. The amount of pre-existing damage in the critical shear area was less than the amount seen in the end-blocks, but more than that seen in the webs.

Shear at Critical Section vs. Average Core Compressive Strength

$$y = 0.0106x + 217.13$$
$$R^2 = 0.9677$$

Legend:
- - - - ACI
- ◆ test values
- —— curve fit

X-axis: Average core compressive strength, lb/in.^{2}

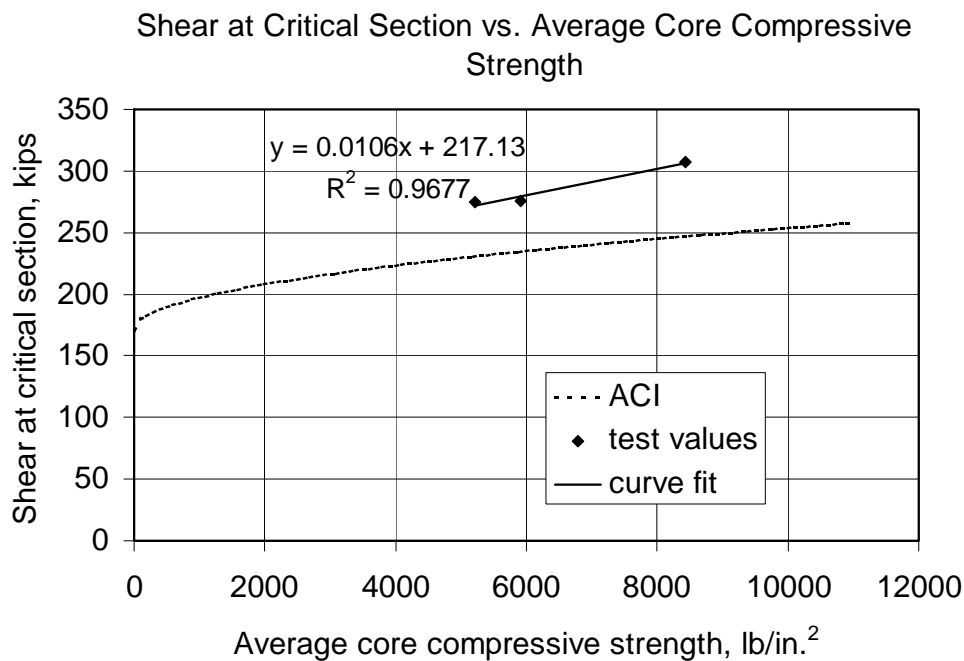Y-axis: Shear at critical section, kips

Figure 5.15 Shear strength versus average core compressive strength

From the limited data available, it appears that ACI Equation 11-2 can safely be used to predict shear strength, based on the compressive strength of concrete cores from the critical region. Because damage reduces not only compressive strength, but also bond strength, as strand slip in BG2S and BG4S and the crumbled concrete in ends of BG2 imply, capacities for specimens with very low compressive strengths might drop below the ACI curve. At very low strengths, the concrete is no longer a solid matrix holding the shear reinforcement and prestressed strand in formation. Table 5.4 shows the maximum strand slip recorded during the shear-dominated tests.

Table 5.4 Maximum strand slip recorded during shear-dominated tests

Specimen	Strand	Maximum Slip, in. (mm)	Average Max Slip, in. (mm)
BG1S	All monitored	0	0
BG2S	P5	0.055 (1.40)	0.097 (2.45)
	P6	0.138 (3.51)	
	All others monitored	0	
BG4S	P1	0.174 (4.42)	0.174 (4.42)
	P2	0.030 (0.762)	
	P3	0.054 (1.37)	
	P4	0.058 (1.470	
	P5	0.238 (6.05)	
	P6	0.409 (10.4)	
	P7	0.356 (9.04)	
	P8	0.074 (1.88)	

Strand slip was noticeably worse in specimens BG2S and BG4S, which had more end damage. This suggests that the premature concrete deterioration reduced the bond between the strand and the concrete matrix. Though strand slip was observed, it was not gross and did not control the failure.

Table 5.5 shows the maximum recorded displacement of the linear potentiometers monitoring web deformation of the shear-dominated specimens. Values for BG2S are taken from the December 16th test. The ratio of maximum displacement to original chord length is also tabulated.

Table 5.5 Maximum web deformations recorded during shear-dominated tests

Specimen	Chord	Maximum Extension, in. (mm)	Max Extension divided by Original Length
BG1S	Compression Diagonal	-0.041 (-1.04)	-7.88×10^{-4}
	Tension Diagonal	0.069 / 1.75	13.3×10^{-4}
	Bottom Chord	----	----
BG2S	Compression Diagonal	-0.016 (-0.406)	-3.72×10^{-4}
	Tension Diagonal	0.025 (0.635)	5.81×10^{-4}
	Bottom Chord	0.041 / 1.04	11.5×10^{-4}
BG4S	Compression Diagonal	-0.036 (-0.914)	-6.92×10^{-4}
	Tension Diagonal	0.090 (2.29)	17.3×10^{-4}
	Bottom Chord	0.037 (0.940)	8.04×10^{-4}

An overall deformation index can be calculated for each shear-dominated specimen by summing the absolute values of the displacement ratios of the diagonals and bottom chord, and multiplying by 10,000 (Table 5.6).

Table 5.6 Total web-deformation indices for shear-dominated specimens

Specimen	Total Web Deformation Index
BG1S	21.2
BG2S	21.0
BG4S	32.3

The proposed elastic model suggests that specimens with lower modulus of elasticity would be more flexible, and would show greater total web

deformation. In this case, the test results are not consistent with that model. BG4 had a lower modulus than BG1, and showed more deformation than BG1. BG2, however, with the lowest modulus of elasticity, had about the same web deformation as BG1.

Shear capacity is plotted against damage index in Figure 5.16. The damage indices and specimens plotted were chosen as described in Section 5.3.

Shear Capacity vs. DI
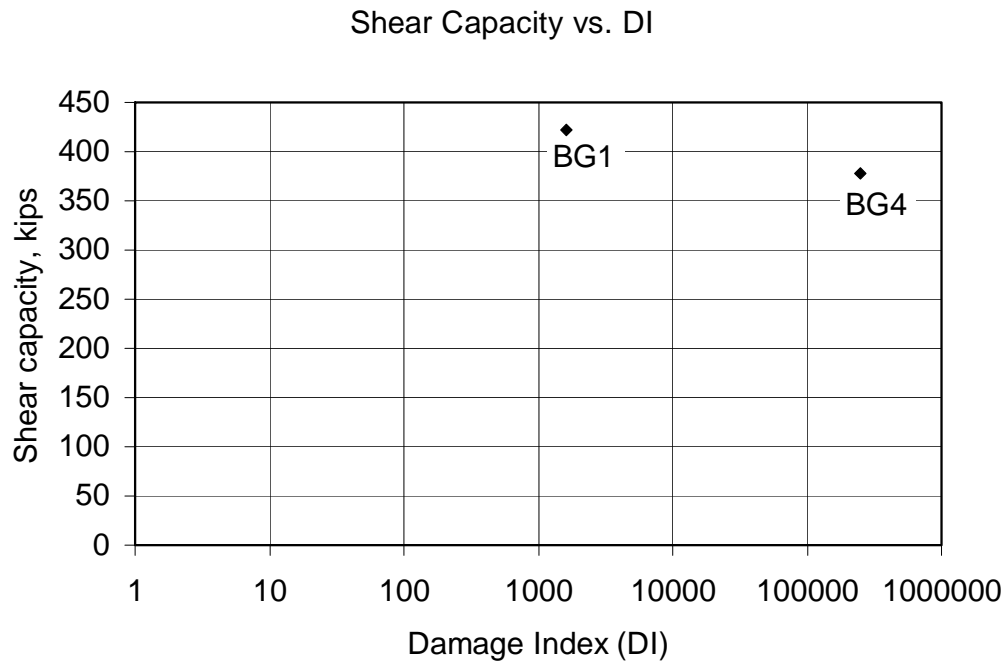
Figure 5.16 Shear capacity versus damage index

Damage histograms for the box girders at two ages are shown in Figures 5.17 and 5.18. They represent the total crack length observed in the

representative squares for cracks of each width. With time, the damage histogram

shifts towards the right (towards more cracks with larger widths).

Damage Histogram of Box Girders
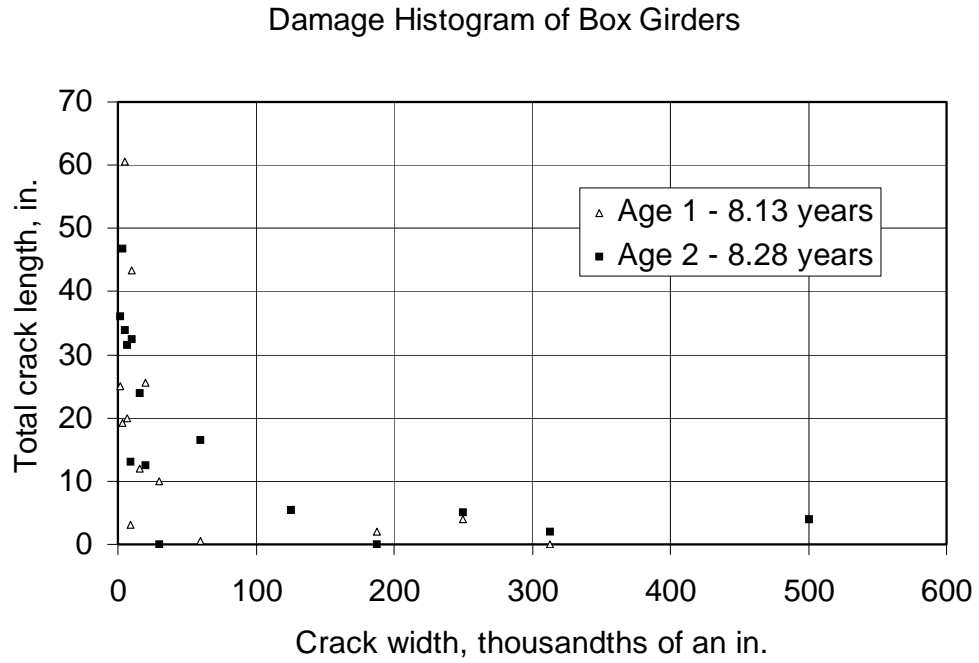
Figure 5.17 Damage histogram of box girders (US Customary units)

Damage Histogram of Box Girders
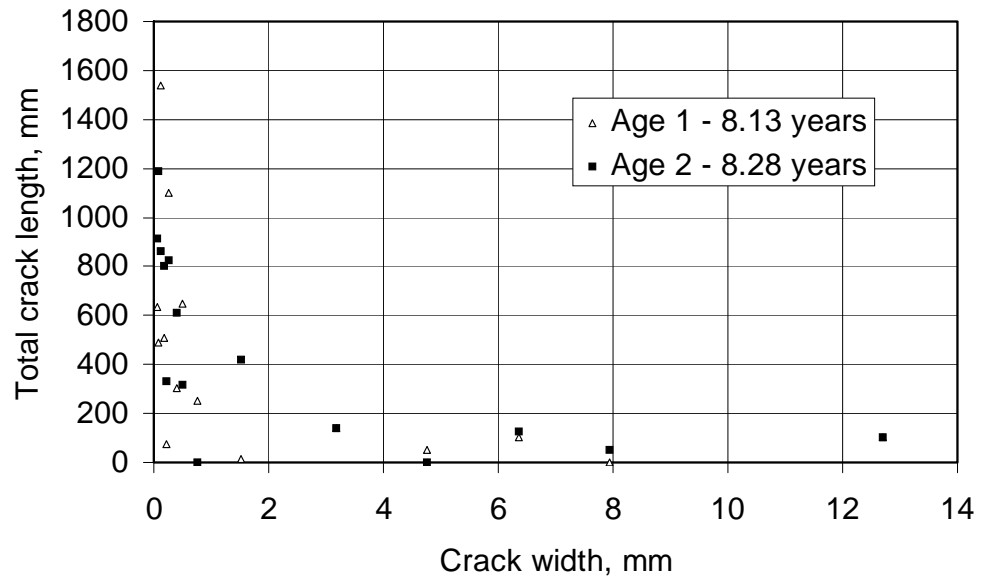
Figure 5.18 Damage histogram of box girders (SI units)

Chapter 6: Development of Field Observation Program

6.1 OBJECTIVES AND PLAN

The goal of the field observation program was to compare the appearance of field structures with those monitored and tested in the laboratory. Premature concrete deterioration was recorded over time in structures subjected to in-service environments, and also in structural elements kept at the laboratory. The rate of deterioration of field structures was compared to that of laboratory specimens, to find out how such deterioration affects the structural capacity of elements over time. The objective is to use the relationship between field and laboratory specimens to predict the degree to which deterioration will continue, and the remaining service life of a damaged element.

6.2 SELECTION OF STRUCTURES STUDIED

As TxDOT became aware of problems with premature concrete deterioration, inspectors noticed unusual map cracking in precast concrete box girders and I-beams in several in-service bridges. Because it is an apparent precursor of premature concrete deterioration, map cracking is used as a general criterion for selecting elements to investigate. Appendix A is a list of structures that TxDOT has identified as having premature concrete deterioration. From this list five structures, representative of the more severely damaged structures in the state, were selected for closer study. Those currently under observation for Project 1857 are:

1. Interstate Highway 10 (I-10) over the Atchison Topeka & Santa Fe Railroad (AT & SF RR)
2. US Highway 90 (US-90) over the San Jacinto River
3. Robinson Road over Interstate Highway 45 (I-45)
4. Beltway 8 (BW8) over State Highway 3
5. FM 1979 over Lake Ivie

6.2.1 I-10 at AT & SF RR

The first structure inspected (Figure 6.1) is in Beaumont, TX on I-10 crossing the Atchison Topeka and Santa Fe railway lines (I-10 eastbound, take 7th Street exit). The affected elements are standard AASHTO Type C prestressed girders, fabricated in 1987.

In November of 1998, two of the exterior girders near the northwest abutment were replaced, and the original girders were sent to the University of Texas for testing.

Figure 6.1 I-10 at AT & SF RR

6.2.2 US-90 at San Jacinto River

The US Highway 90 structure crossing the San Jacinto River (Figure 6.2) is approximately 25 miles northeast of Houston (US-90 eastbound, exit before San Jacinto River). The affected elements are Type 54 prestressed girders, cast in 1986.

Figure 6.2 US-90 at San Jacinto River

6.2.3 Robinson Road at I-45

The Robinson Road overpass of I-45 (Figure 6.3) is located north of Houston in the Woodlands (I-45 northbound, exit before Woodlands Parkway). The affected elements are Type IV prestressed girders, fabricated in 1987.

Figure 6.3 Robinson Road at I-45

6.2.4   Beltway 8 at State Highway 3

Beltway 8 over State Highway 3 (Figure 6.4) is approximately 15 miles southeast of downtown Houston. The affected elements are Type IV prestressed girders over the northbound lanes of State Highway 3, fabricated in 1987.

Figure 6.4 Beltway 8 at State Highway 3

6.2.5   FM 1979 at Lake Ivie

FM 1979 crosses Lake Ivie (Figure 6.5) near San Angelo, TX. The bent caps and columns, built in 1989, are affected.

Figure 6.5 FM 1979 at Lake Ivie

6.3 METHODS USED

Four methods were used to assess damage to the field structures: visual inspection; crack comparator; Demec gage; and measurement using a magnifying eye scope.

6.3.1 Visual inspection

The overall appearance of the damage is noted. General condition of paint and cracks is described. This method is fast and requires no tools, but is highly subjective.

6.3.2 Crack comparator

A crack comparator is a transparent ruler with lines of different widths, varying from 0.002 to 0.06 in. (0.08 to 1.50 mm). By placing the ruler over a crack and identifying the calibrated line with the same width, the width of the

crack is determined (Figure 6.6). This method offers quantitative results, but retains an element of subjectivity.

Figure 6.6 Crack comparator

6.3.3 Demec gage

The Demountable Mechanical Strain gage (Demec gage) is a mechanical dial gage used to measure the distance between two steel discs glued to a surface. For field measurements of cracks, a disc was glued to either side of a crack (Figure 6.7). Since this method was considered the least subjective and most accurate, changes in Demec measurements on successive field visits were used to indicate crack growth or shrinkage.

Figure 6.7 Demec gage

6.3.4   Magnifying eye scope

The magnifying eye scope consists of a magnifying lens with 0.005 in. (0.127 mm) divisions and a light (Figure 6.8).

Figure 6.8 Magnifying eye scope

This instrument is well suited to measuring larger cracks (> 0.02 in., or 0.5 mm wide), but is less suited to measuring smaller cracks. It is difficult to hold sufficiently still in the field to estimate the distance between the closest gradations.

6.4 BRIEF SUMMARY OF FIELD VISITS

The structures visited and activities performed during seven field trips are described below.

Trip on November 28, 1998

On November 28, 1998, 10 Demec points were installed on the I-10 structure in Beaumont. Initial measurements taken were intended to serve as a reference for crack growth in that structure, which has the longest duration of measurements.

Trip on February 6, 1999

On February 6, 1999, the I-10 structure was monitored again, and another set of Demec points was added. Two structures were monitored for the first time: US-90 over the San Jacinto River and Robinson Road over I-45 in Houston. Demec points were installed and initial measurements taken.

Trip on April 9, 1999

On April 9, 1999, the three previous structures were monitored again, and another structure (Beltway 8 over State Highway 3) was added to the research. No Demec points were added at that time, since a man-lift would have been required to install them.

Trip on June 5, 1999

On June 5, 1999, Demec gages were installed on the Beltway 8 structure, and all the previous structures were monitored again.

Trip on September 29, 1999

On September 29, 1999, a visual inspection was conducted on the bents of the FM 1979 structure over Lake Ivie. Based on this preliminary visual examination, an underwater investigation was conducted on columns of two of the bents.

Trip on October 21, 1999

On October 21, 1999, the four structures in southeast Texas (I-10, US-90, Robinson Road and BW8) were monitored again. Using the crack comparator, crack widths were measured at existing locations of Demec points, and at other significant locations.

Trip on February 11, 2000

On February 11, 2000, Demec and crack-comparator measurements were taken at the four structures in southeast Texas, and the magnifying eyescope was used for the first time.

Chapter 7: Results from Field Observations

7.1 NOMENCLATURE

At each structure, the most severely affected elements were monitored. Girders were labeled according to their position in the structure; for example, NW Girder 1 denotes Northwest Girder 1. The nomenclature of Figure 7.1 is used in this chapter to identify faces of the girders.
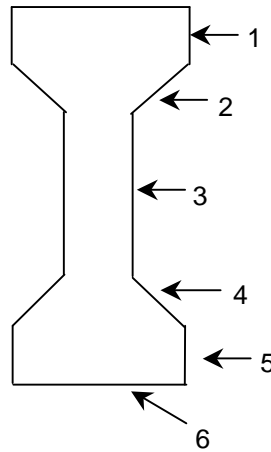
Figure 7.1 Nomenclature used to designate faces of girders

7.2   OBSERVATIONS FROM STRUCTURES STUDIED

The condition of each structure is described as observed during the site visits outlined in Section 6.4. Schematics are included describing the locations of Demec points installed on each structure. The distance of each point from the end of the girder is listed in Appendix H.

7.2.1   I-10 at AT & SF RR

Figure 7.2 shows the relative locations of measurement points on the I-10 structure. SW Girders 3 and 4 were cast on June 26, 1987; the cast date of SW Girders 1 and 2 could not be determined.
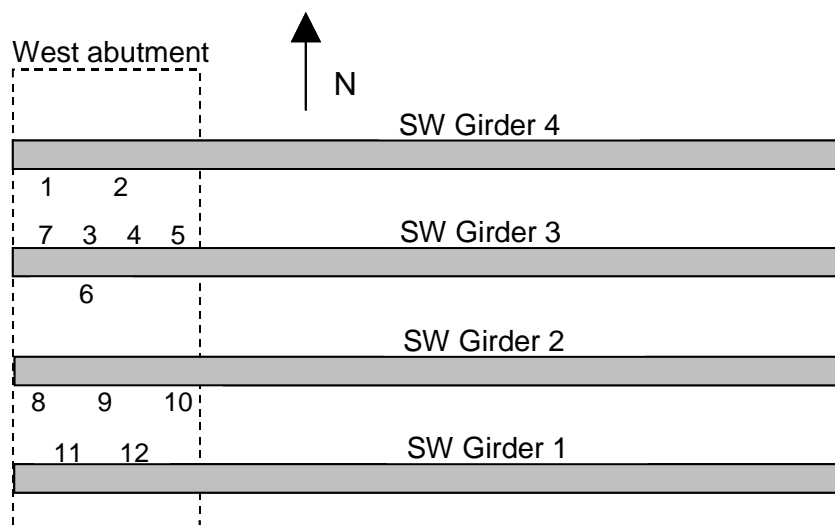
Figure 7.2 Schematic of measurement points on I-10 structure

Observation of the Beaumont site began on November 28,1998. Demec points were placed on the four southernmost girders near the west abutment, and initial measurements were made.

On February 6, 1999 the I-10 structure in Beaumont was inspected again. The most obvious cracks were at the ends of the girders on Faces 4 and 5. In some cases these extended the complete length of the girder. Other longitudinal cracks had also developed on Faces 1, 2 and 6. Changes in crack length and width since the November trip were observed. Deterioration of the girders was significantly worse in areas exposed to water, such as the exterior girders and

girders near an open expansion joint. Particularly advanced deterioration was noticed near the abutments. At the west abutment it was estimated that the cracks had grown 5 to 10% in length since the last visit.

Two types of repair materials were observed in some of the cracks. One was hard and gray, and appeared to be applied to the surface only. According to TxDOT, it was a paste-type epoxy[1]. The other type, less common than the first, was clear, yellow, and more pliable. It was probably an elastometric sealant, injected through ports that are apparent on the face of the girder (Figure 7.3).

Figure 7.3 Injected sealant on I-10 structure

At one bearing point, the bearing pad had slipped out, causing the girder to rest directly on the concrete support. This had caused a portion of the support to spall off (Figure 7.4).

---

[1] Personal communication, Brian Merrill (TxDOT), 1999

Figure 7.4 Missing bearing pad at I-10 structure

On April 9, 1999 increases in length of existing cracks were marked. One new crack by Demec Point 8 was noted. All old girders at the west abutment had fully developed cracks along their bottom faces (Face 6). The northernmost girder (new, replacing one now at FSEL) had no cracks.

On June 5, 1999, the epoxy that had been applied to several cracks on the bottom flanges was cracked along its full length of application. Many cracks were noted to have extended from 6 to 12 in. (0.15 to 0.30 m).

On October 22, 1999, the role of water in accelerating damage was more evident. In Figure 7.5, the west abutment between SW Girder 2 and SW Girder 3 is shown. Note the staining that indicates more water on SW Girder 2 than on SW Girder 3. In Figures 7.6 and 7.7, respectively, damage to SW Girder 2 is seen to be heavier than to SW Girder 3.

Figure 7.5 View of west abutment between SW Girder 2 (left) and SW Girder 3
          (right)

Figure 7.6 View of greater damage to SW Girder 2

Figure 7.7 View of lesser damage to SW Girder 3

7.2.2 US-90 at San Jacinto River

Figure 7.8 shows the relative locations of measurement points on the US-90 structure. NW Girders 1 and 2 were cast on October 31, 1986.
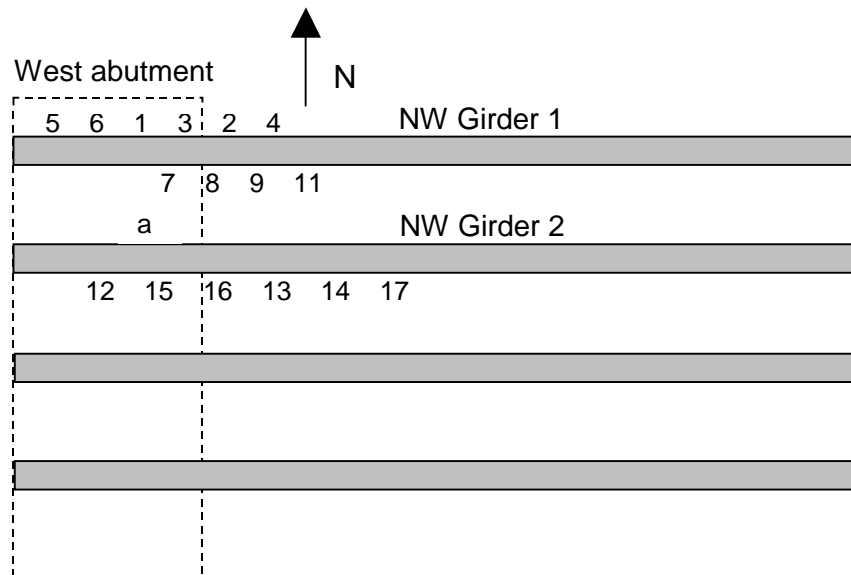
Figure 7.8 Locations of measurement points on US-90 structure

On February 6, 1999, the same type of cracks as in seen in the I-10 structure were observed at the west abutment of the US-90 structure. These were longitudinal cracks on Faces 4 and 5, beginning at the ends of the beams and extending towards midspan. Crack patterns along the end 15 ft (4.6 m) at the west abutment of both sides of the exterior of NW Girder 1 were sketched and are included in Appendix?.

TxDOT personnel had filled some cracks with some type of repair material, and had also monitored their length in September 1998. The markings they left suggested that while the cracks had not grown much, new cracks had formed slightly above and below the old ones. These new cracks extended several inches past the ends of the old ones (Figure 7.9).

Figure 7.9 New cracks extending past the end of the old crack

Cores had been taken from other girders in the span (Figure 7.10). Some core holes had been filled with grout; others were left unfilled. In one of the holes, a strand had also been cut and was exposed. The anchor bolts for the coring machine seemed to have been set into existing cracks, making them wider.
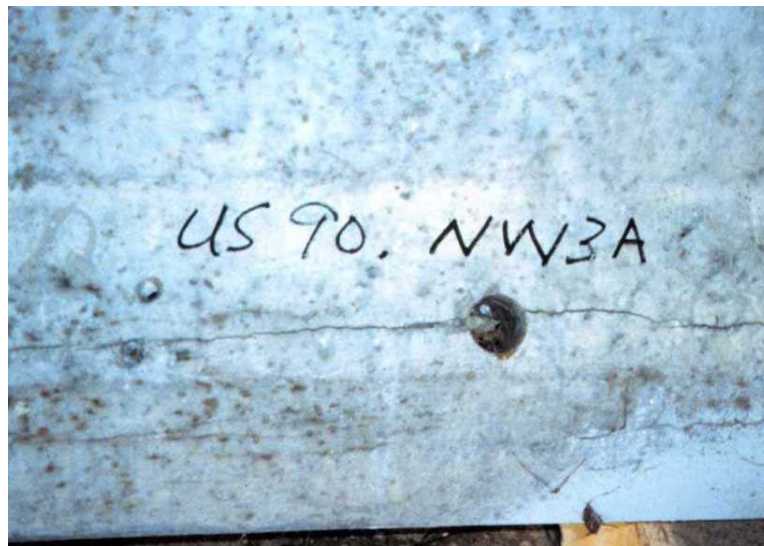
Figure 7.10 Core removed from US-90 girder

More severe damage was present on girders below where a section of the rubber seal, normally compressed between two spans of slab, had fallen out (Figure 7.11).

Figure 7.11 Rubber seal dropped from joint above at west abutment of US-90
            structure

On April 9, 1999, many girders had fully developed cracks on their bottom faces (Face 6). Girders on the eastbound lanes had similar but less severe damage. Cracks on exterior faces of outside girders in both directions may have grown in length, but were possibly obscured by paint.

On June 5, 1999, the crack on Face 3 on NW Girder 1 had propagated about 6 in. (0.15 m) up into Face 2. A few cracks on the bottom flanges had also extended about 6 to 10 in (0.15 to 0.30 m).

On October 22, 1999, cracking on the outside of the NW Girder 1 appeared markedly more severe than on previous trips, probably because the paint there had begun to peel, exposing the cracking beneath. At the north side of NW Girder 2, Point "a" was marked (Figure 7.12). The crack at that location was more than 1/4 in. (6.4 mm) wide.

Figure 7.12 Point "a" on NW Girder 2 of US-90 structure

The apparent role of exposure to water was more evident than before. In examining overall damage on the northwest portion of the bridge, horizontal cracks were clearly visible on Face 5 of the northwest girders, directly below each drain scupper (Figure 7.13).

Figure 7.13 Cracking on Face 5 of exterior girder under drain scupper

On February 11, 2000, the location of Point "a" was not apparent. The crack on Face 3 parallel with the top flange seemed to be continuous now where it had been intermittent before – either because of growth or the loss of more paint. A few cracks on the bottom flanges had also extended about 6 to 10 in. (0.15 to 0.30 m), and new cracks were apparent within 6 in. (0.15 m) of the west end on the bottom flange (Faces 5 and 6).

7.2.3   Robinson Road at I-45

Throughout the period of monitoring, this site was relatively clean and dry. Figure 7.14 shows the relative locations of measurement points on the Robinson Road structure. NW Girder 1 was cast on March 27, 1987; NW Girders 2 and 3 were cast on March 25 1987.
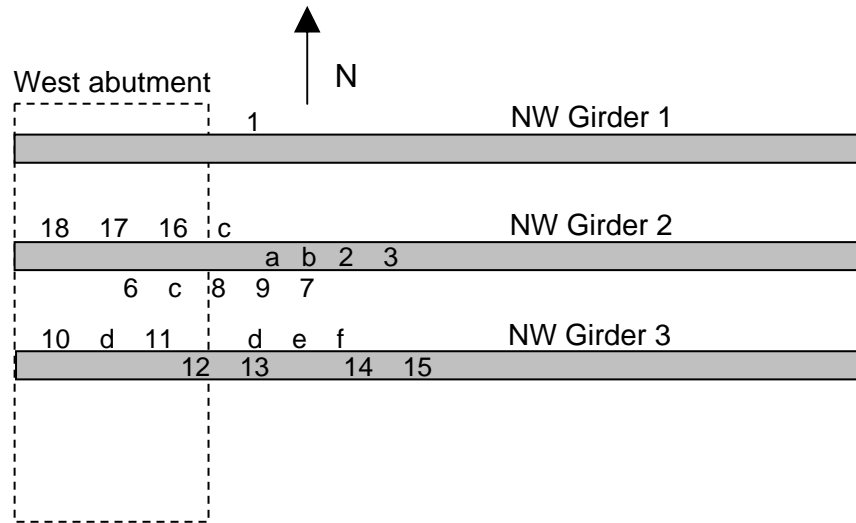
Figure 7.14 Locations of measurement points on Robinson Road structure

On February 6, 1999, the east abutment girders did not have visible damage. The girders at the west abutment had two parallel cracks on their bottom faces (Face 6), some of which extended the entire length, and others which stopped within 15 ft (4.6 m) from the end. Horizontal cracks on the sides of the girders were most prevalent on Faces 1, 4 and 5, and these for the most part stopped within 15 ft (4.6 m) of the end. A few cracks had been marked by TxDOT and their ends had been dated "9/98." These cracks had lengthened approximately 3 in. (0.08 m) since that date. Repair material (probably epoxy) had been applied to a few cracks, which had obviously elongated since the application. There was no paint on NW Girder 1.

On April 10, 1999, damage was still most severe at the west abutment. Cracks on Face 6 of NW Girders 1, 2, and 3 had extended. Webs had extensive map cracking. Paint on the outside girders may have obscured cracks in them. Three new sets of Demec points (Points 16, 17, and 18) were set on the north face of NW Girder 2.

On October 22, 1999, cracks on Face 6 of NW Girder 3 had not propagated since the last visit. On the north face of NW Girder 3, previously identified cracks on Face 2 had continued to propagate (Figure 7.15). Lettered Points "a" through "f" were marked and measured with the crack comparator.

Figure 7.15 Extension of crack on Face 2 of NW Girder 3 at Robinson Road
structure

On February 10, 2000, the lettered points showed either no change or a
decrease in width. At Points 8, 11, and 17 the cracks were less than 0.002 in.
(0.05 mm) wide. No crack was visible at Point 9.

7.2.4 Beltway 8 at State Highway 3

The locations monitored on the Beltway 8 structure are shown in Figure
7.16.
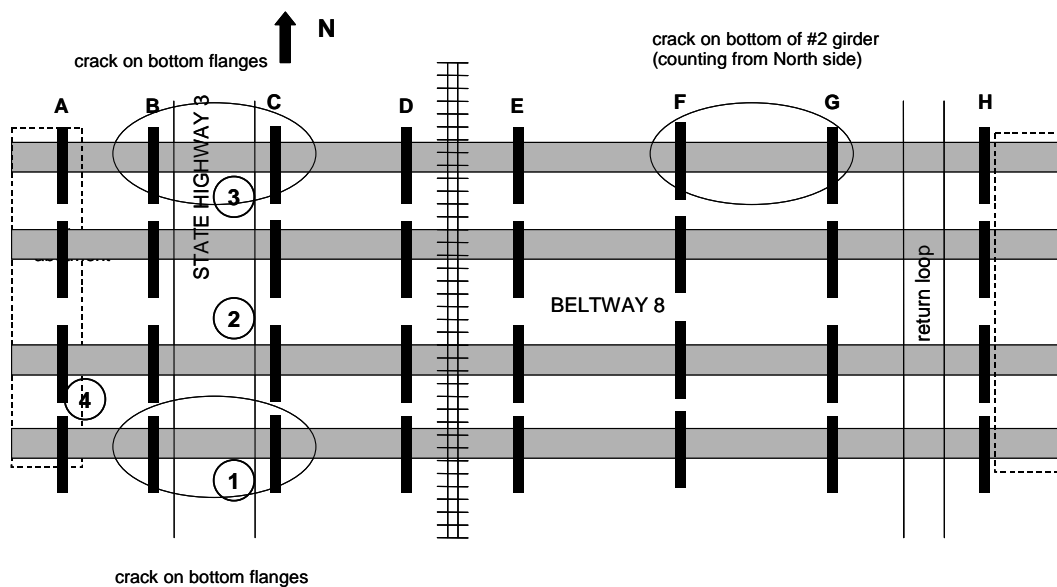
Figure 7.16 Schematic of Beltway 8 structure

On April 10, 1999, a preliminary investigation of the Beltway 8 structure was conducted. Accessibility and general damage were assessed. The two spans with the most damage were over State Highway 3. It was recommended that we mark cracks, measure crack widths, and set Demec points on the next visit. Damage appeared similar to that at the US-90 site.

On June 4, 1999, Location 1 and Location 2 were chosen for closer study. At Location 1 large cracks were noticed on Face 5 of the southernmost girder, as well as minor cracking in the web and top flange. The paint was peeling excessively, and remaining paint seemed to obscure some minor cracks (Figure 7.17). At Location 1, the contrast between damaged and undamaged girders is quite striking (Figure 7.18).

Figure 7.17 Typical cracks on bottom flange of Beltway 8 girders

Figure 7.18 Contrast between damaged and undamaged girders at Location 1

Cracks were mapped, and two Demec points were placed on the bottom flange of the east end of the girder: Point 1 on Face 5, and Point 2 on Face 4. At Location 2, cracks approximately 0.06 in. (1.5 mm) wide and 5 to 10 ft (1.5 to 3.0 m) long were noted directly on either side of the midspan diaphragm (Figure 7.19). Three additional Demec points were placed to the west of this diaphragm on the exterior of the north girder: Points 3 and 5 on Face 4, and Point 4 on Face 5.

Figure 7.19 Cracks on Face 5 of exterior girder at Location 2

On October 22, 1999, at Location 1, Points "a," "b," "c," and "d" were marked (Figure 7.20).

Figure 7.20 Marked points at Location 1

Cracks at Location 1 were about 1/8 in. (3.2 mm) wide. On the bottom flange, cracks were as wide as 1/4 in. (6.4 mm). The Demec discs had fallen off at Points 1 and 4. At Location 2, Points "e" through "l" on the bottom and sides of the bottom flange were marked and measured. Points "e" and "f" correspond to Points 4 and 5 respectively (Figures 7.21). Cracks at Locations 3 and 4 looked very similar to those at Location 1.

Figure 7.21 Marked points on Faces 4 and 5 at Location 2

On February 10, 2000, none of the points marked with letters on October 22, 1999 was visible. Two new cracks were noted at Location 1 on Face 4, and one had developed on the Face 3. These were about 1 ft (0.30 m) long. The horizontal cracks at Location 2 on Face 4 and Face 5 had extended several feet to the east and west. The apparently new and longer cracks might have been pre-existing, but just recently exposed by the severe paint loss.

7.2.5   FM 1979 at Lake Ivie

The east profile of the FM 1979 structure is shown in Figure 7.22. A schematic of a typical bent is shown in Figure 7.23.
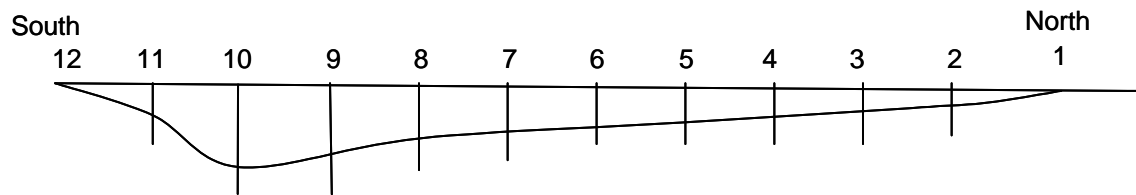
Figure 7.22 East profile of FM 1979 structure
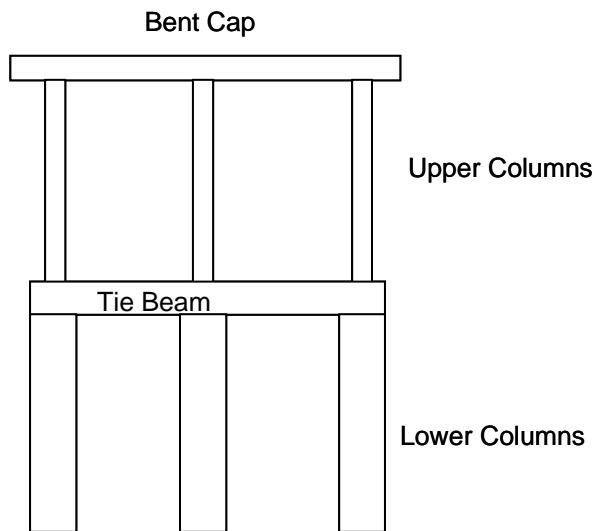
Figure 7.23 Schematic of a bent in FM 1979 structure

On September 29, 1999, cracks could be seen at each bent. Damage was concentrated at bents with expansion joints, probably because of greater exposure to rain of bent caps and girders in those locations. Bents 5, 9, 10 and 11 were visually assessed. Bent 10 showed clearly visible cracks, about 1/8 in. (3 mm) wide, over the entire height of the lower columns. The cracks appeared to coincide with the locations of the longitudinal reinforcement in the lower columns. Bents 9 and 11 show similar cracks, about 1/16 in. (2 mm) wide. Examples of these cracks are shown in Figure 7.24. Bent 5 shows similar vertical cracks, about 1/16 in. (2 mm) wide. It also showed clearly visible horizontal cracks, about 1/32 in. (1 mm) wide, apparently in line with the locations of the transverse reinforcement in the lower columns. This cracking is shown in Figure 7.25.

Figure 7.24 Vertical cracking typical of Bents 9, 10 and 11 of FM 1979 structure (Bent 10)

Figure 7.25 Horizontal and vertical cracking in Bent 5 of FM 1979 structure

An underwater investigation revealed that the vertical cracks go all the way to the mud line. At Bent 10 the cracks are 1/8 in. (3 mm) wide and at Bent 5, 1/16 in. (2 mm) wide down to the mud line.

Observations on the west side of the structure revealed damage on the bent caps, upper columns and tie beams in those same bents. At Bent 5, the girder ends showed horizontal cracking on their bottom flanges, and map cracking on their webs (Figures 7.26 and 7.27). The bent cap showed extensive map cracking, with a typical width of 1/16 in. (2 mm), on the top, sides and ends (Figure 7.28). On the sides of the bent cap, some diagonal cracks propagated outward from the top of the upper column (Figure 7.29).

Figure 7.26. Horizontal cracking on bottom flanges of outside girder ends (Bent 5)
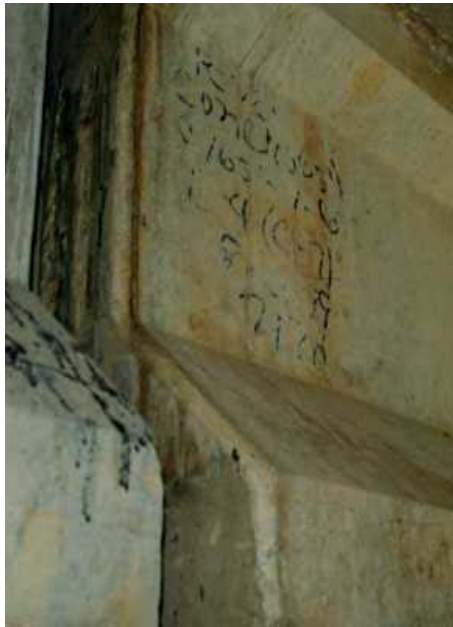
Figure 7.27. Horizontal cracking at bottom flanges of inside girder ends (Bent 5)

Figure 7.28 Map cracking at ends of bent cap (Bent 5)

Figure 7.29 Map cracking on side of bent cap (Bent 5)

At Bent 5, map cracking was clearly visible on the upper columns, and on the upper surfaces of the tie beams (Figure 7.30). The vertical cracks on the lower columns extended upward to the upper surface of the tie beam (Figure 7.31).

Figure 7.30 Map cracking on upper surface of tie beam (Bent 5)

Figure 7.31 Propagation of vertical cracks in lower column to top of tie beam (Bent 5)

At Bent 9, similar damage was evident to the bent caps (Figure 7.32) and girder ends (Figure 7.33).

Figure 7.32 Map cracking at ends of bent cap (Bent 9)

Figure 7.33 Horizontal and map cracking at girder ends (Bent 9)

7.3   RESULTS FROM CRACK-WIDTH MEASUREMENTS

Figures 7.34 through 7.39 show the crack widths and change in crack widths determined from Demec gage measurements over time. Due to the loss of Demec points, only crack comparator measurements are presented for the Beltway 8 structure (Figure 7.40). Note that different locations were measured on each date.
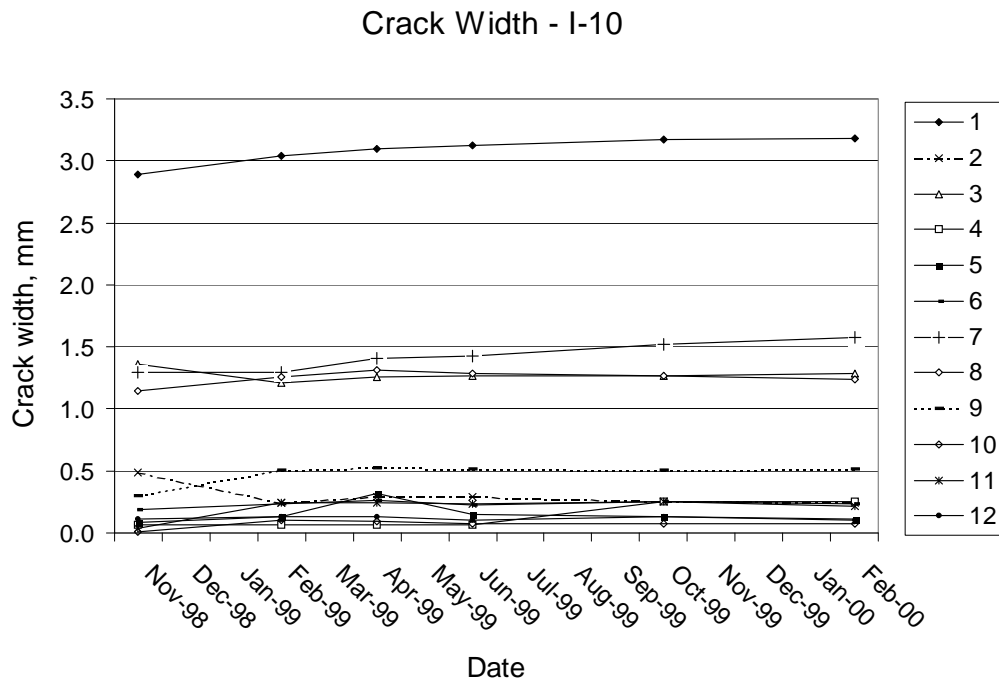
Figure 7.34 Crack width over time for I-10 structure

Change in Crack Width - I-10
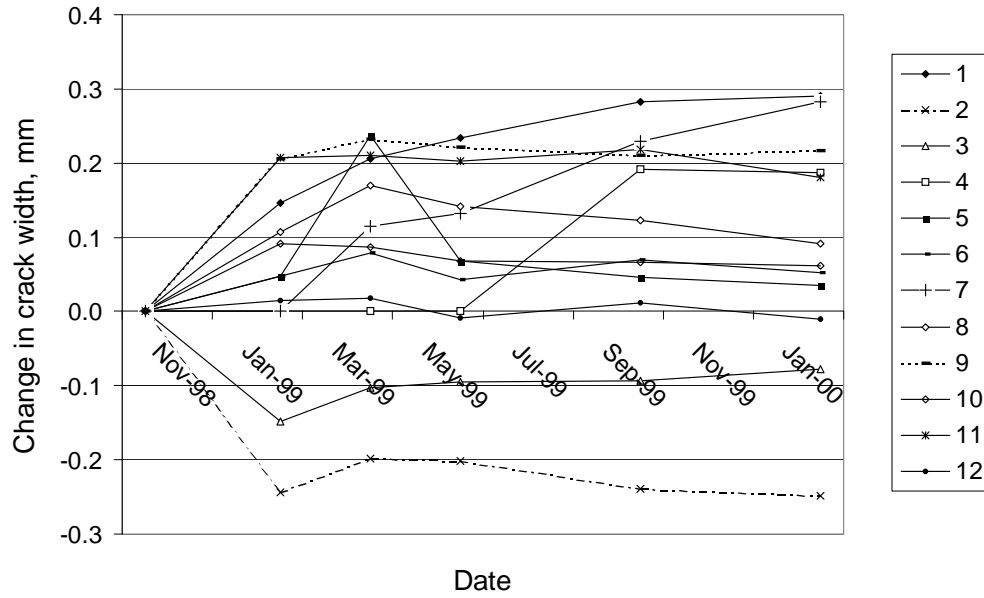
Figure 7.35 Change in crack width over time for I-10 structure
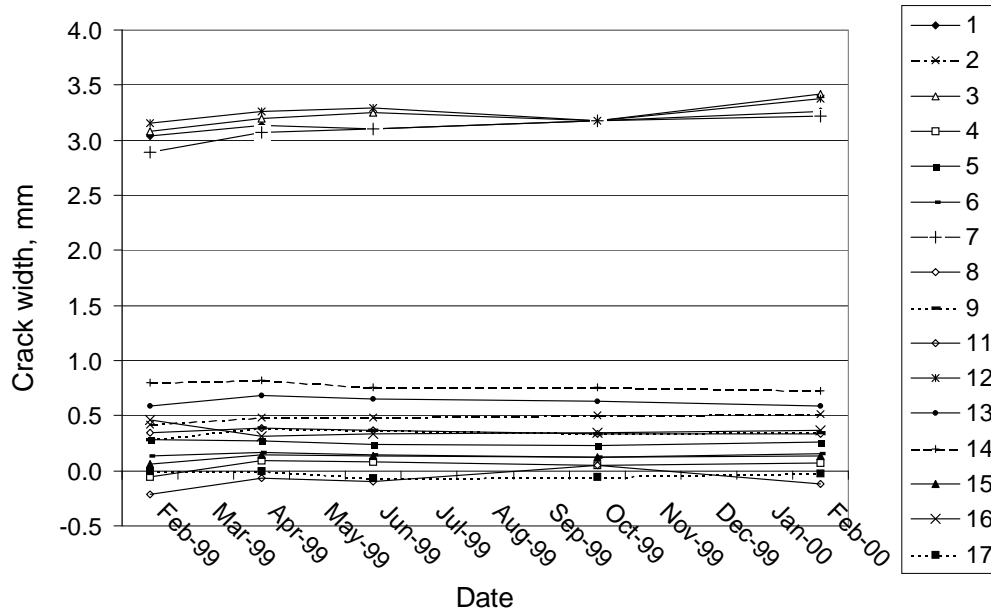
Figure 7.36 Crack width over time for US-90 structure

158

Change in Crack Width - US-90
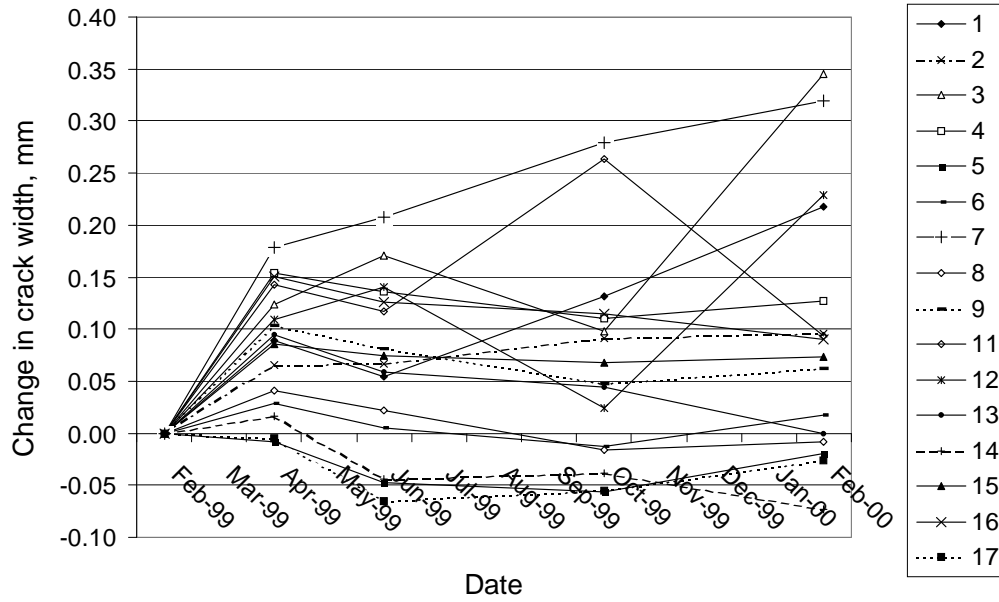
Figure 7.37 Change in crack width over time for US-90 structure

Crack Width - Robinson Road
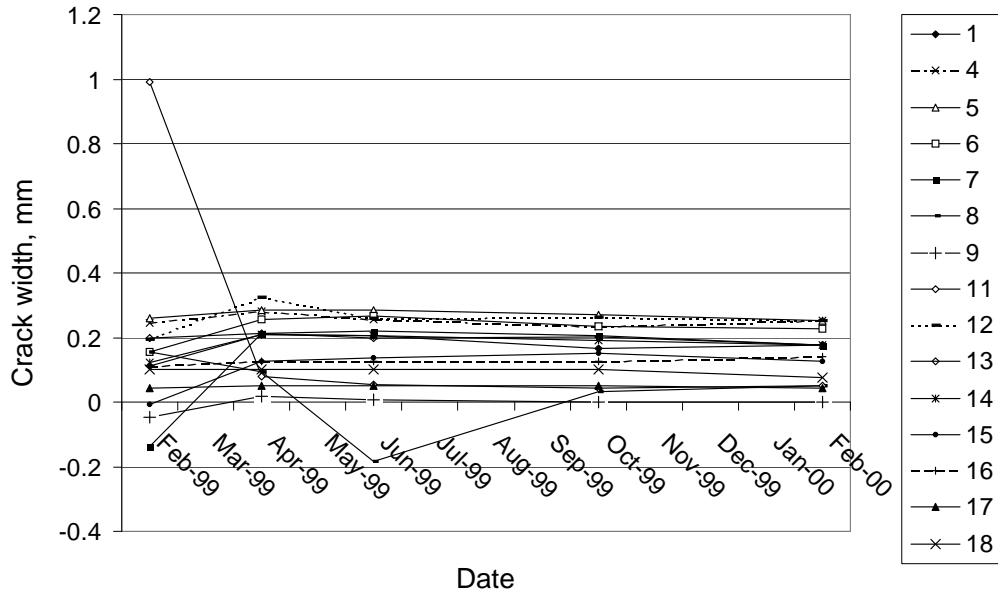
Figure 7.38 Crack width over time for Robinson Road structure

Change in Crack Width - Robinson Road
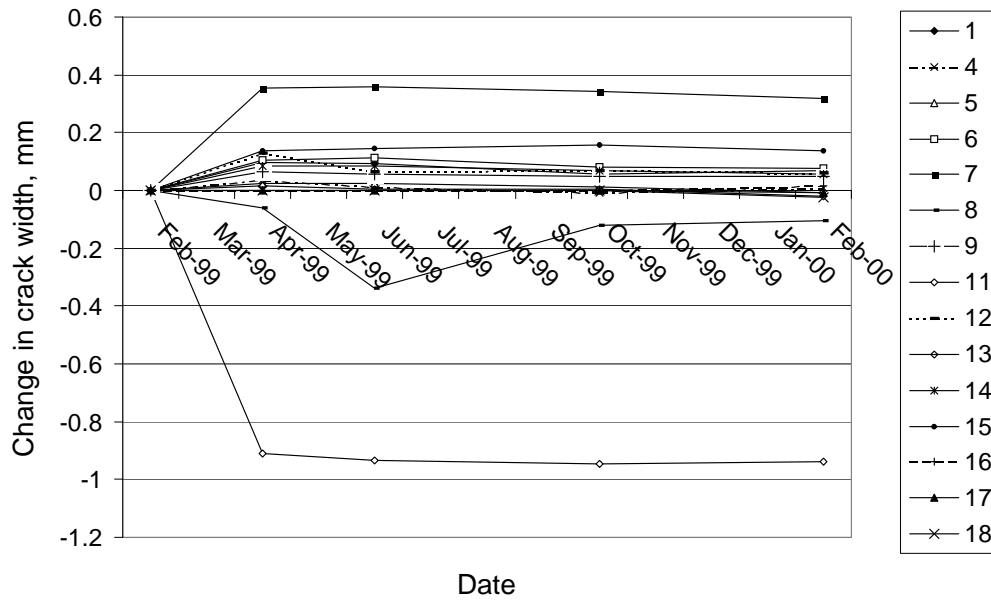
Figure 7.39 Change in crack width over time for Robinson Road structure
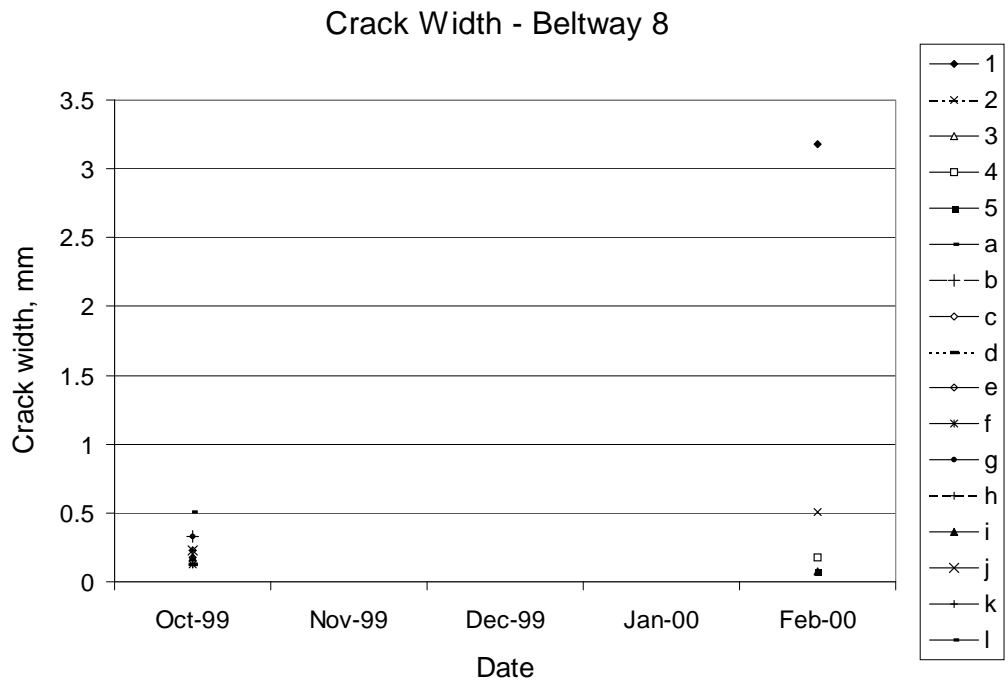
Figure 7.40 Crack width over time for Beltway 8 structure

Chapter 8: Significance of Field Results

In this chapter, the significance of the field observations presented in Chapter 7 is discussed.

From visual inspection, structures with severe exposure are located in areas of high rainfall (about 50 in. or 1.3 m per year), and have poorly-sealed joints causing water penetration at girder ends. Structures with mild exposure are located in areas of lower rainfall, and have with well sealed joints. The I-10 structure, US-90 structure, and Beltway 8 structure can be considered to have severe exposure; the Robinson Road structure has mild exposure.

The crack monitoring corroborates this. Figures 8.1 and 8.6 show the crack widths and change in crack widths determined from Demec gage measurements versus the age of the girders for the structures monitored.
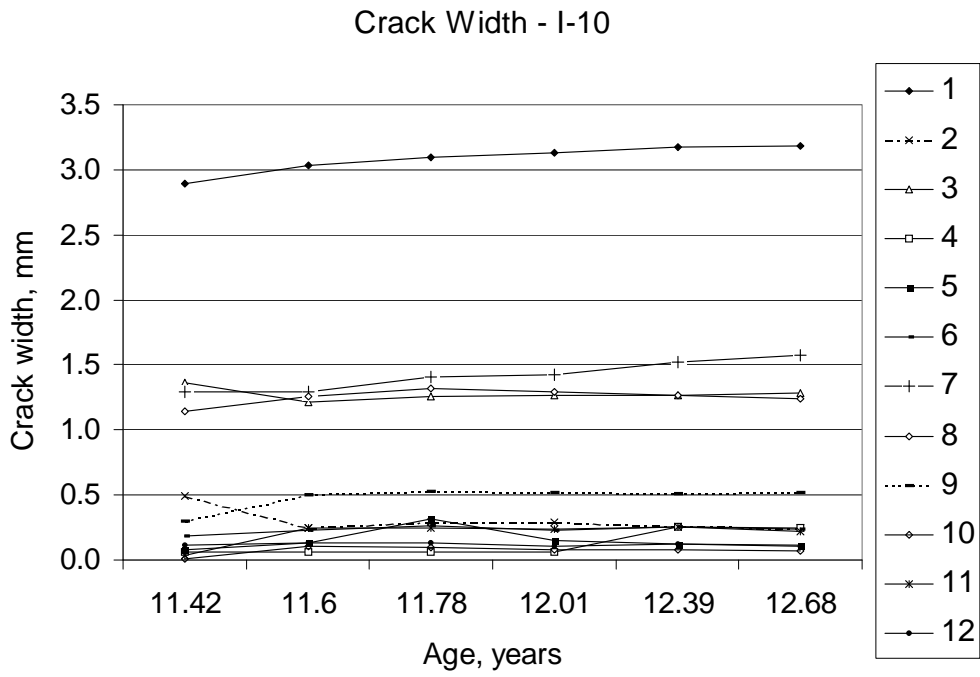
Figure 8.1 Crack width versus age of beam for I-10 structure
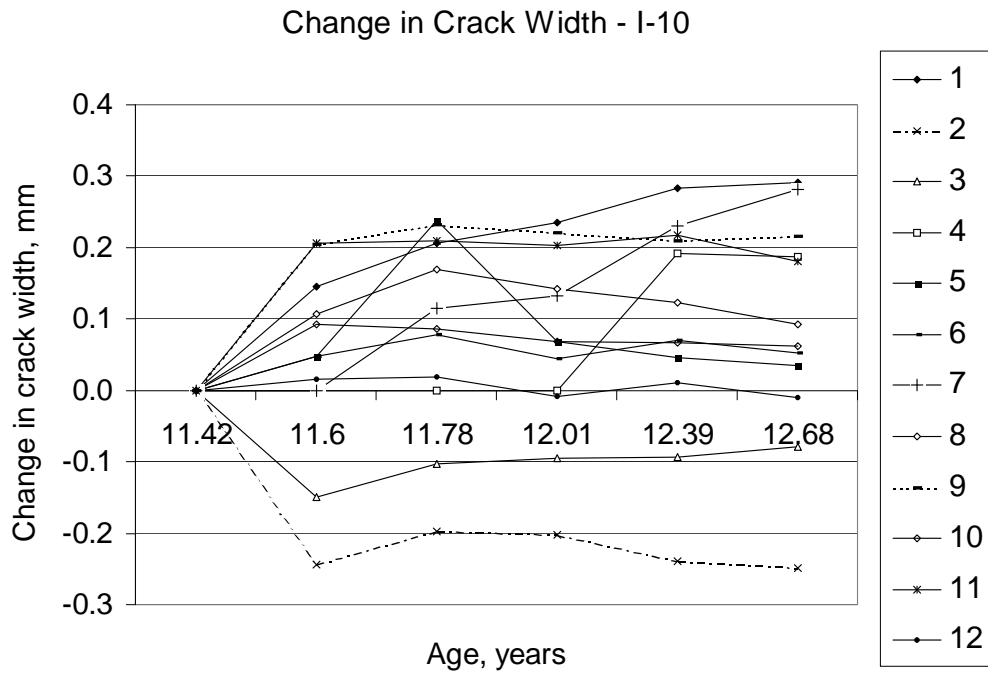
Figure 8.2 Change in crack width versus age of beam for I-10 structure
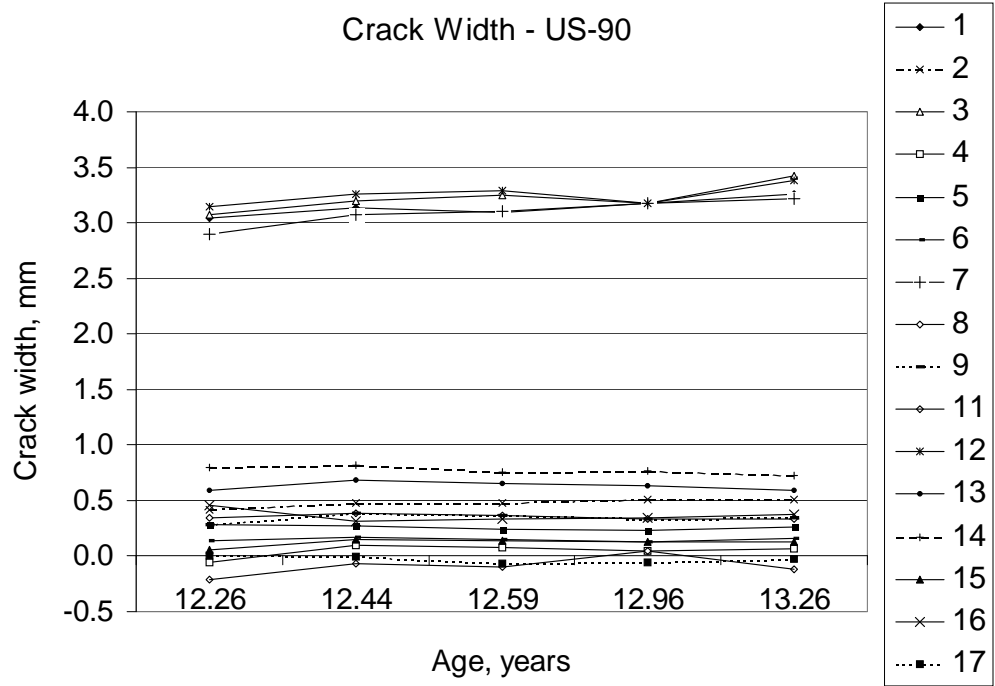
Figure 8.3 Crack width versus age of beam for US-90 structure
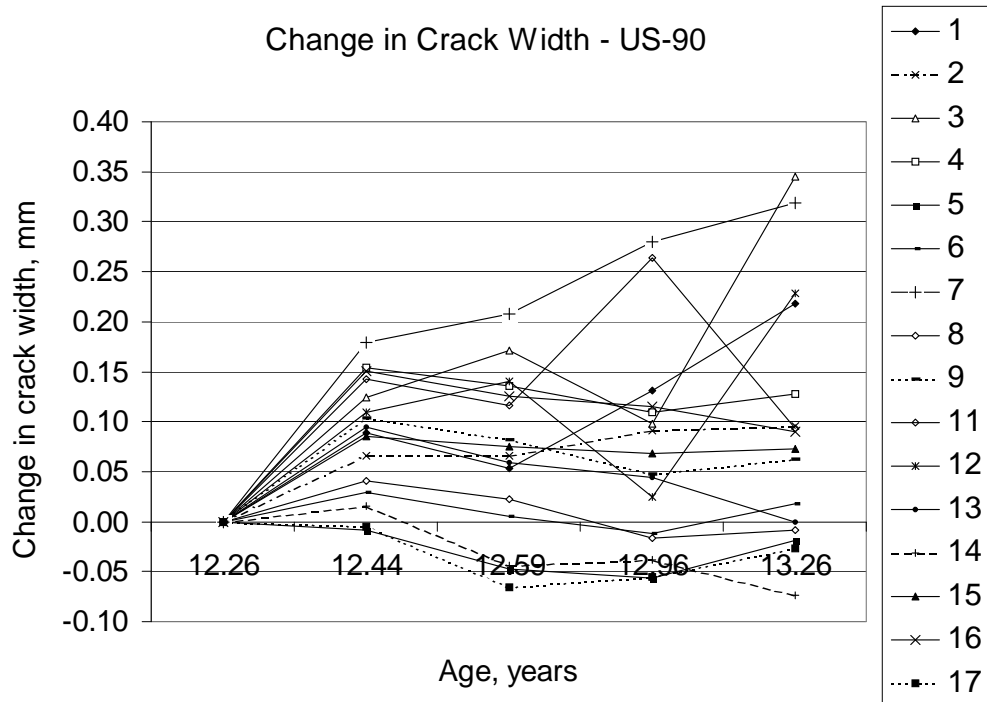
Figure 8.4 Change in crack width versus age of beam for US-90 structure
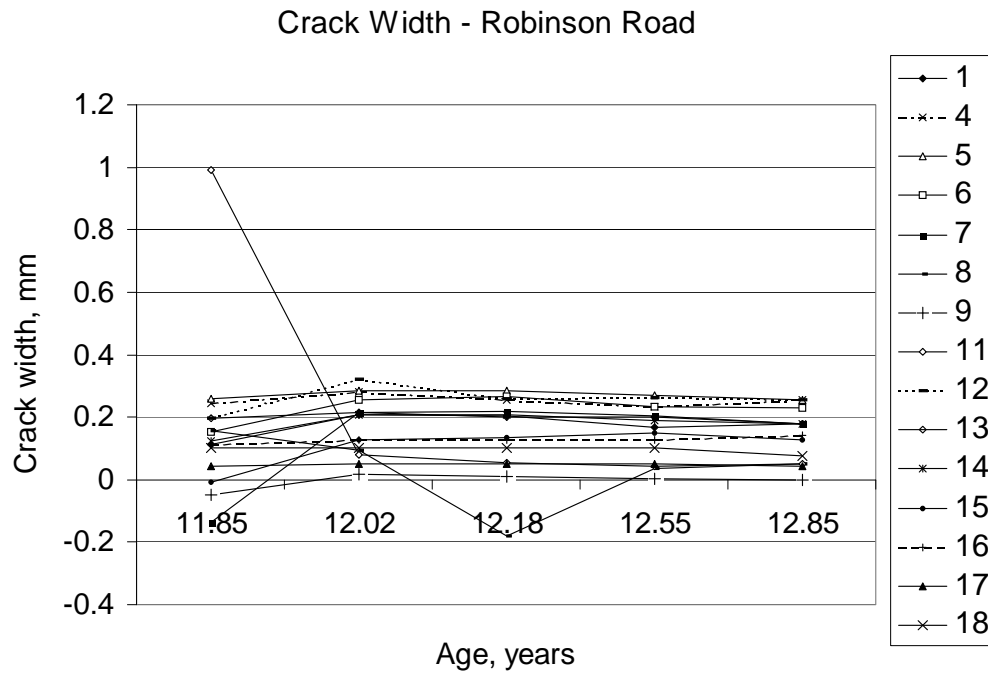
Figure 8.5 Crack width versus age of beam for Robinson Road structure
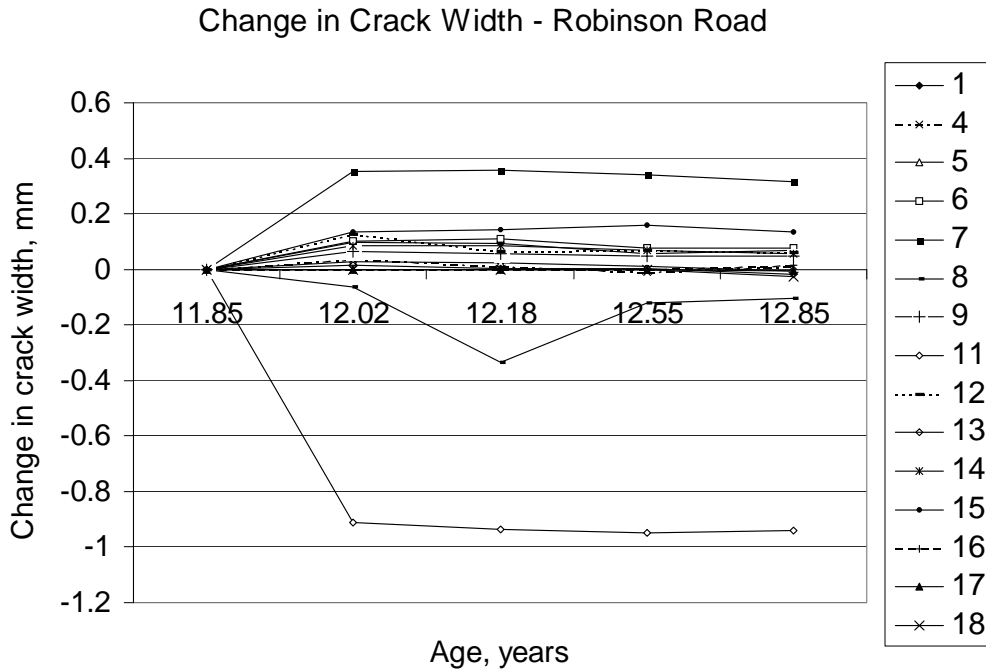
Figure 8.6 Change in crack width versus age of beam for Robinson Road structure

On the I-10 structure, cracks at Points 1, 3, 7 and 8 were significantly wider than others, and were all within 65 in. (1.65 m) of the ends of the girders. Cracks at Points 1 and 7, which consistently grew in width, were within 36 in. (0.91 m) of the ends. On the US-90 structure, cracks at Points 1, 3, 7 and 12 were significantly wider than others, and were all within 53 in. (1.35 m) of the ends of the girders. Only Point 1 consistently grew in width; it was 24 in. (0.61 m) from the ends. No significant crack growth was observed on the Robinson Road structure. Conclusions regarding the Beltway 8 structure cannot be made at this time.

All documented points where cracks grew significantly were near the ends of the girders, where they were subjected to a more extreme exposure.

Figure 8.7 shows the maximum crack widths of the field girders studied.

Maximum Crack Width of Field Girders
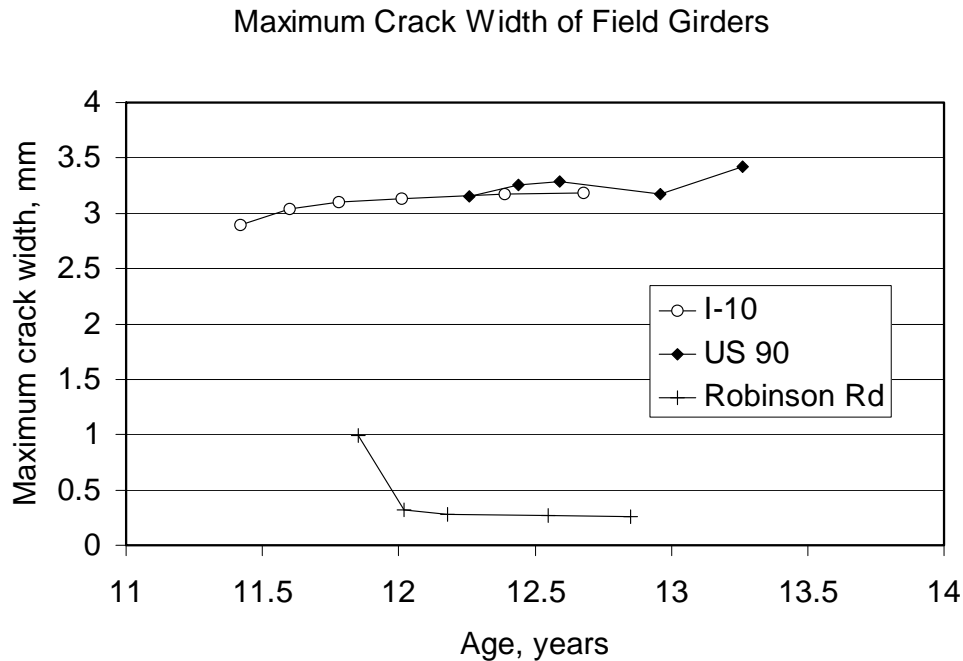
Figure 8.7 Maximum crack width of field girders

Effect of exposure on level of damage and rate of deterioration is evident. For a common age of 12.5 years, structures with severe exposure had maximum crack widths 13 times greater than structures with mild exposure. In structures with severe exposure, maximum crack widths continued to increase; in the structure with mild exposure, maximum crack widths were relatively stable.

For the age of structures monitored, some cracks stop growing, while others continue to grow. Looking at one crack could lead one to conclude that the

damage has stopped progressing. Looking at a different crack, however, could lead one to conclude that the damage is progressing rapidly. Visual inspection shows that most cracks that stopped growing are adjacent to a new crack that is growing. The rate of change in width of individual cracks may indicate that the rate of damage is increasing or decreasing. The plot of maximum crack width, however, along with visual inspection, confirms that overall damage is progressing.

Figure 8.8 compares the maximum crack widths of box and field girders versus their ages.

Maximum Crack Width of Box and Field Girders
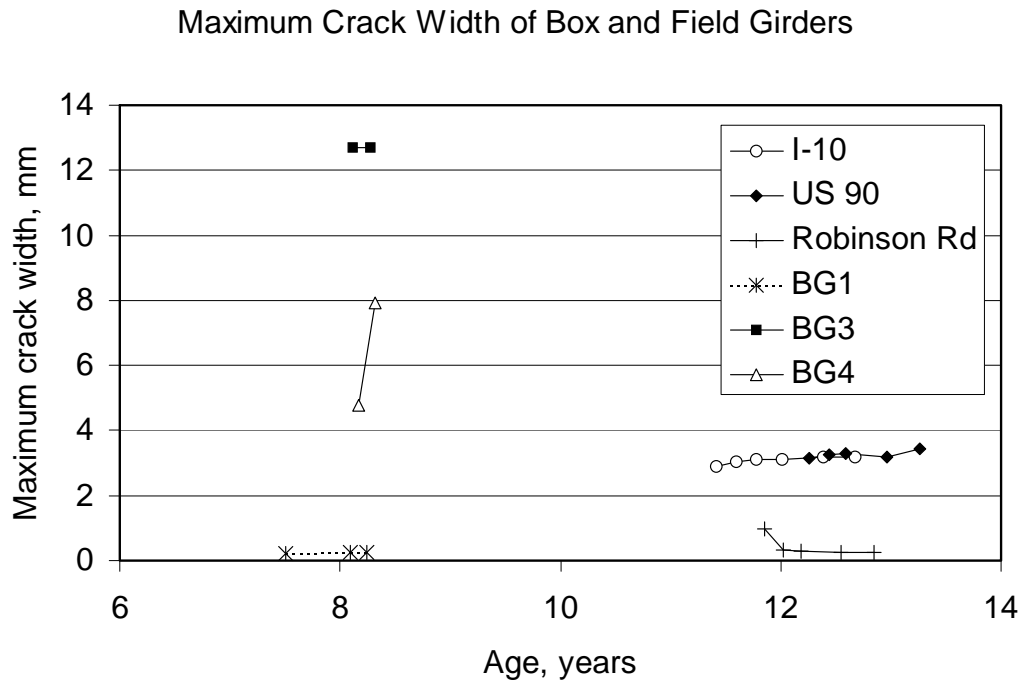
Figure 8.8 Maximum crack width of box and field girders

This shows similar trends in the structures with mild exposure and low inherent problems (BG1 and Robinson Road). Though the field girders with severe exposure show an increase in maximum crack width, they have lower maximum widths than the younger box girders studied in the laboratory. This might be explained by lower inherent problems. No structure or girder showed as drastic an increase in maximum crack width as BG4 (wetted). This is consistent with its severity of exposure. Although some field girders may have been located in areas with rainfall as severe as the wetting exposure of BG4, field girders would not generally have as severe exposure, because they would be protected to some degree by overlying slabs.

Chapter 9: Summary, Conclusions and Recommendations

9.1   SUMMARY

This thesis describes part of the work associated with TxDOT Study 1857 ("Structural Assessment of In-Service Bridges with Premature Concrete Deterioration"). That study comprises five tasks:

1) Field investigation of in-service structures and monitoring of laboratory specimens with premature concrete deterioration to develop damage indices over time;

2) Laboratory investigations of local effects of premature concrete deterioration on cores and slices removed from larger specimens;

3) Developing nondestructive evaluation techniques for determining damage indices that correlate with physical damage indices;

4) Developing petrographic techniques for identifying Delayed Ettringite Formation (DEF), alone or in combination with Alkali-Silica-Reaction (ASR); and

5) Using the damage indices developed to predict the capacity of large elements as a function of premature damage.

The particular focus of this thesis is using observations from in-service structures and laboratory specimens with premature concrete deterioration, along with core tests and large-scale tests of the laboratory specimens, to predict the capacity of a large element with any level of damage. The theoretical background of premature concrete deterioration, while not the focus of this thesis, is reviewed.

Large-scale tests to failure were conducted on 3 flexure-dominated and 3 shear-dominated specimens. Results from those tests were compared with tested compressive strength and elastic modulus of cores removed from the specimens, and with visual damage indices. Results were also evaluated in the light of observed damage to in-service structures, obtained over two years of field observation of 5 large TxDOT structures in different parts of Texas. These comparisons are used to propose approaches for evaluating the structural integrity of in-service structures with premature concrete deterioration.

9.2 CONCLUSIONS

1) Premature concrete deterioration is the result of an internal expansion mechanism in the concrete. Its basic causes are Delayed Ettringite Formation (DEF) and ASR (Alkali-Silica Reaction), which usually occur together in some degree. Both mechanisms are accelerated by exposure to water.

2) Premature concrete deterioration and the rate of increase of that deterioration can be described by various damage indices. The one used in this thesis, the summation of crack length times the square of crack width of each crack in a defined area (Figures 5.7 through 5.9 and Figures 8.1 through 8.8), showed promising results.

3) Premature deterioration in field and laboratory specimens can be directly correlated to the inherent susceptibility of the concrete itself, and to the severity of exposure. Susceptibility of the concrete itself may be correlated with high temperatures during curing and high levels of slowly

soluble sulfates in the clinker phase of the cement. Structures with non-susceptible concrete and mild exposure showed little or no premature concrete deterioration, while structures with susceptible concrete and severe exposure showed significant concrete deterioration. For example, in field and laboratory structures, premature concrete deterioration was concentrated in areas subjected to wetting. In the field, most wetting, and therefore most premature concrete deterioration, occurs at the ends of girders, which are exposed to water entering from joints in the roadway surface, and on the exterior faces of outside girders. Because of their massiveness (high ratio of internal volume to surface area), the solid end-blocks and intermediate diaphragms of concrete box girders often experience higher curing temperatures than the rest of the girder, and may therefore be inherently more susceptible to damage. In laboratory specimens, the most damage was observed in these areas.

4) Visual damage from premature concrete deterioration is correlated to reductions in the compressive strength and modulus of elasticity of concrete taken from affected regions. In particular, the modulus of elasticity of cores taken from damaged regions is far below the value that would be expected, even considering the reduced compressive strength (Figure 5.6). This uncharacteristically low modulus can perhaps be correlated with non-destructive evaluation techniques to develop faster techniques for quantifying premature concrete deterioration in the field.

5)   Reductions in compressive strength are very strongly correlated to damage indices (Figure 5.11).

6)   Reductions in compressive strength can be correlated to reductions in structural capacity, using strut-and-tie models. Structural capacity of prestressed girders can be governed by the tensile capacity of prestressing strand and by the bond of that strand to the surrounding concrete. It can also be governed by the compressive strength of the compression diagonals and compression chords comprising the strut-and-tie model. Gross strand slip, while not observed in these tests, is another possible failure mechanism. It is being investigated in a separate part of this overall study.

7)   Because the prestressed girders examined in this study showed premature concrete deterioration primarily at their ends, because they did not experience gross strand slip, and because they did not show much damage in the compression chord (top flange) in the region of maximum moment, their flexural capacity was not significantly lower than that predicted for undamaged girders.

8)   Because the prestressed girders examined in this study showed premature concrete deterioration near their ends, their shear capacity was reduced by 14% over that corresponding to otherwise identical but undamaged girders. This reduced capacity could still be predicted, however, using Equation 11-2 of ACI 318-99 (nominal shear capacity from V_c plus V_s), provided that reduced concrete strengths were used in that equation.

9)   Structures with high inherent susceptibility and severe exposure may experience enough of a decrease in compressive strength so that with overloads, shear-dominated failure may be possible near their ends.

9.3   RECOMMENDATIONS

1)   Crack widths in field structures and laboratory specimens should be monitored further, to document their trends over a longer time. Representative squares, similar to those of the laboratory specimens, should be used on the field girders to calculate and compare damage indices.   Those damage indices should be used to determine the relationship between maximum crack width and damage index for field girders. Curves like those of Figure 5.10 could be used for preliminary diagnostic purposes; structure-specific curves should be developed as needed.

2)   Field observations should be combined with NDE techniques to estimate the loss in compressive strength of particularly affected regions of structures in the field.

3)   To predict capacity of a field girder with premature concrete deterioration, two methods are recommended:

- Determine a damage index. Use that damage index with Figure 5.11 to estimate the compressive strength of the deteriorated concrete. Use that compressive strength with ACI Equation 11-2 to estimate the remaining shear strength.

- Remove cores from the most damaged areas (usually the ends) and test them in compression. Use that tested compressive strength with ACI Equation 11-2 to estimate the remaining shear strength.

The first method should be used as a preliminary assessment tool. For example, the latest maximum crack width measured on the US-90 structure is 0.13 in. (3.4 mm). Using Figure 5.10, this corresponds to a damage index of 13,097 (US customary units). Using Figure 5.11, the compressive strength is estimated as 5170 lb/in.[2]. If this is below the specified compressive strength, ACI Equation 11-2 should be used to estimate the reduced shear capacity of end regions of affected girders. If the shear capacity estimated in this way fell significantly below that used for design, compressive strengths could be verified by core tests.

4) If significantly reduced shear capacities were confirmed, measures should be developed and implemented to control the probability of shear failures. These could include rating the structure for a lower load than that for which it was originally designed.

5) Techniques should be investigated for delaying or preventing premature concrete deterioration in existing structures.

Appendix A: List of Structures in Texas with Premature Concrete Deterioration

Appendix B: Fabrication Details of Box Girders

Appendix C: Sketches of Crack Patterns of Box Girders

Appendix D: Calculations for Predicted Behavior of Laboratory Tests

The predicted ultimate capacity of flexure-dominated and shear-dominated specimens was calculated using a simplified model of the cross section (Figure D.1) and ACI 318-99. Equation numbers here refer to that document. Neglecting the solid blockouts, the cross-sectional area and the moment of inertia were calculated to be 688 in.^{2} and 21,950 in.^{4} respectively.
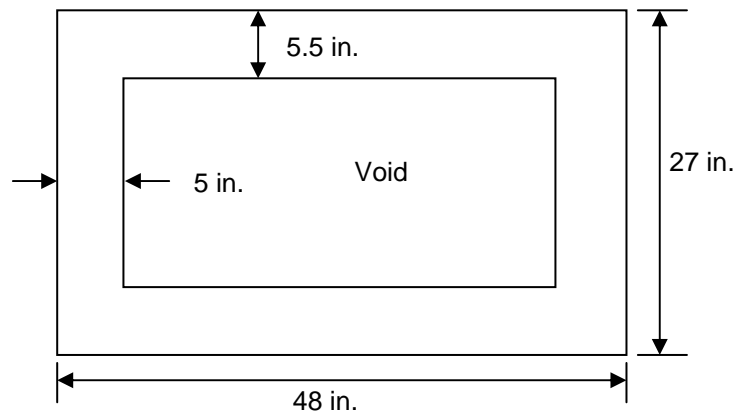
Figure D.1 Simplified box girder cross-section used for calculations

D.1   FLEXURE-DOMINATED TESTS

A simple span of 68.25 ft (Figure D.2) was used for analysis of the flexure-dominated specimens.
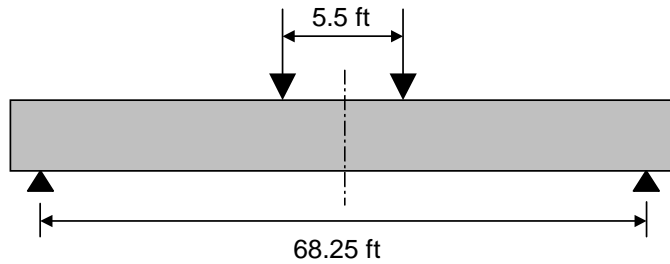
Figure D.2 Simple span of flexure-dominated specimens

Since BG1 was representative of the best material available, its core strengths were considered to determine the concrete strength to be used in the analysis. The compressive strength of cores taken from the endblock of BG1 was 7340 lb/in.^{2}, and the strength of the cores taken from the webs nearer to midspan was 10550 lb/in.^{2}. Because the damage near the ends of BG1 appeared to be limited to those areas, and because flexural behavior for such a long specimen is less affected by the end properties of the specimen, the concrete strength for analysis was assumed to be 10,000 lb/in.^{2}.

The stress in the bonded prestressed reinforcement is:

$$f_{ps} = f_{pu}\left\{1 - \frac{\gamma_p}{\beta_1}\left[\rho_p \frac{f_{pu}}{f_c'} + \frac{d}{d_p}(\omega - \omega')\right]\right\} = 257,400 \text{ lb/in.}^2 \qquad (18\text{-}3)$$

where

$$f_{pu} = 270,000 \text{ lb/in}^2$$

$$\gamma_p = 0.28 \text{ for low-relaxation prestressing steel}$$

$$\beta_1 = 0.65$$

$$\rho_p = \frac{A_{ps}}{bd_p} = \frac{30(0.153 \text{ in.}^2)}{(48 \text{ in.})(23.67 \text{ in.})} = 0.004$$

$$f_c' = 10,000 \text{ lb/in.}^2$$

$$d = 0 \quad \text{(distance to nonprestressed tension reinforcement).}$$

Assuming the prestressed reinforcemen takes all the tension, the maximum tensile force developed, is:

$$T = A_{ps} f_{ps} = 1,182,000 \text{ lb}$$

The compression carried by the compression reinforcement is:

$$C_s = 6(0.44 \text{ in.})(60,000 \text{ lb/in}^2) = 158,000 \text{ lb}$$

$$T = C = C_s + C_c$$

$$C_c = T - C_s = 1,023,000 \text{ lb} = 0.85 f_c' ba$$

$$a = 2.51 \text{ in.}$$

$$M_u = C_s(d_p - d') + C_c\left(d_p - \frac{a}{2}\right) = 26,230,000 \text{ lb-in.} = 2186 \text{ k-ft}$$

Ignoring the blockouts, the weight per foot of the girder is:

$$w = 0.150 \text{ k/ft}^3 (688 \text{ in}^2)\left(\frac{1 \text{ ft}^2}{144 \text{ in.}^2}\right) = 0.717 \text{ k/ft}$$

Considering the weight of the solid blockouts, the total weight of the box girder is approximately 54.5 kips. Using this estimate to determine an average self weight-per-foot gives:

$$w = \frac{54.5 \text{ k}}{68.25 \text{ ft}} = 0.799 \text{ k/ft}$$

A self-weight, w, of 0.75 k/ft was used for the static analysis (Figure D.3).

P/2

w

M_max

34.13 ft

P/2 + 25.59 k
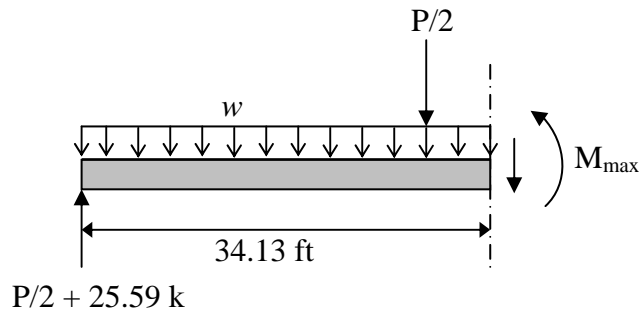
Figure D.3 Free body diagram of one half of flexure specimen

By setting M_{max} equal to M_n, a maximum expected capacity of 111.5 kips (111,500 lb/ 496 kN) was calculated.

Following the procedure outlined by Lin and Burns (1981), a moment-curvature analysis was conducted. Concrete strength of 10,000 lb/in.[2] and an effective prestress, f_{se}, of 160,000 lb/in^2 were assumed. Figure D.4 shows the moment-curvature relationship of the box section. Figures D.5 through D.18 plot curvature versus position along the girder for different loads, where 0 in. represents the support and 409.5 in. represents midspan. The moment-area method was used to calculate the deflection at midspan for each load. Figure D.19 shows the load-deflection curve developed with this procedure.

Moment-Curvature of Box Girder
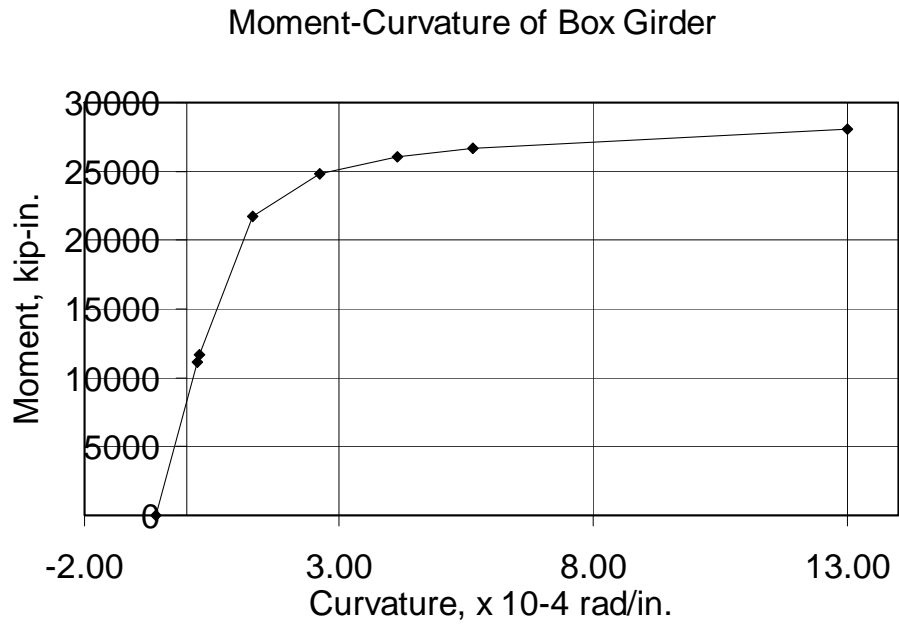
Figure D.4 Moment-curvature of box girders

Curvature vs. Position - P=0 kips
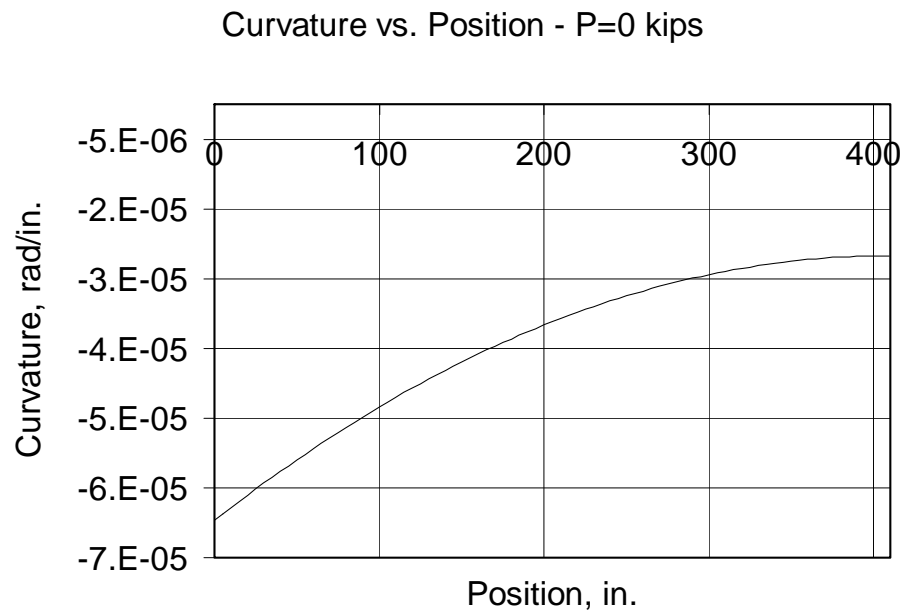
Figure D.5 Curvature along the girder at zero applied load

Curvature vs. Position - P=10 kips
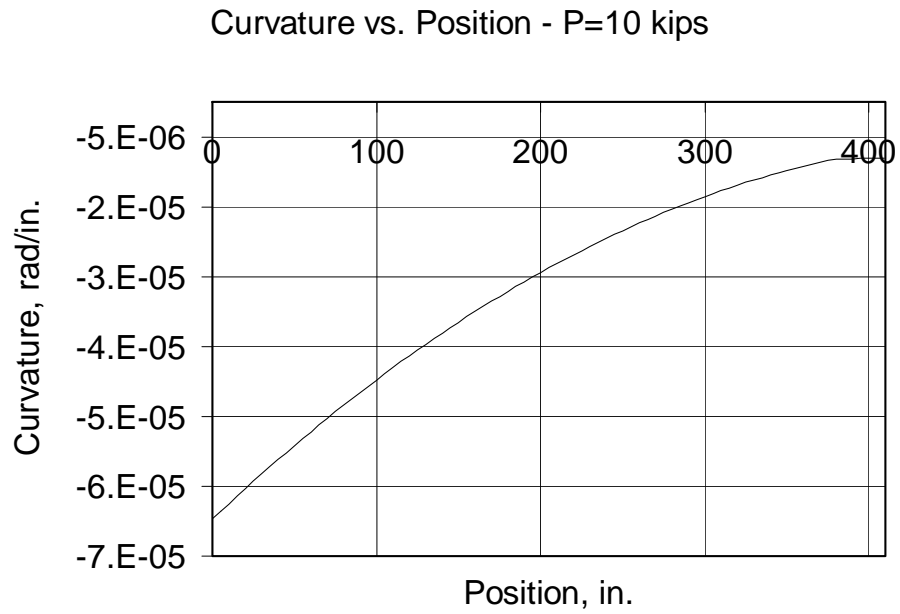
Figure D.6 Curvature along the girder at 10 kips applied load

Curvature vs. Position - P=20 kips
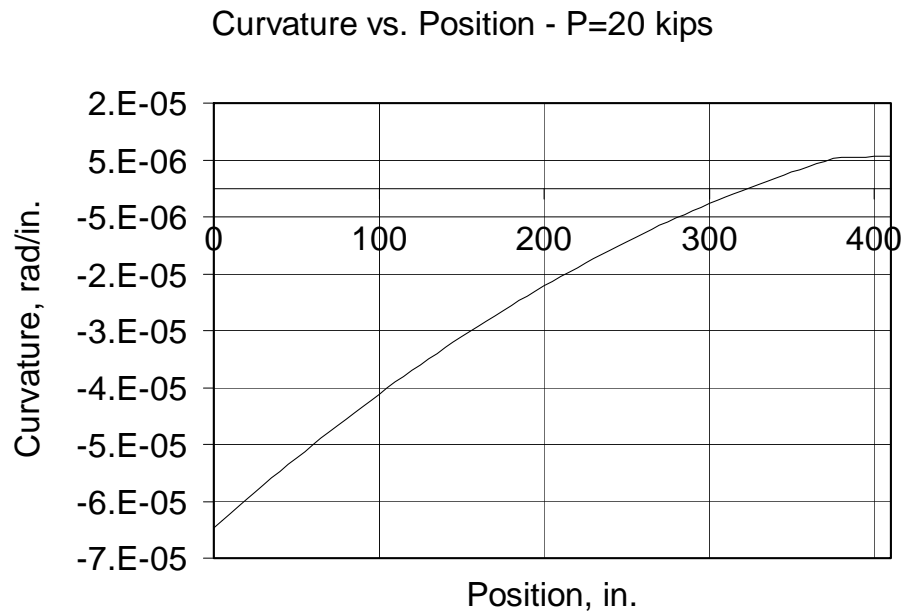
Figure D.7 Curvature along the girder at 20 kips applied load

Curvature vs. Position - P=30 kips

Curvature, rad/in.
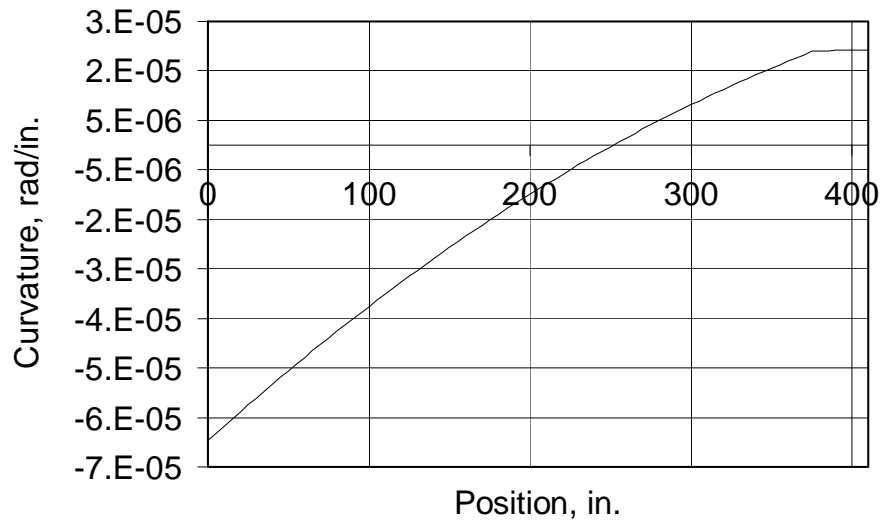
Position, in.

Figure D.8 Curvature along the girder at 30 kips applied load

Curvature vs. Position - P=40 kips

Curvature, rad/in.
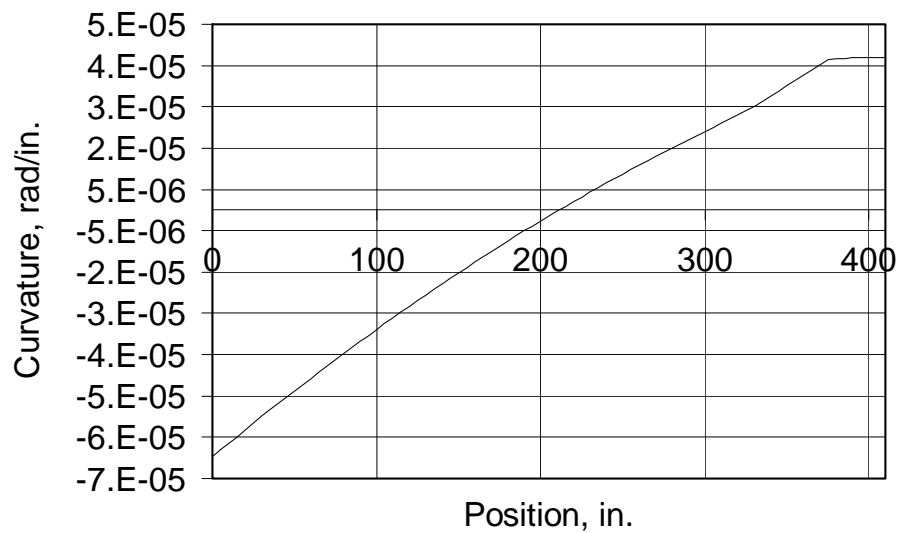
Position, in.

Figure D.9 Curvature along the girder at 40 kips applied load

Curvature vs. Position - P=50 kips

Curvature, rad/in. (y-axis)
Position, in. (x-axis)
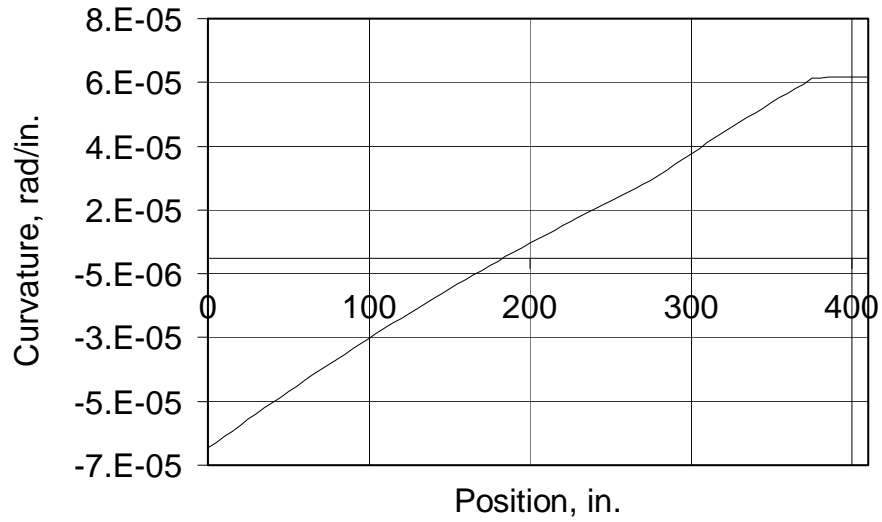
Figure D.10 Curvature along the girder at 50 kips applied load

Curvature vs. Position - P=60 kips

Curvature, rad/in. (y-axis)
Position, in. (x-axis)
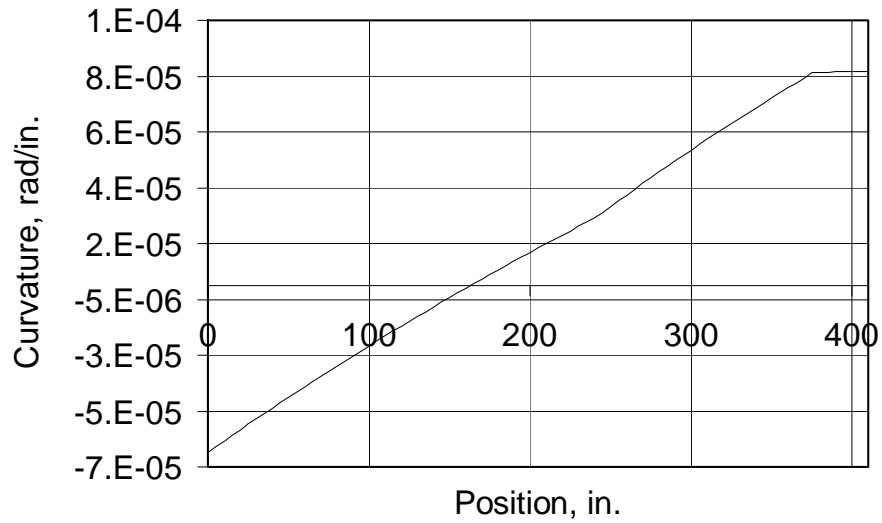
Figure D.11 Curvature along the girder at 60 kips applied load

Curvature vs. Position - P=70 kips
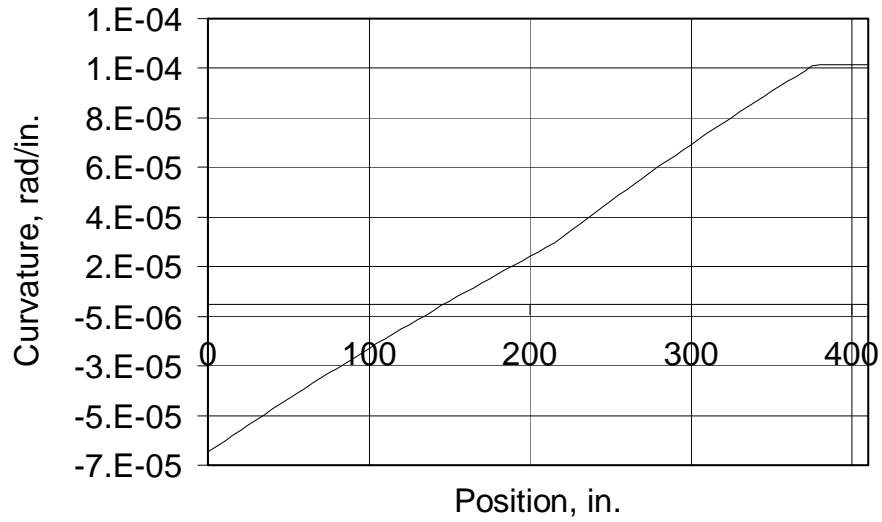
Figure D.12 Curvature along the girder at 70 kips applied load

Curvature vs. Position - P=80 kips
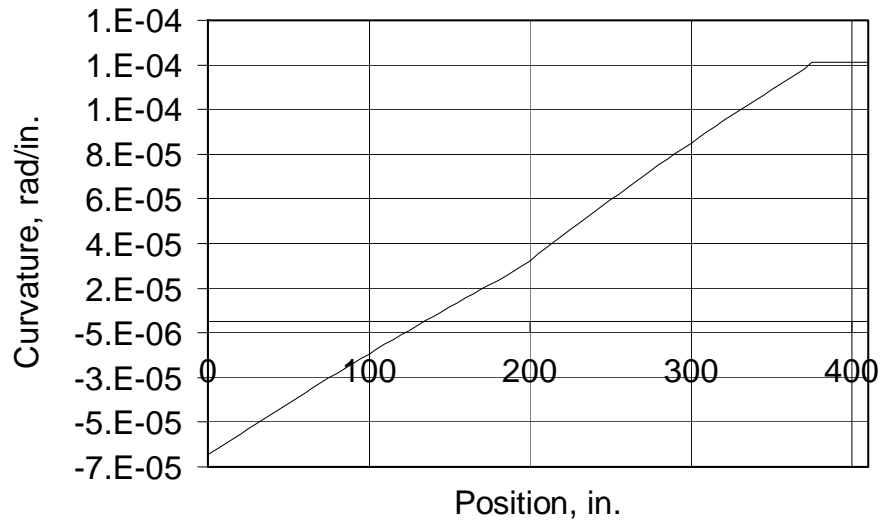
Figure D.13 Curvature along the girder at 80 kips applied load

Curvature vs. Position - P=90 kips
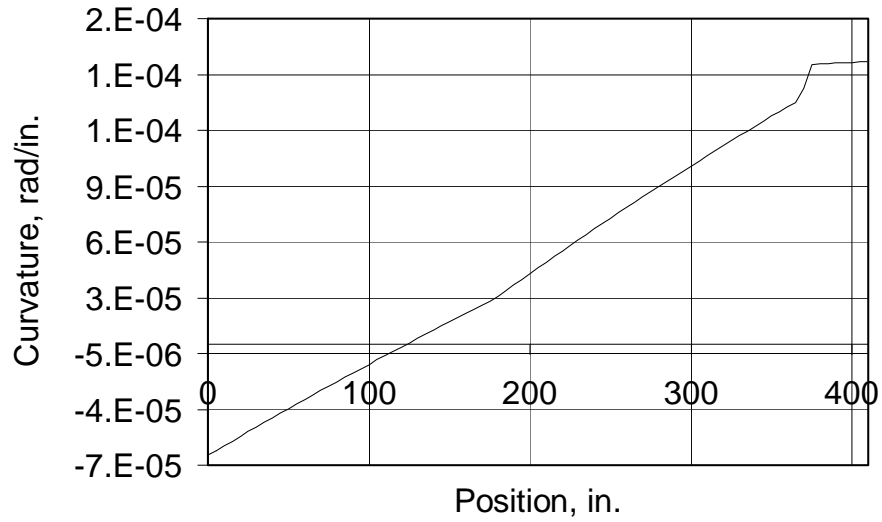
Figure D.14 Curvature along the girder at 90 kips applied load

Curvature vs. Position - P=100 kips
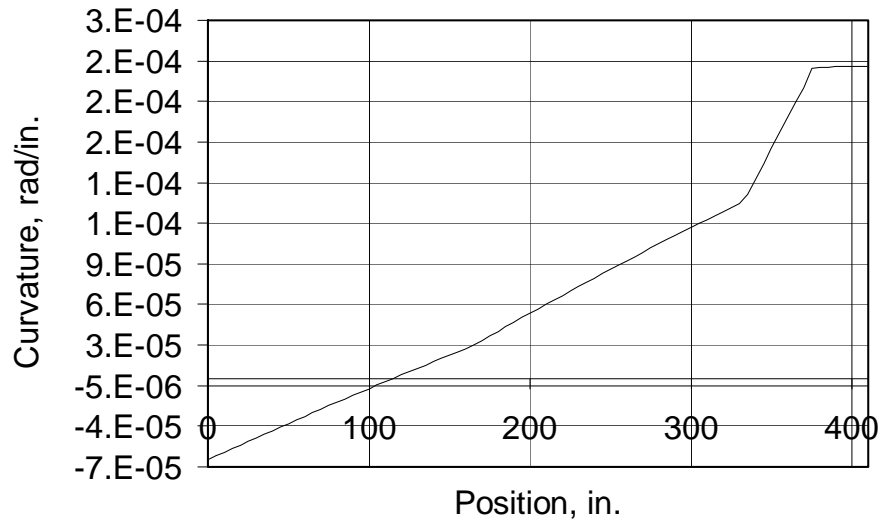
Figure D.15 Curvature along the girder at 100 kips applied load

Curvature vs. Position - P=110 kips
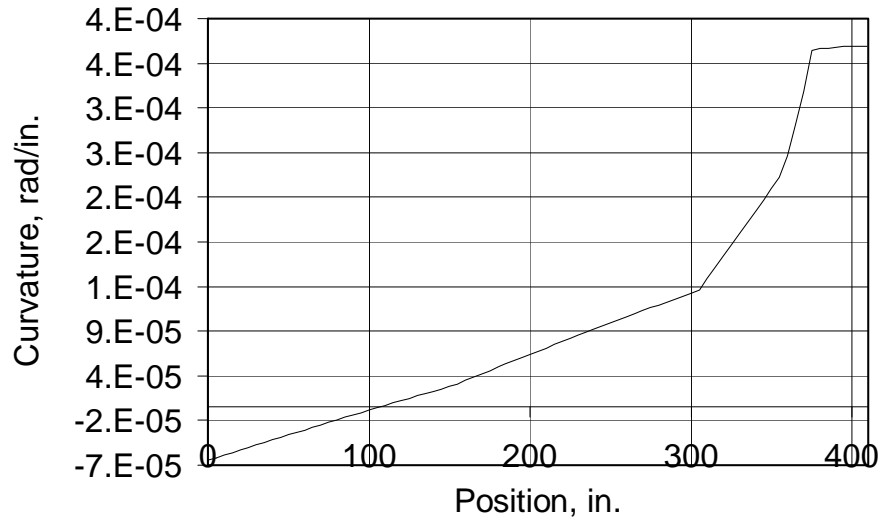
Figure D.16 Curvature along the girder at 110 kips applied load

Curvature vs. Position - P=120 kips
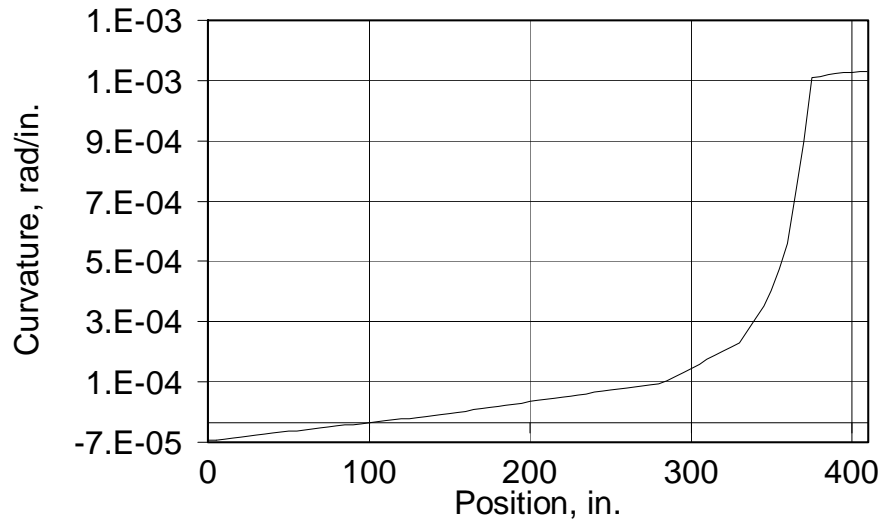
Figure D.17 Curvature along the girder at 120 kips applied load
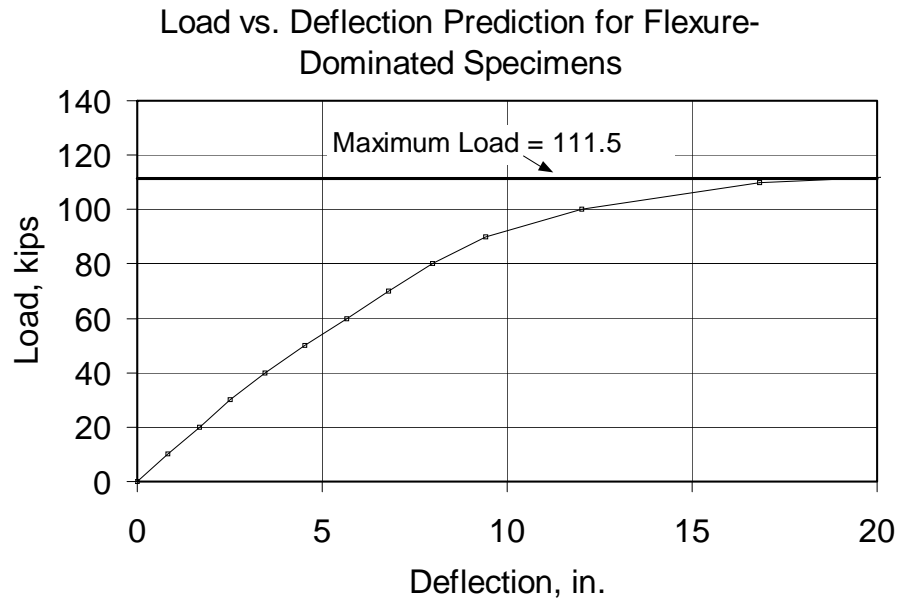
Figure D.18 Predicted load-deflection curve for flexure-dominated specimens

D.2 SHEAR-DOMINATED SPECIMENS

The simple spans and locations of load application for Case 1 and Case 2, shown in Figures 3.23 and 3.24, were used for analysis of the shear-dominated specimens. A lower concrete compressive strength, 6,000 lb/in.^{2}, was used to reflect the diminished integrity of the ends of the girders and the design strength. This value was confirmed by core tests (Section 4.4).

The nominal shear strength provided by concrete when diagonal cracking results from excessive principal tensile stress in the web is:

$$V_{cw} = \left(3.5\sqrt{f_c^{'}} + 0.3f_{pc}\right)b_w d + V_p = 140{,}000\,\text{lb} \qquad (11\text{-}12)$$

where

211

$$f_{pc} = \frac{f_{se}}{A} = \frac{30 \text{ strands} \left(0.153 \text{ in.}^2\right)\left(160 \text{ lb/in.}^2\right)}{688 \text{ in.}^2} = 1067 \text{ lb/in.}^2 \text{ (compressive}$$

stress in concrete (after allowing for all prestress losses) at centroid of cross section resisting externally applies loads or at junction of web and flange when the centroid lies within the flange, lb/in.^{2})

$b_w = 10$ in. (web width)

$d = 23.7$ in. (distance from extreme compression fiber to centroid of longitudinal tension reinforcement, but need not be less than 0.80h for circular sections and prestressed members)

$V_p = 0$ (vertical component of effective prestress force at section)

Using #4 stirrups spaced at 6 in. on center, the nominal shear strength provided by shear reinforcement is:

$$V_s = \left(\frac{A_v f_y d}{s}\right) = \left(\frac{0.4 * 60{,}000 \text{lb/in.}^2 * 23.67 \text{in.}}{6 \text{ in.}}\right) = 94{,}700 \text{ lb} \qquad (11\text{-}15)$$

The nominal shear strength of the box girders is:

$$V_n = V_c + V_s = 235{,}000 \text{ lb} \qquad (11\text{-}2)$$

Including the self-weight of the girder of 0.75 k/ft for the static analysis, the maximum calculated load was 308.0 kips (1370 kN) for Case 1, and 319.7 kips (1420 kN) for Case 2. Figures D.19 and D.20 show the moment and shear diagrams for Case 1; Figures D.21 and D.22 show the moment and shear diagrams for Case 2. In both cases, the maximum moment corresponding to the

maximum load calculated for shear failure was much less than the moment
capacity calculated in Section D.1.

Shear Diagram for Case 1
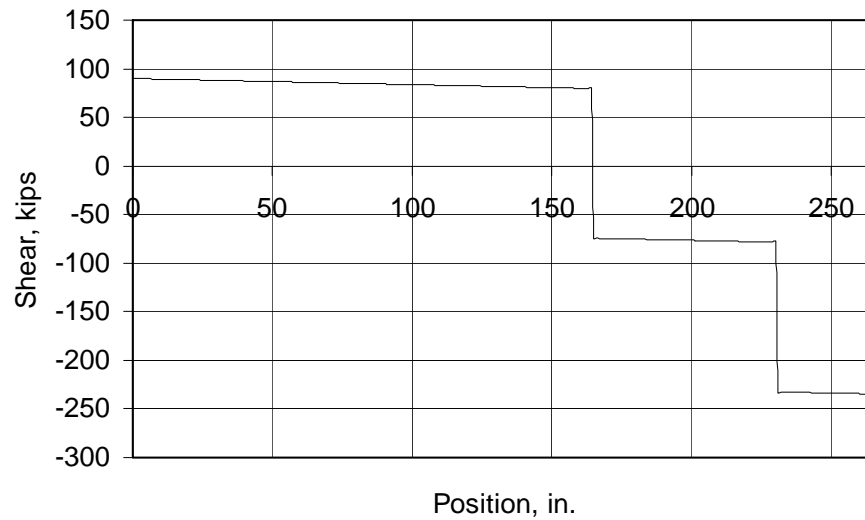
Figure D.19 Shear diagram for Case 1 loading

Moment Diagram for Case 1
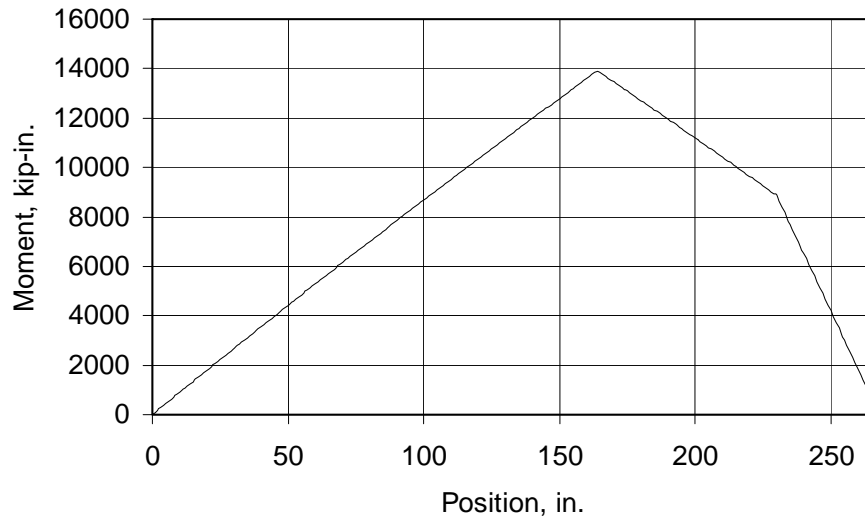
Figure D.20 Moment diagram for Case 1 loading

Shear Diagram for Case 2
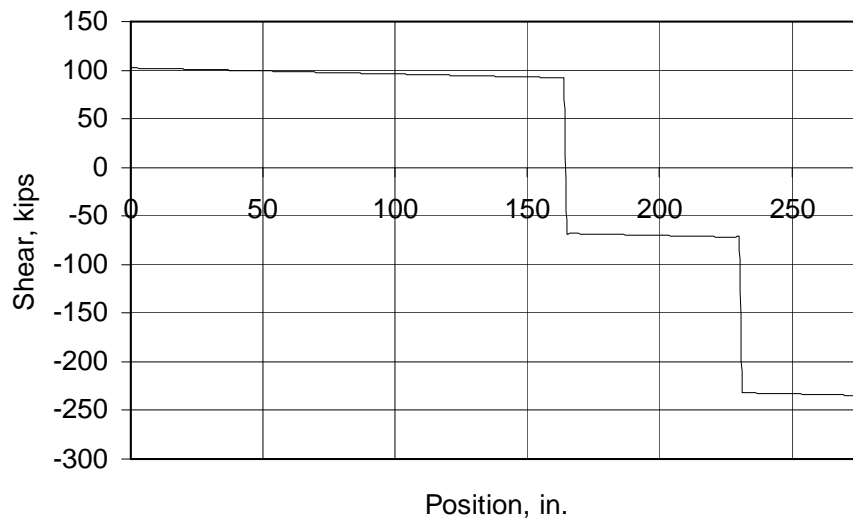
Figure D.21 Shear diagram for Case 2 loading

Moment Diagram for Case 2
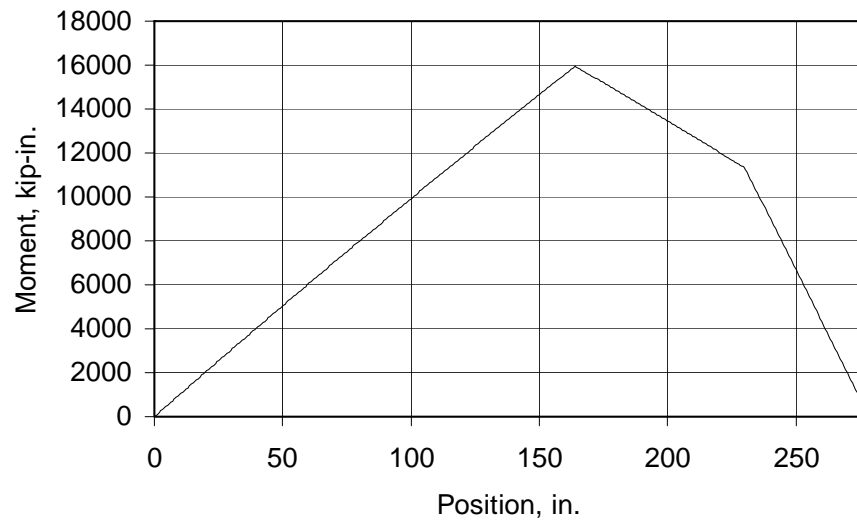
Figure D.22 Moment diagram for Case 2 loading

Appendix E: Data from Flexure-dominated Tests

BG1F

BG1F - North Bearing Pad
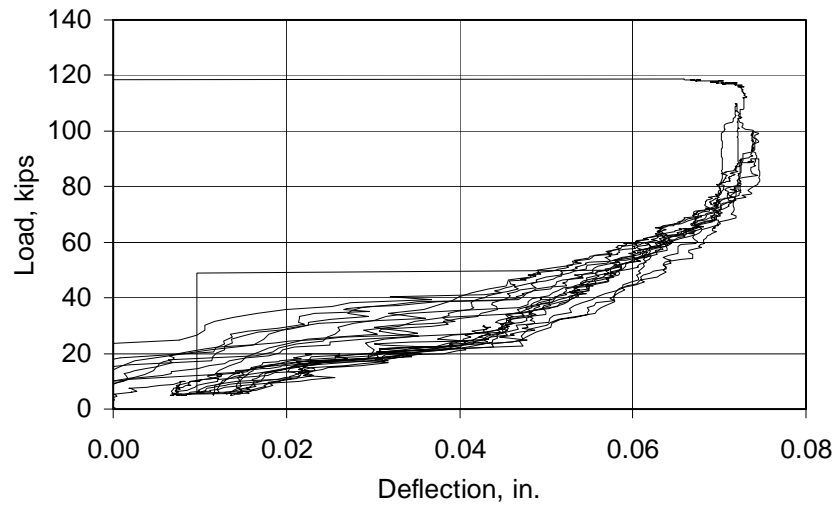
BG1F - South Bearing Pad
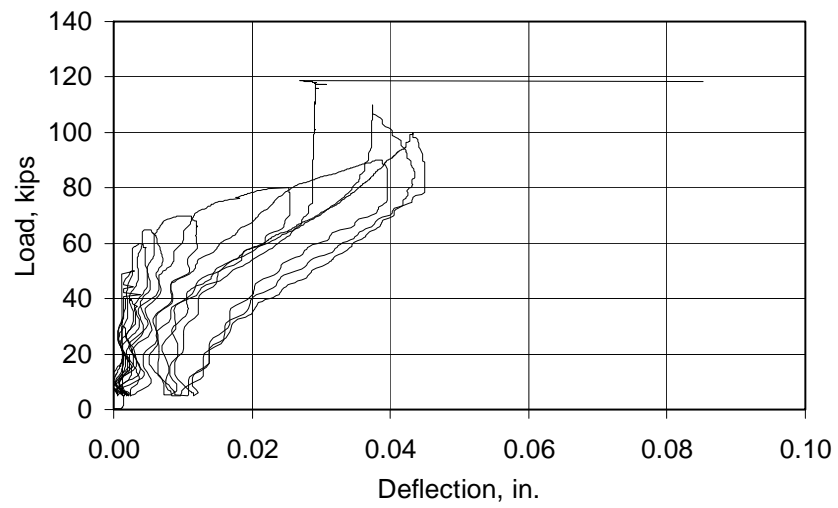
BG1F - P1
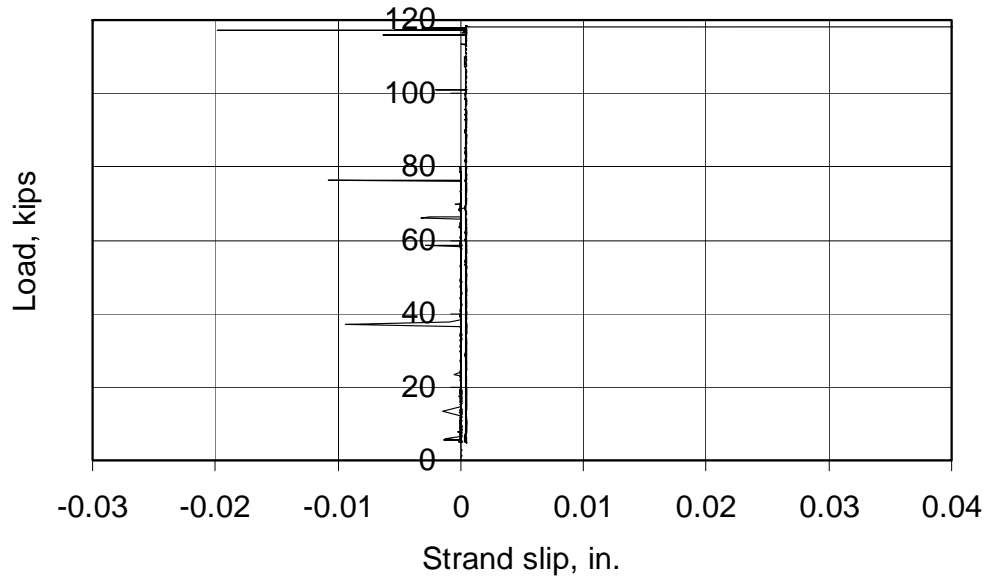
BG1F - P2

BG1F - P3

BG1F - P4

218

BG1F - P5

BG1F - P6

219
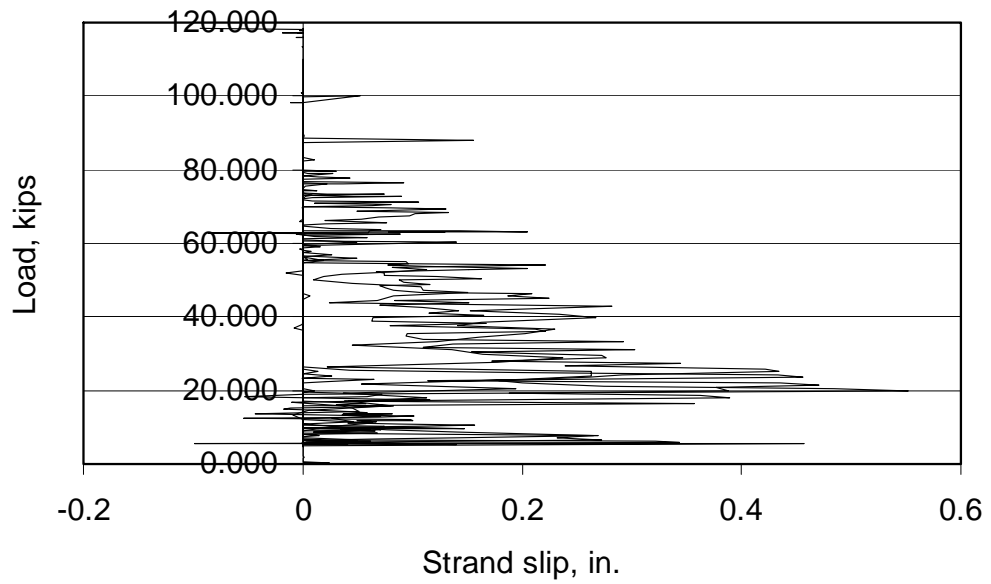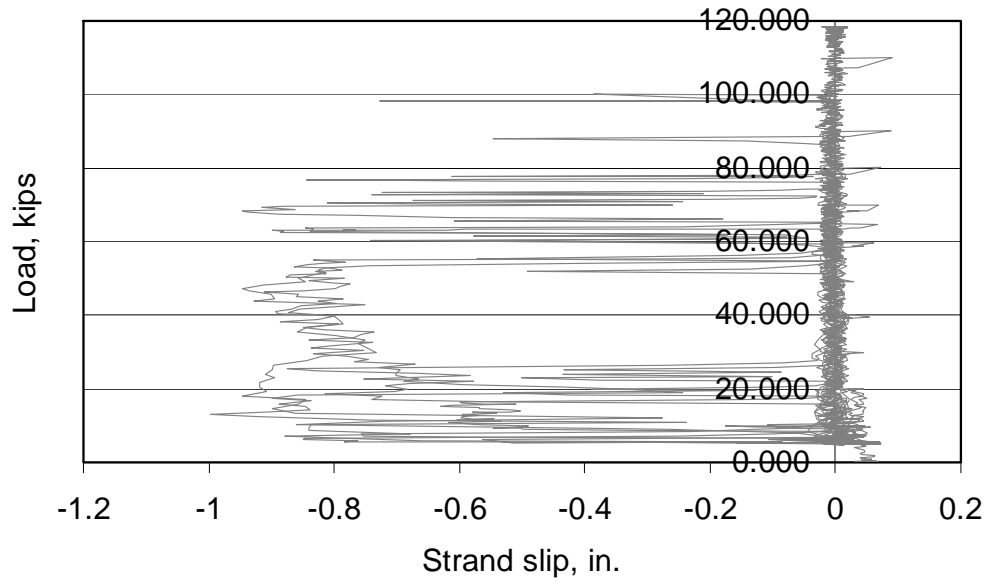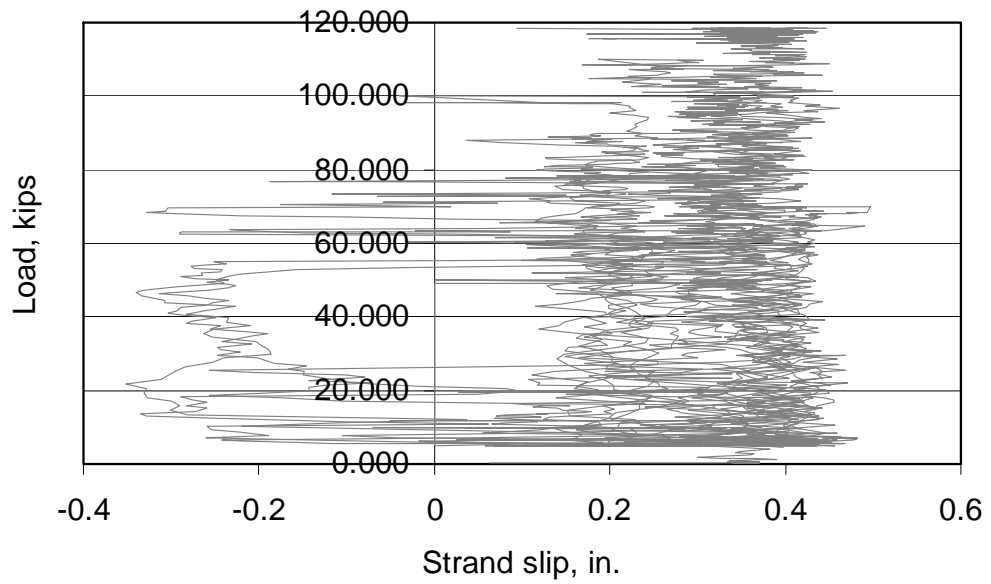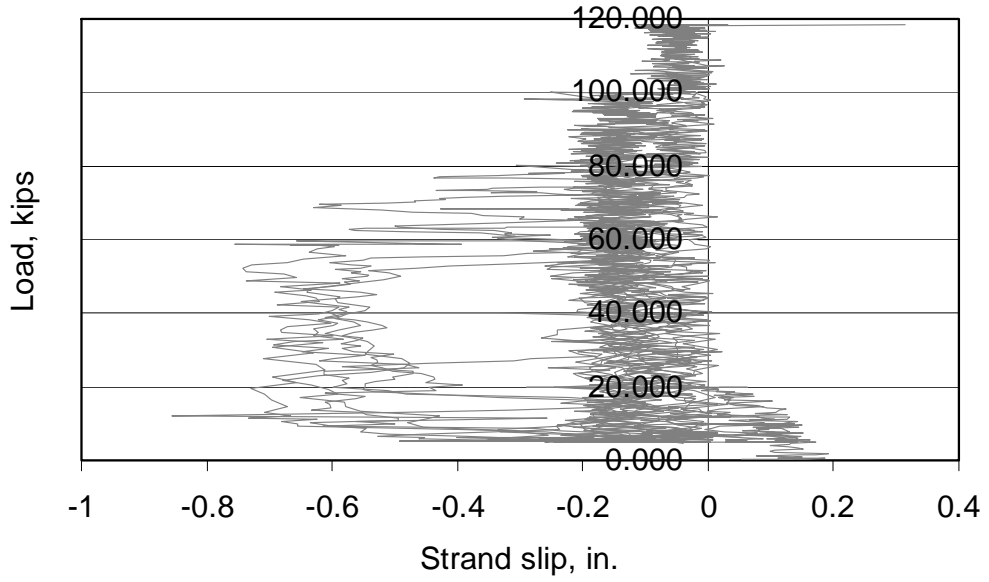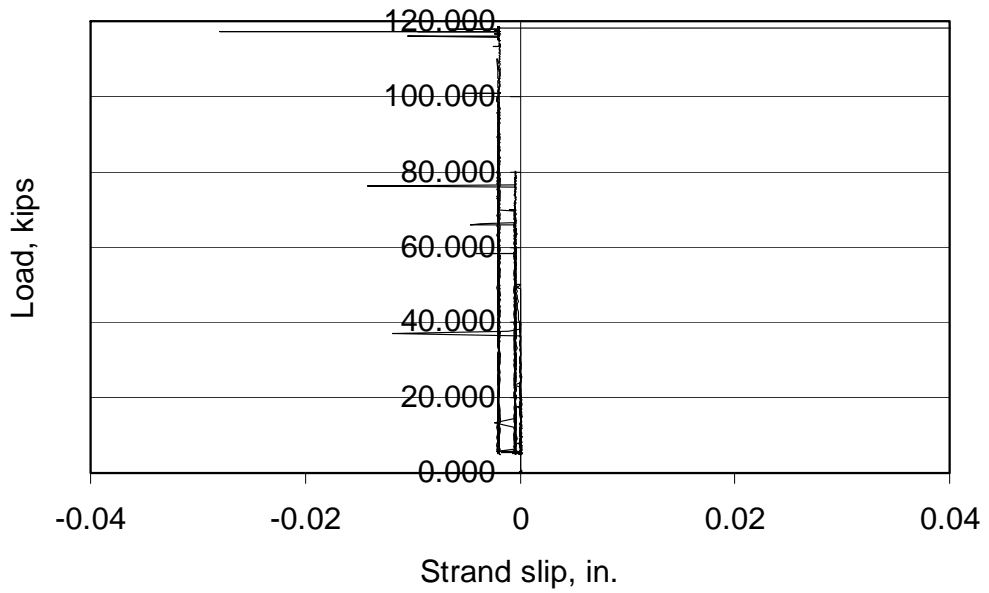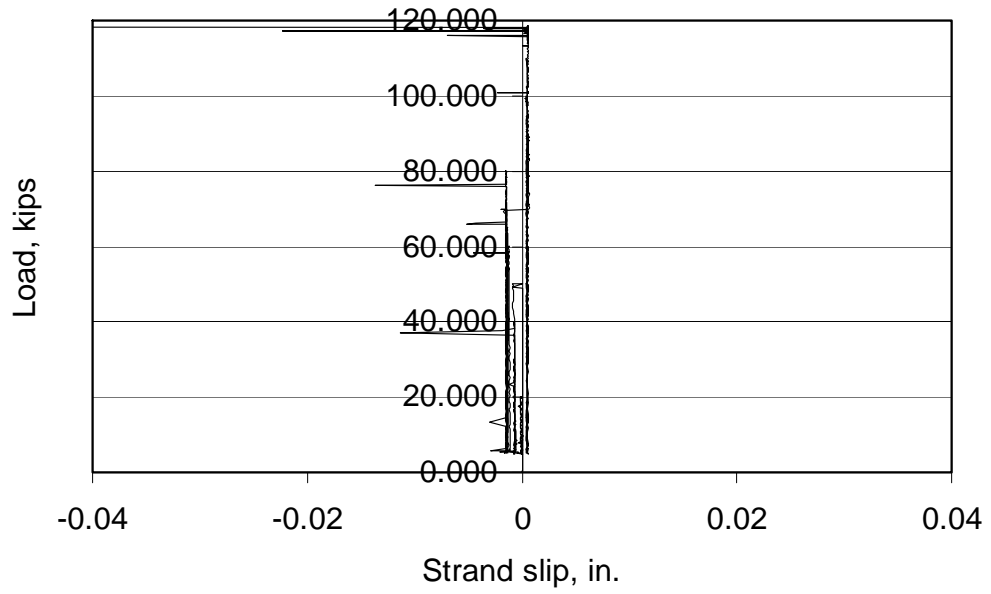
BG1F - P7

BG1F - P8

BG1F Strain Gradient
1 ft south of midspan

Distance from bottom, in.

- 20 kips
- 40 kips
- 60 kips
- 80 kips
- 100 kips
- 118.6 kips

Microstrain

-3000   -2000   -1000   0   1000   2000   3000

25

20

15

10

5

0

BG1F - C1

Load, kips

120.000

100.000

80.000

60.000

40.000

20.000

0.000

Change in crack width, in.

-0.08   -0.06   -0.04   -0.02   0.000   0.02
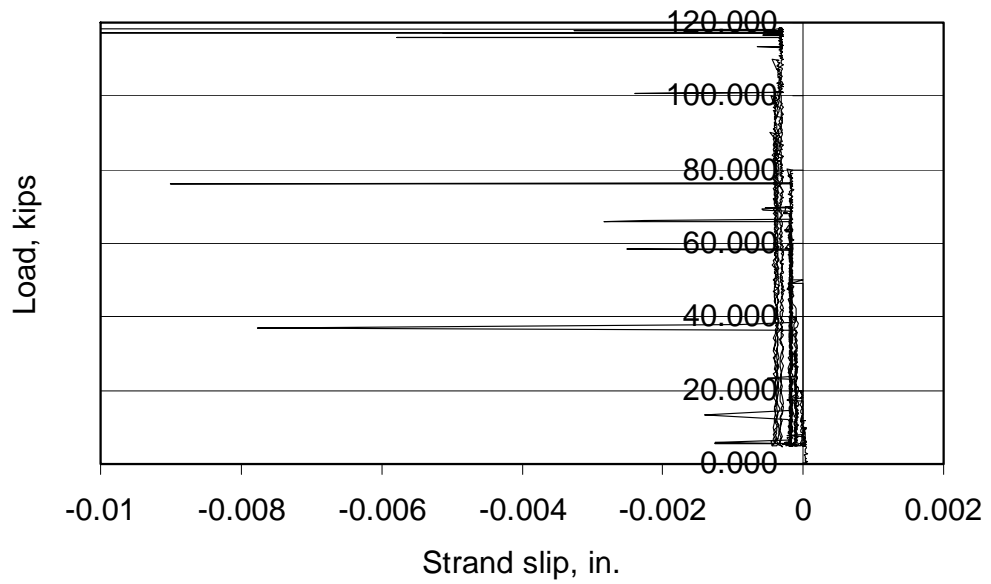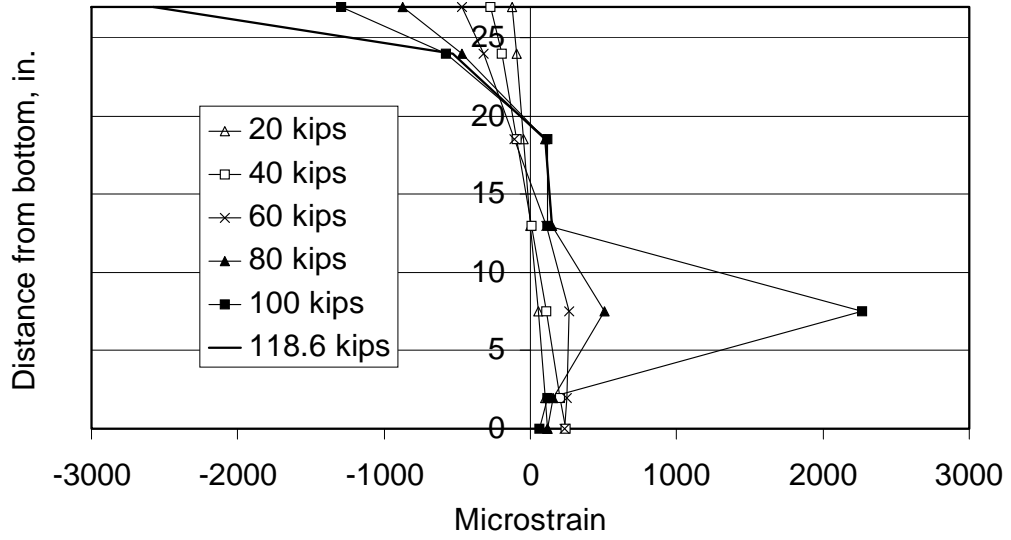
221
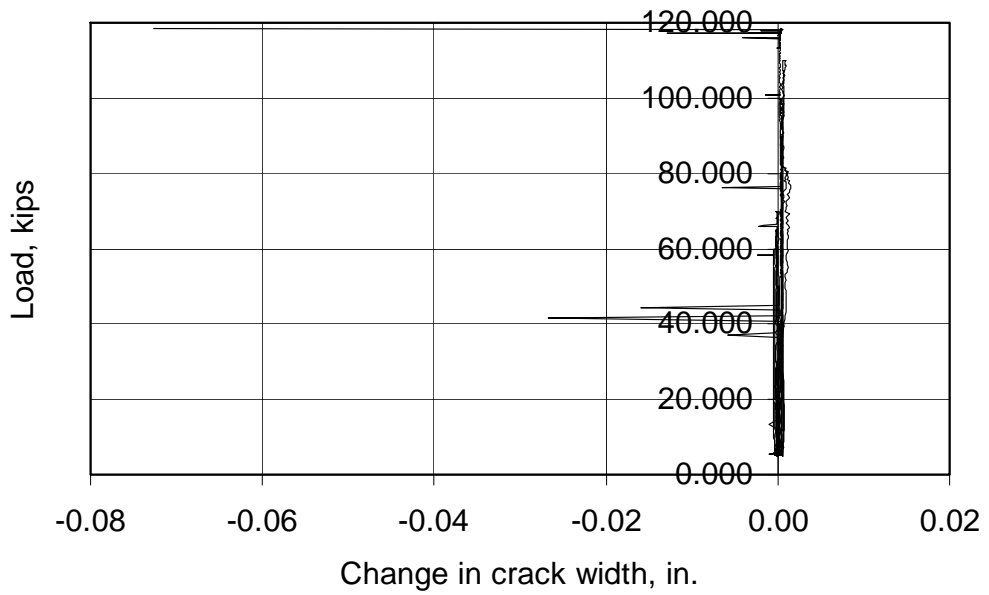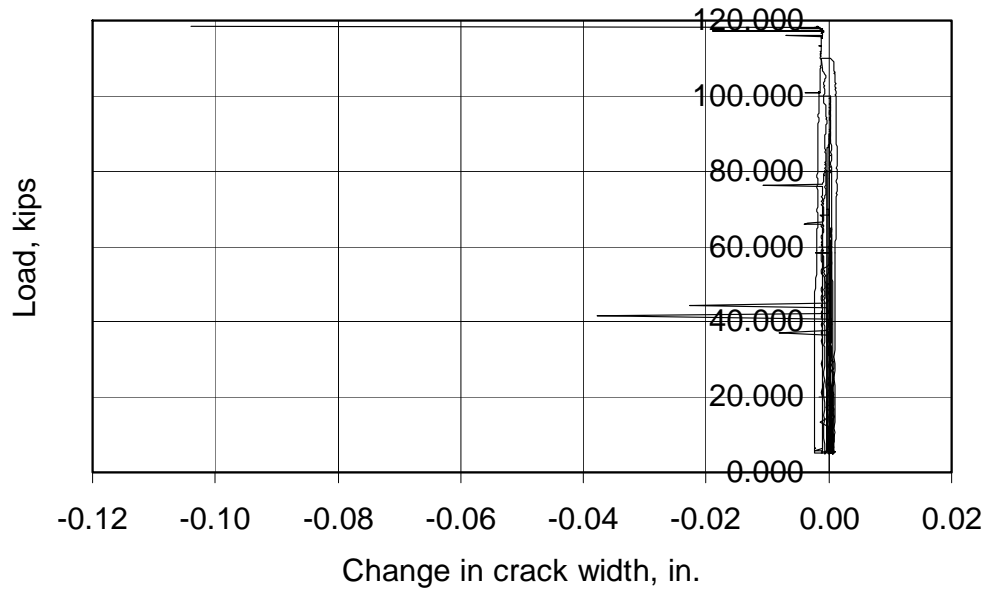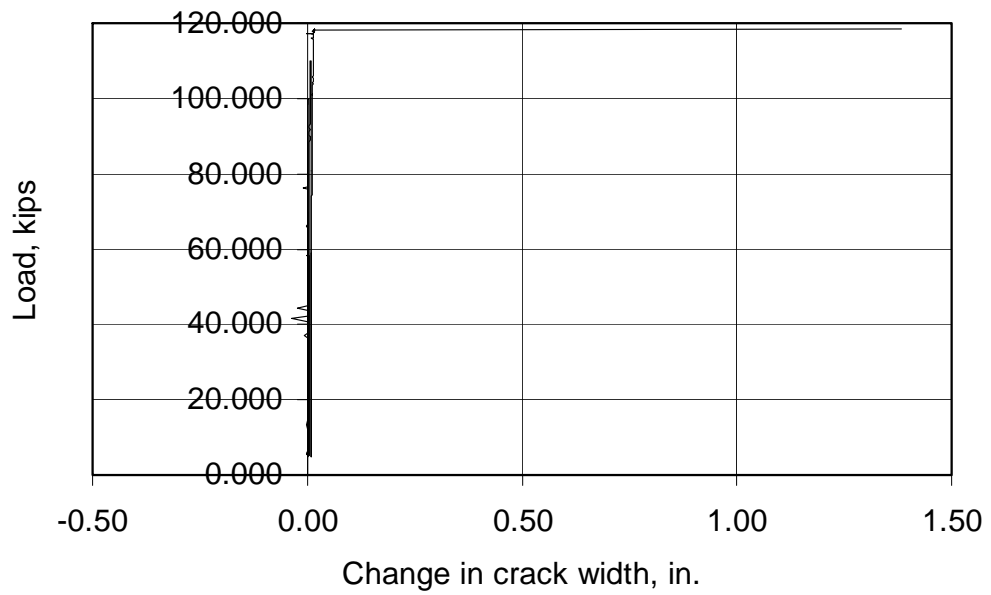
BG1F - C2
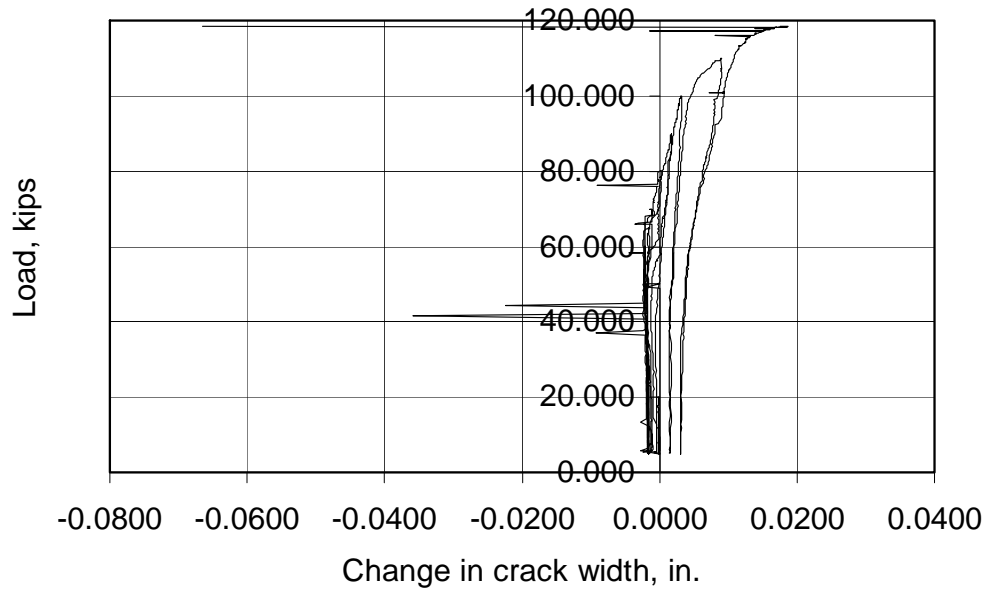
BG1F - C3

BG1F - C4

BG1F - C5
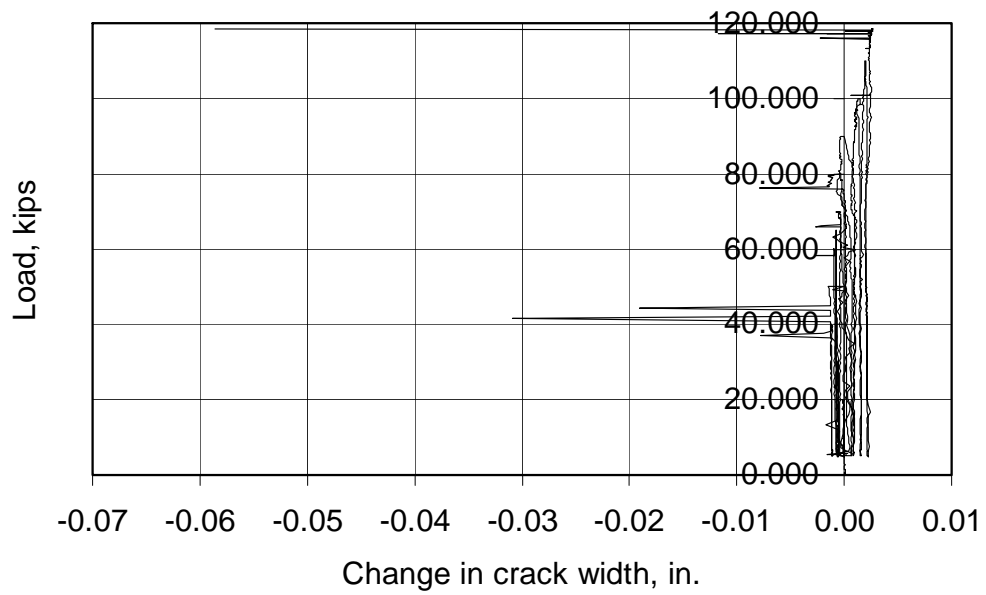
BG1F - C6
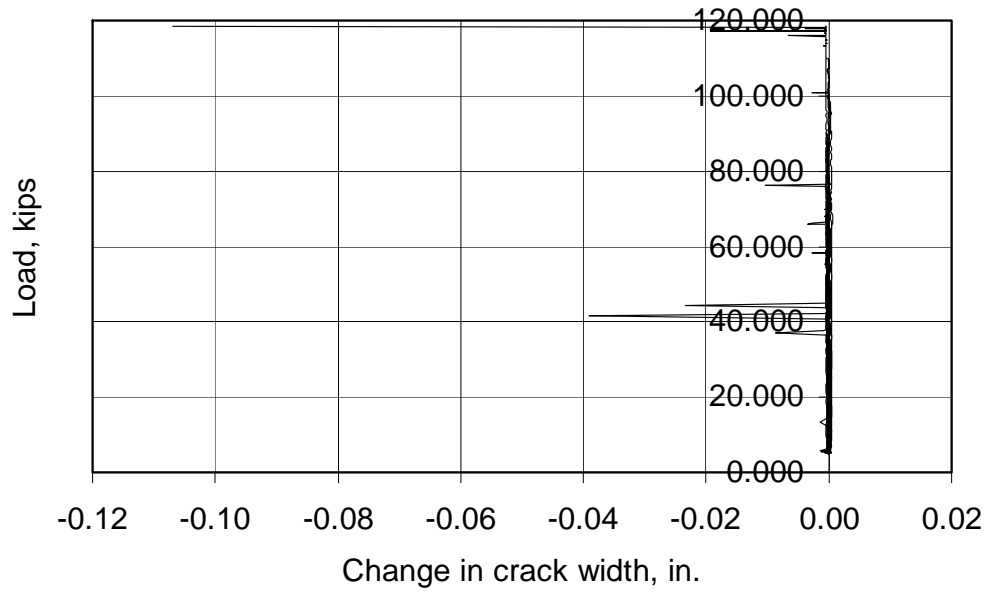
BG1F - C7
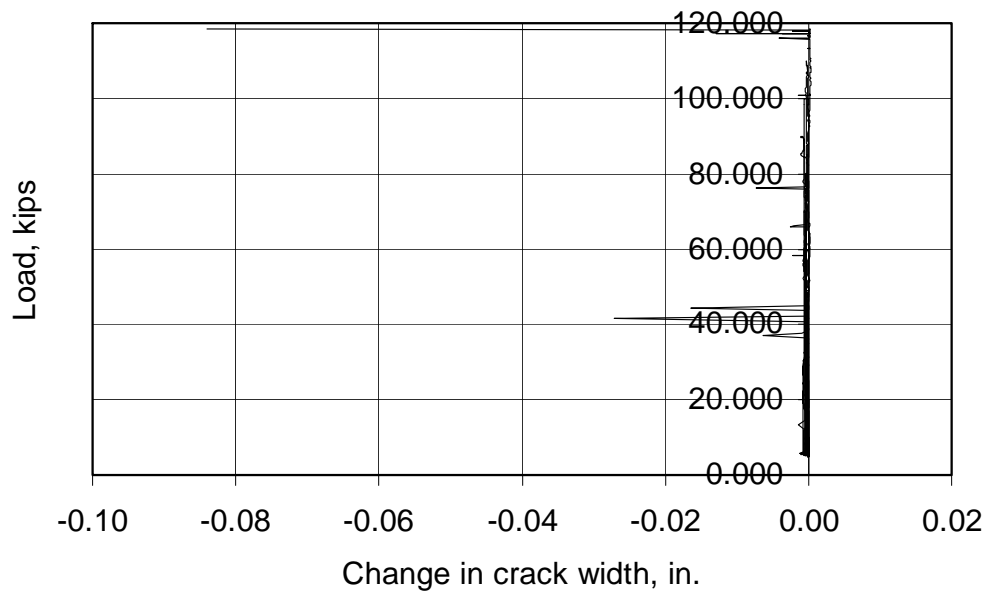
BG2F

BG2F - North Bearing Pad
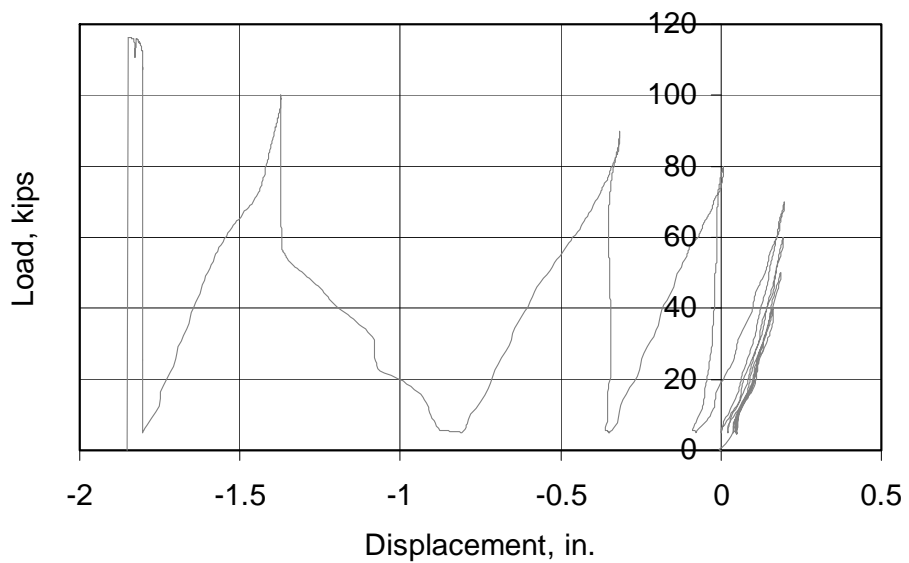
BG2F - South Bearing Pad

225

BG2F - P1

BG2F - P2

226
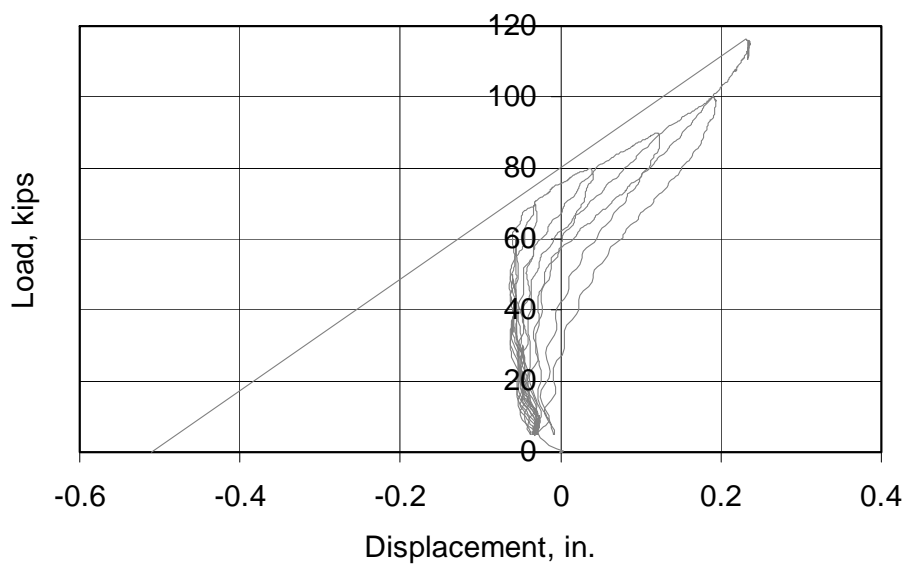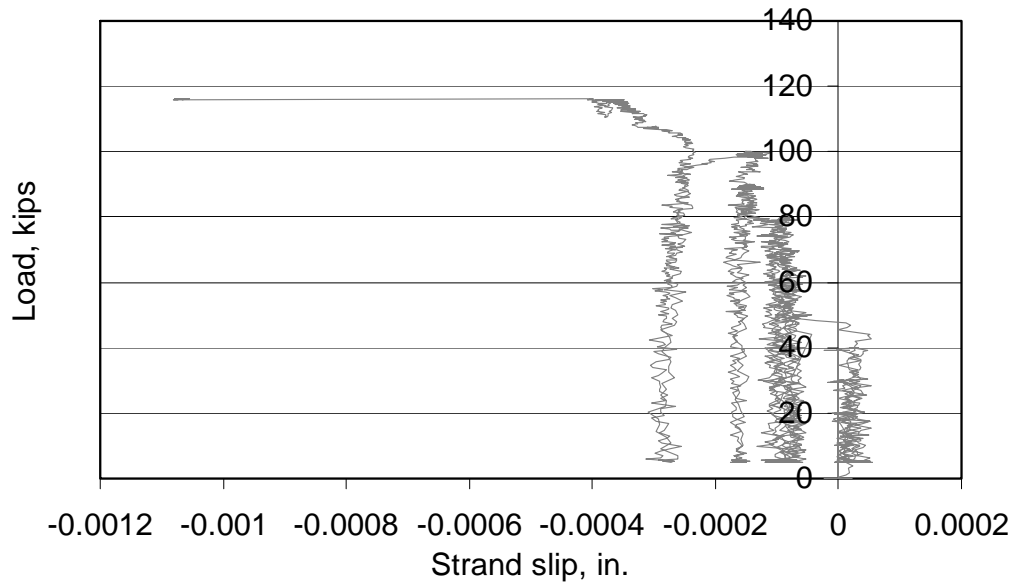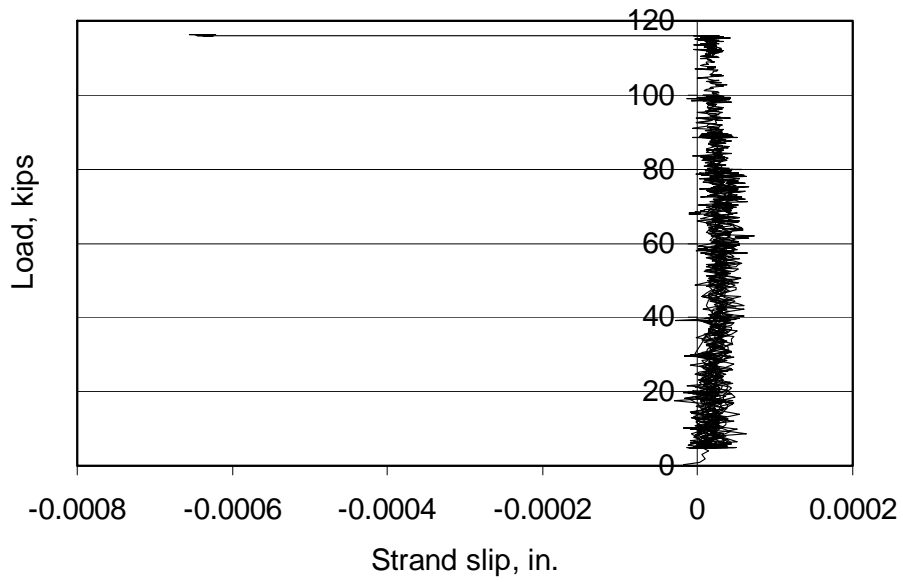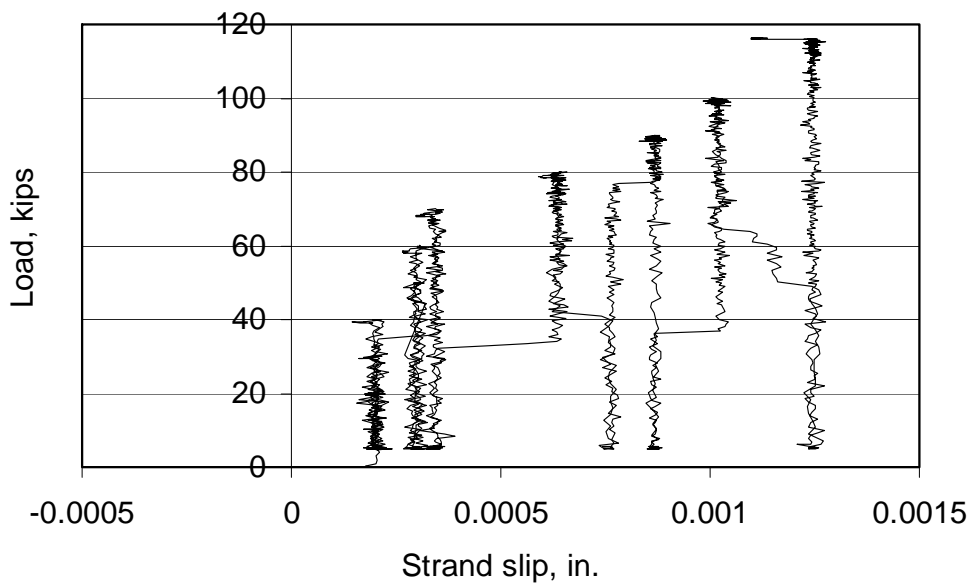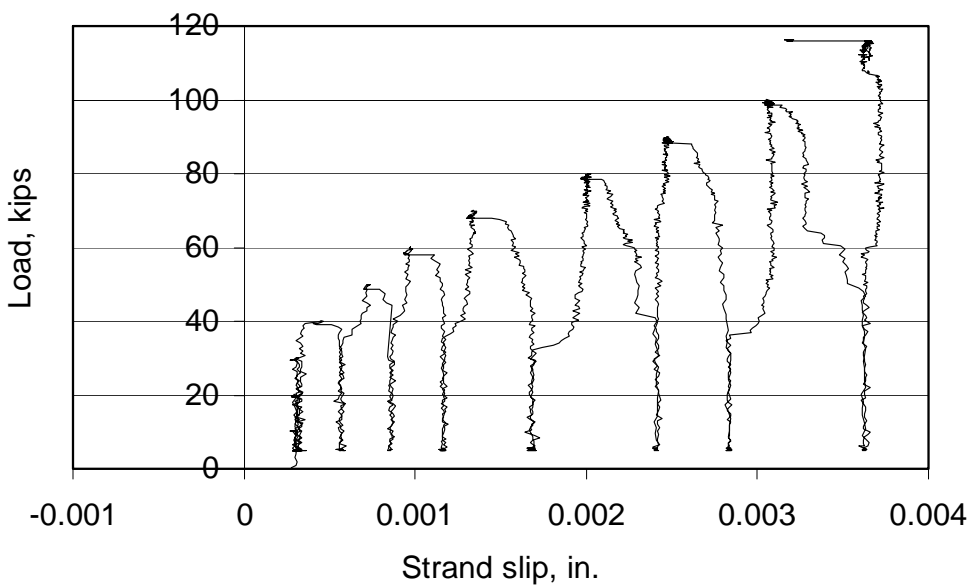
BG2F - P3

BG2F - P4

BG2F - P5
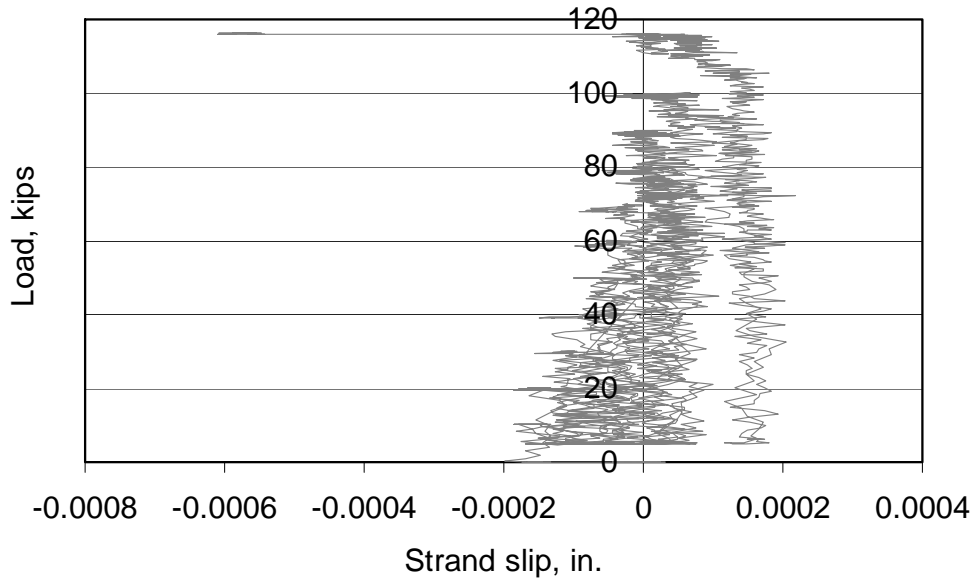
BG2F - P6
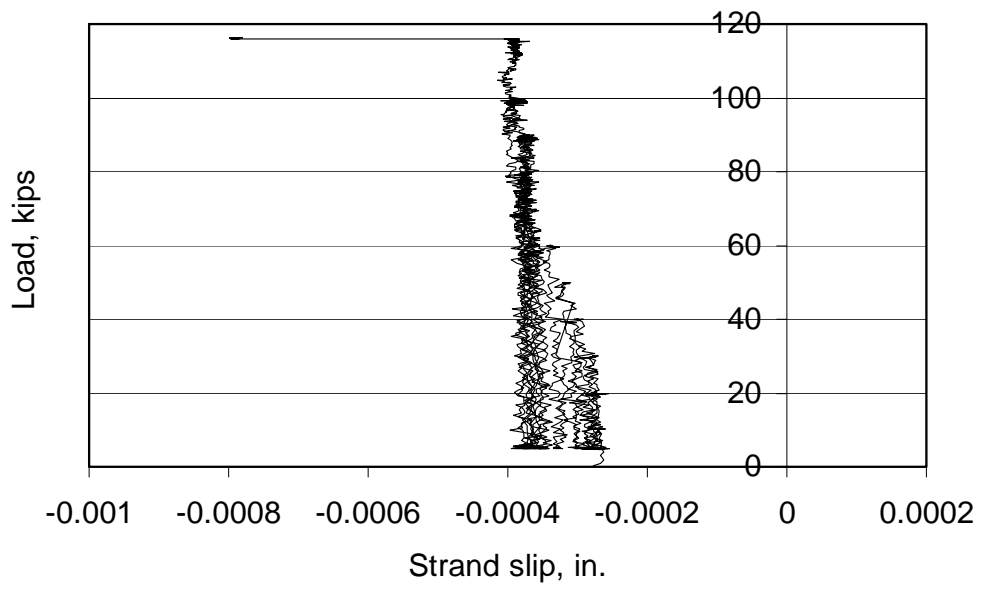
BG2F - P7
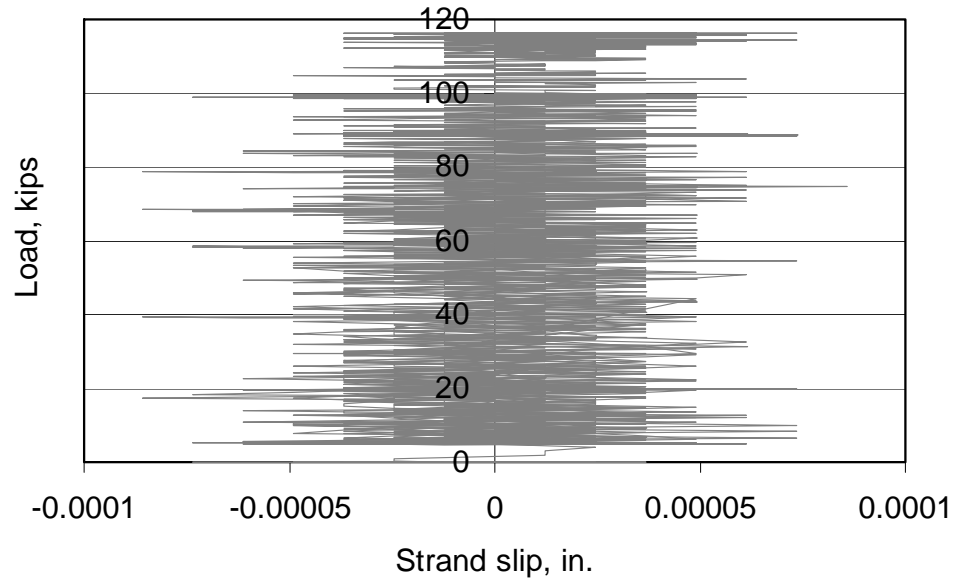
BG2F - P8

BG2F Strain Gradient
1 ft south of midspan

Legend:
- 20 kips
- 40 kips
- 60 kips
- 80 kips
- 100 kips
- 116.3 kips

Y-axis: Distance from bottom, in.
X-axis: Microstrain

BG2F - C1

Y-axis: Load, kips
X-axis: Change in crack width, in.

BG2F - C2

BG2F - C3

231
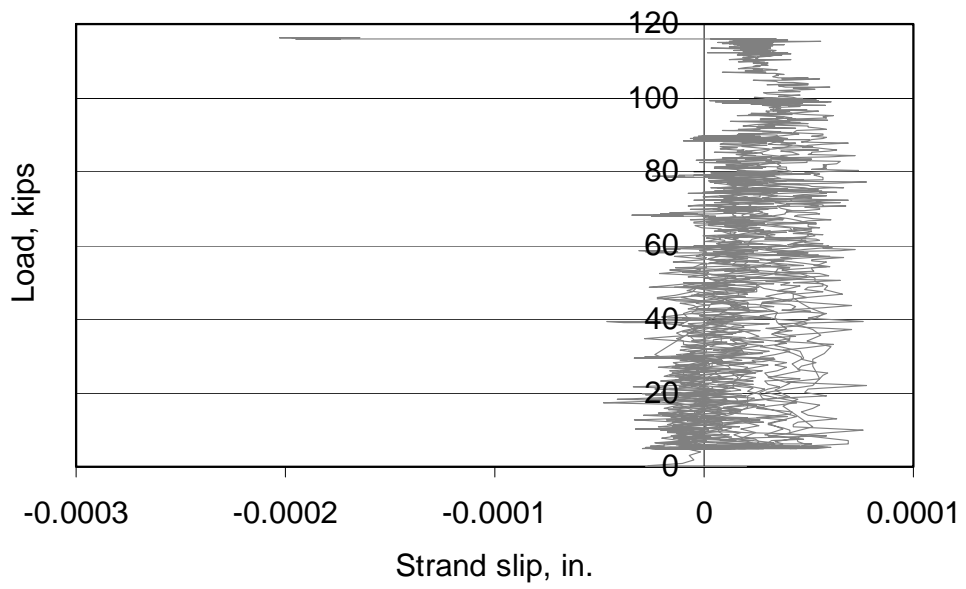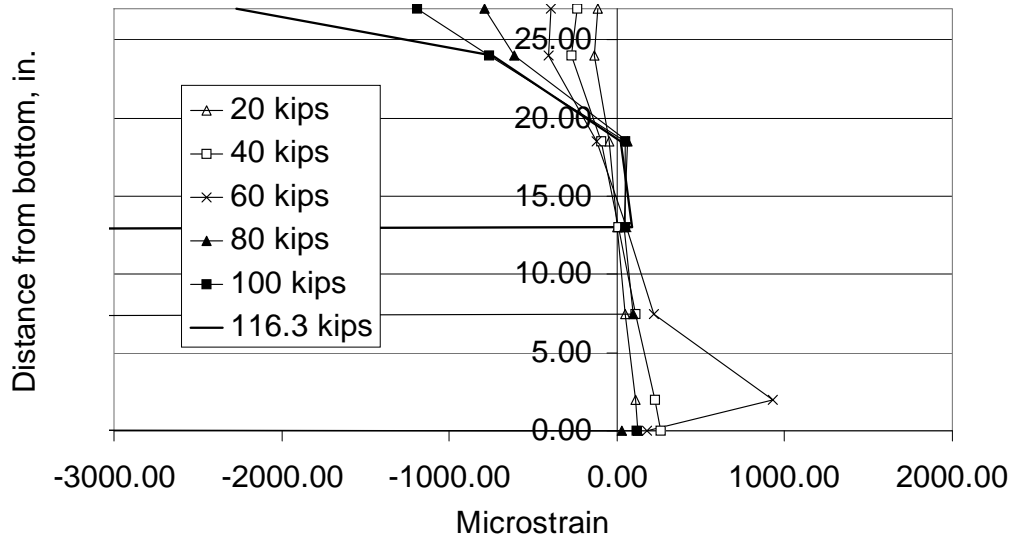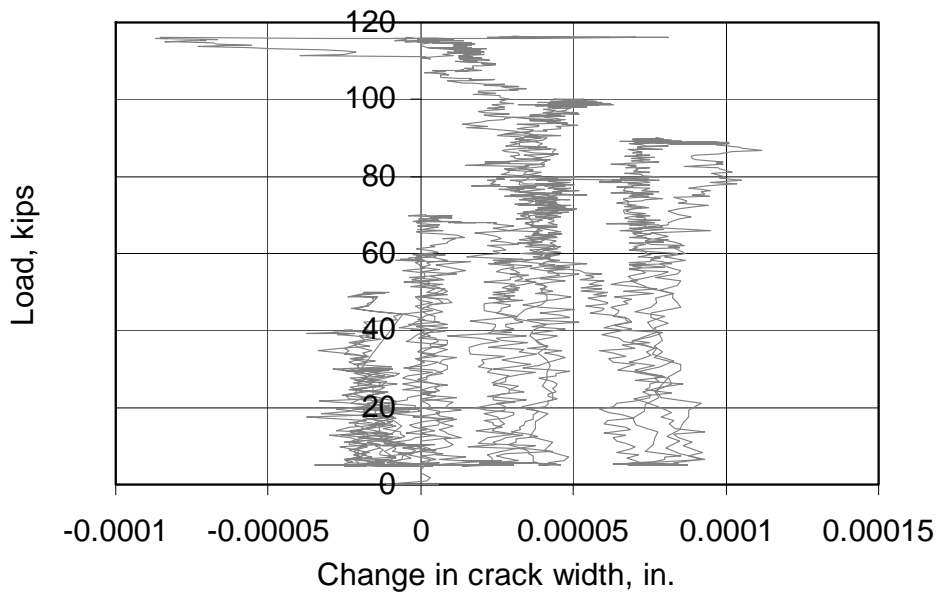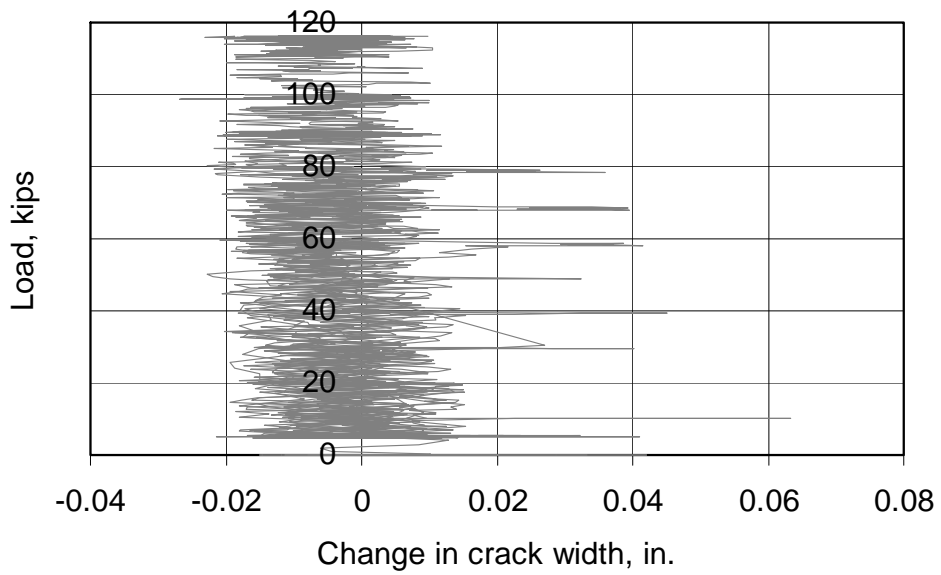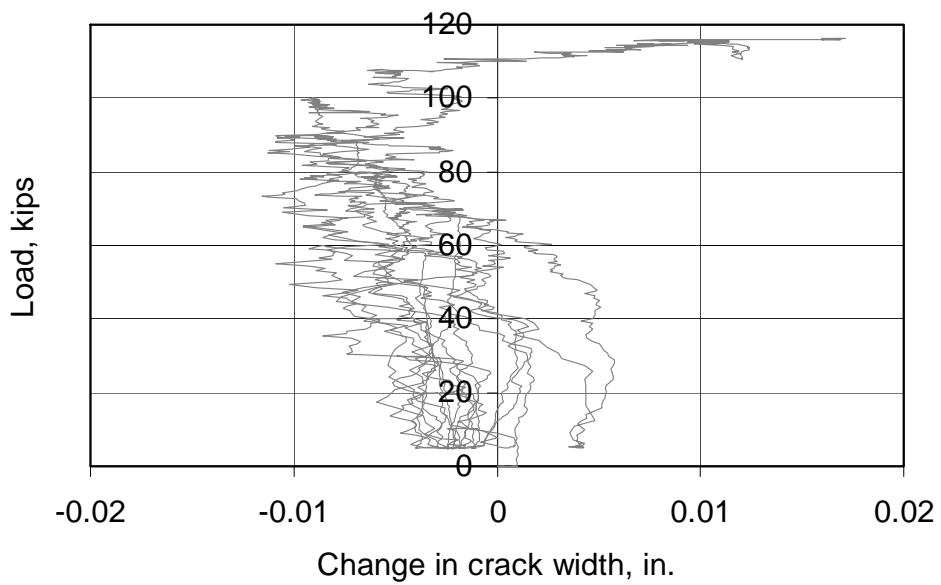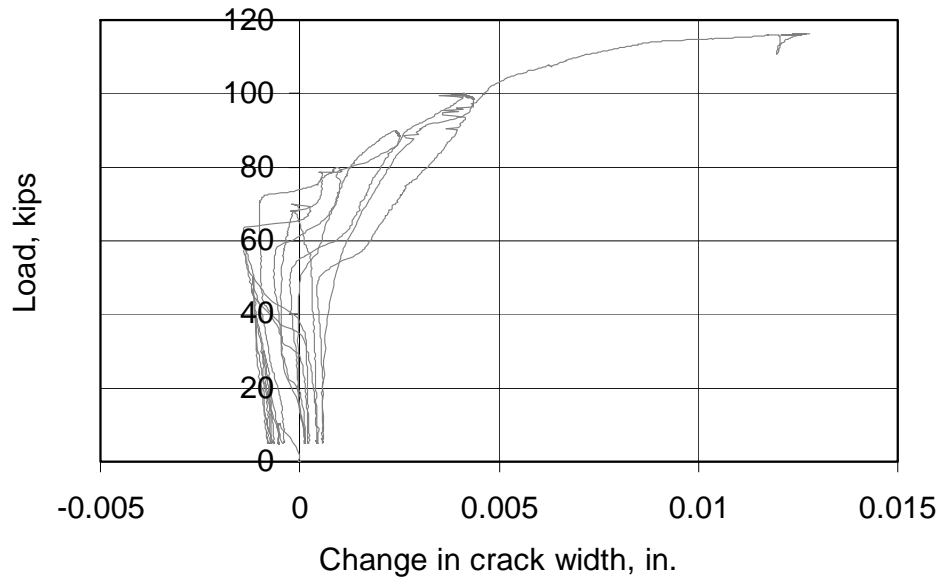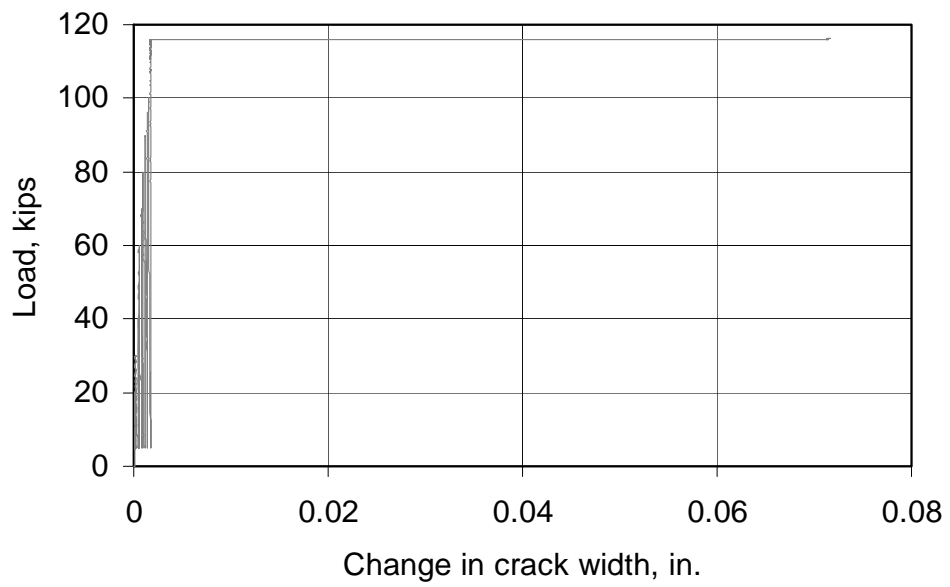
BG2F - C4
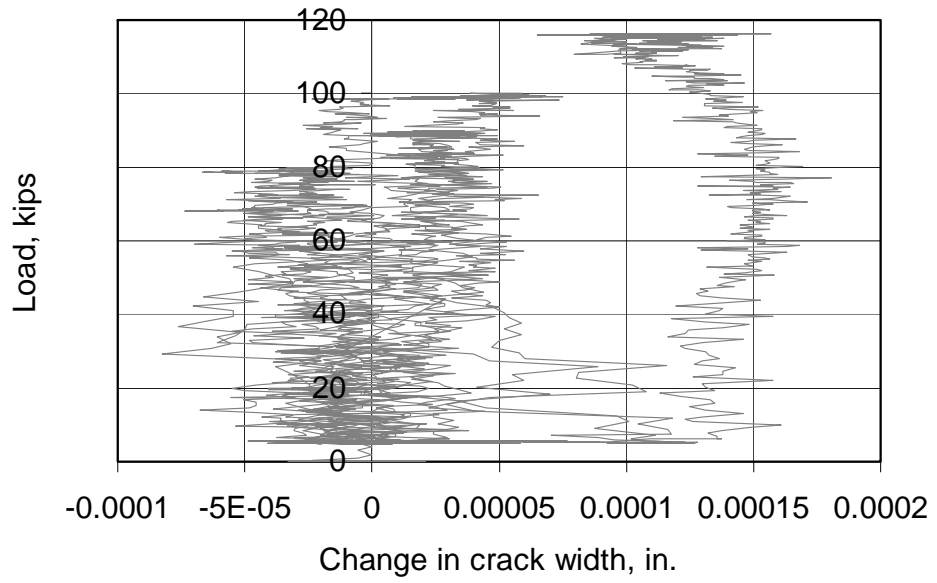
BG2F - C5

BG2F - C6

BG2F - C7
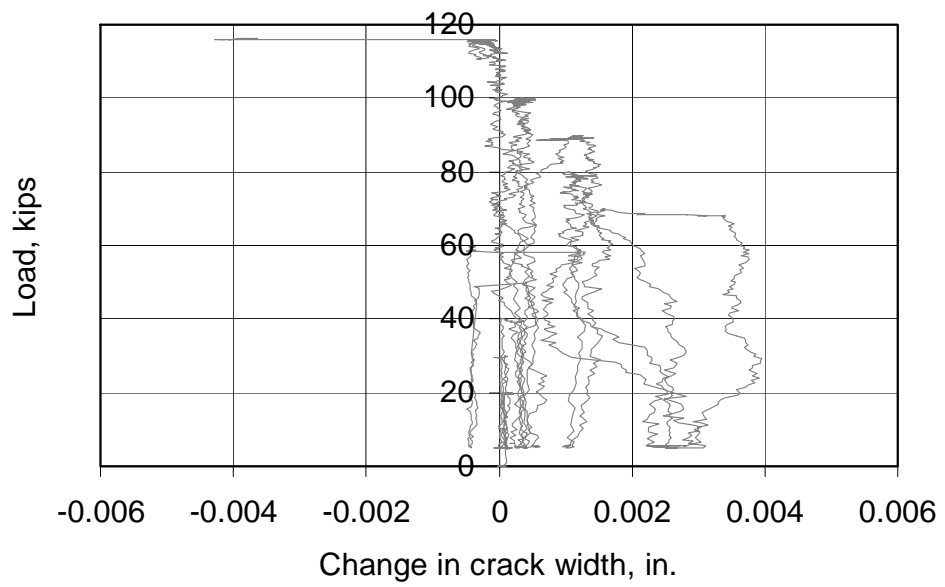
BG4F

BG4F - North Bearing Pad

Load, kips

Displacement, in.

BG4F - South Bearing Pad

Load, kips

Displacement, in.
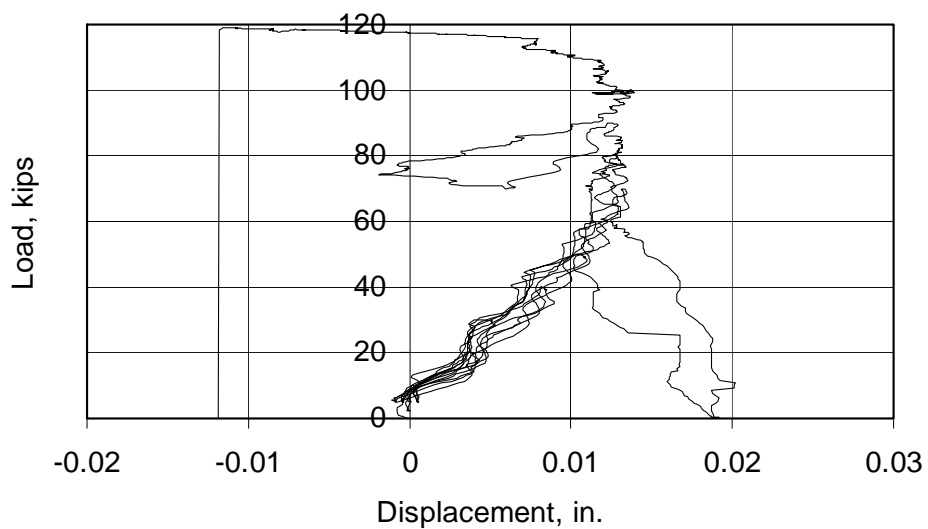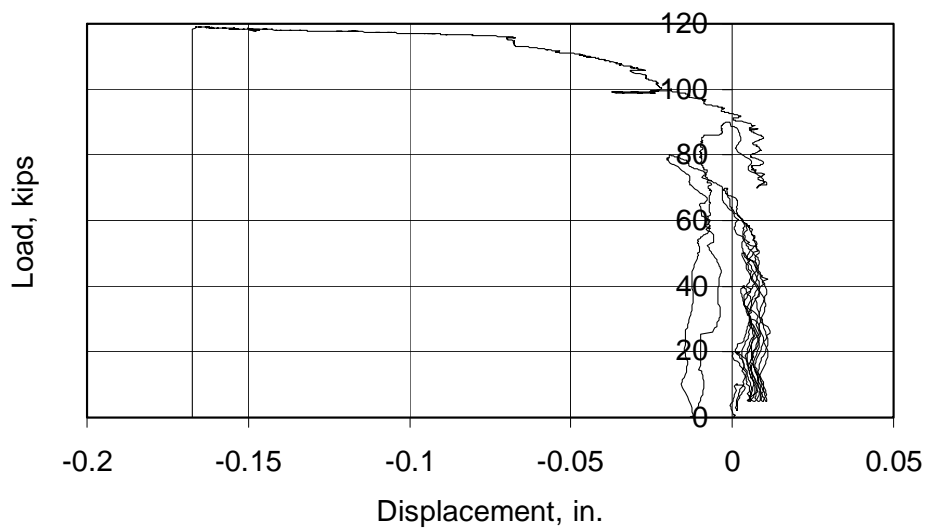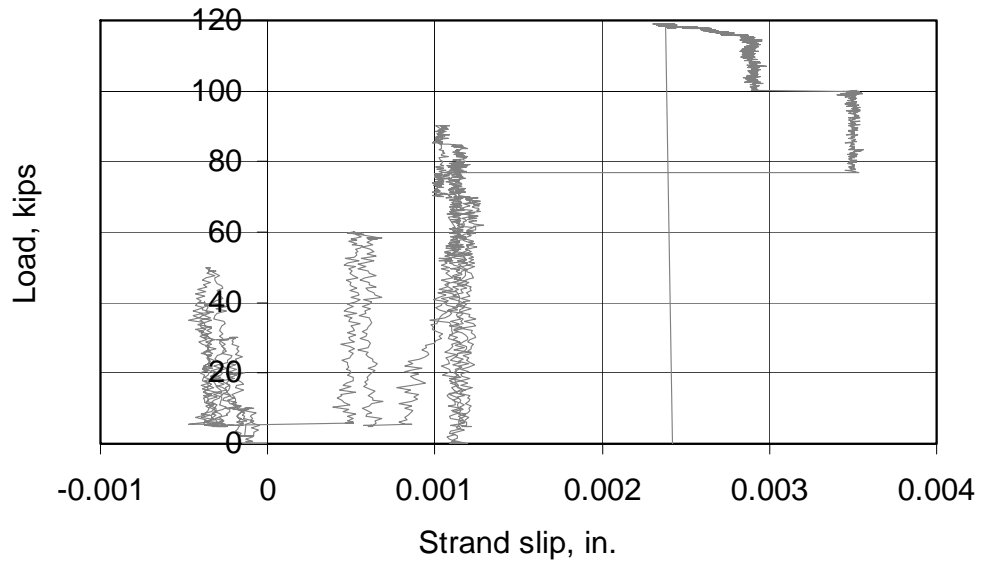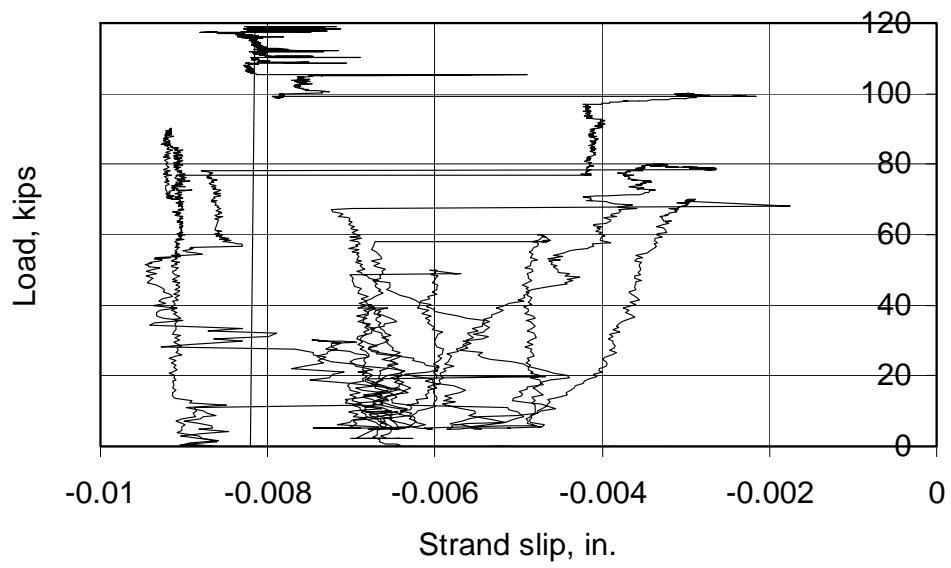
BG4F - P1
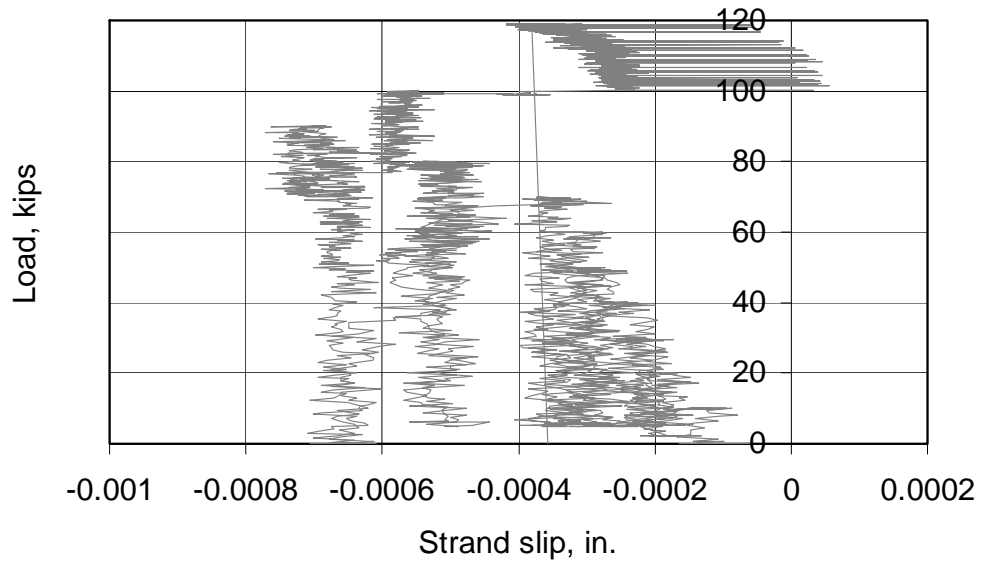
BG4F - P2

BG4F - P3

BG4F - P4
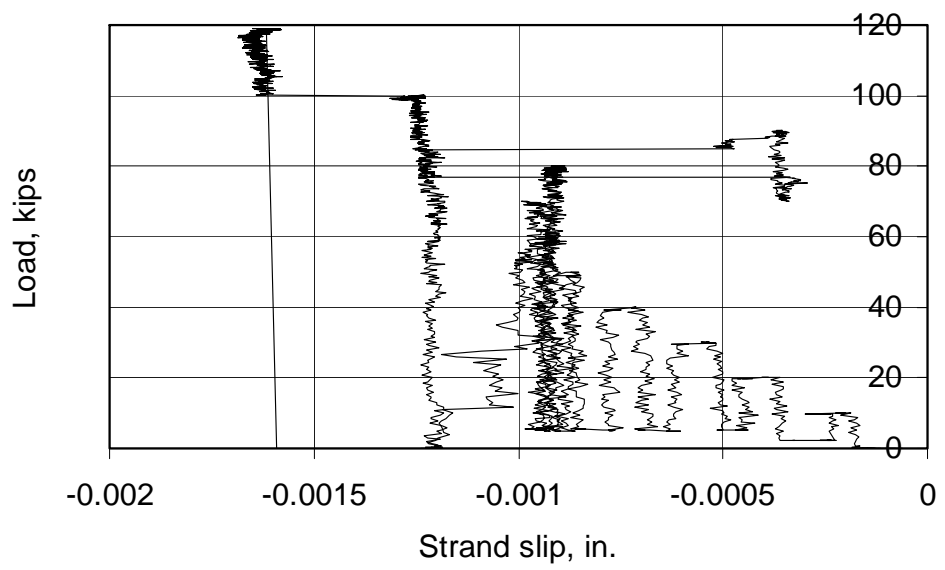
BG4F - P5
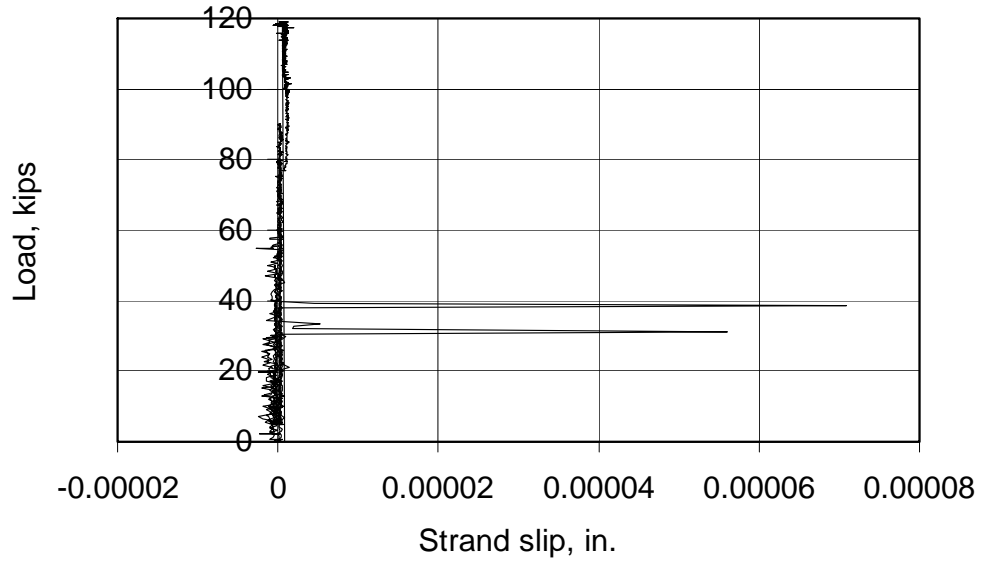
BG4F - P6
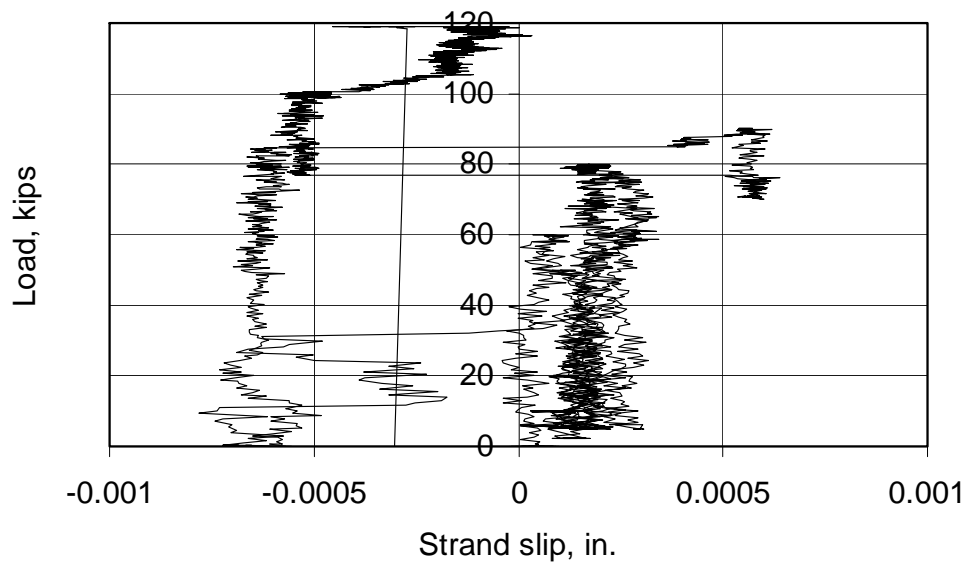
BG4F - P7

BG4F - P8

BG4F - C1

BG4F - C2

239

BG4F - C3

Load, kips

Change in crack width, in.
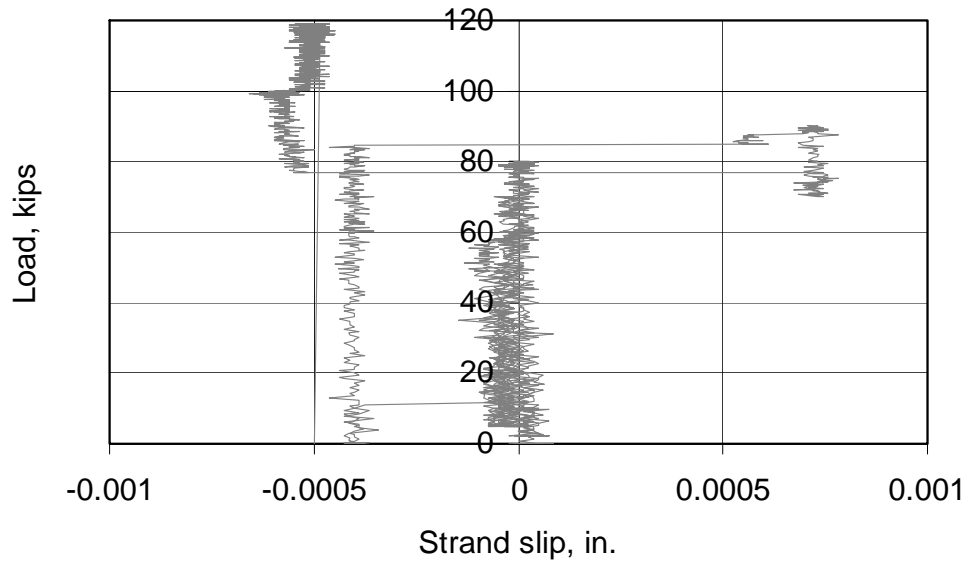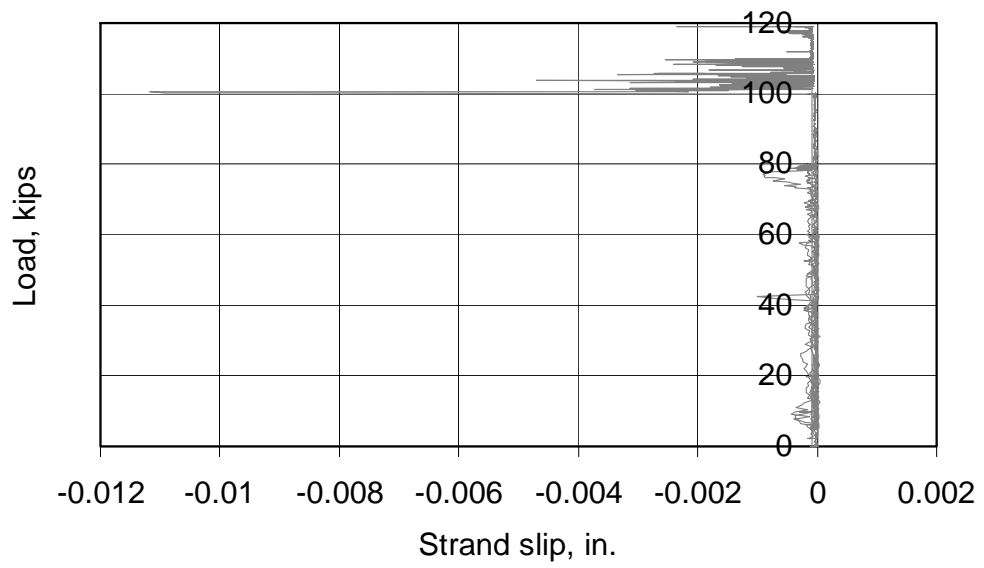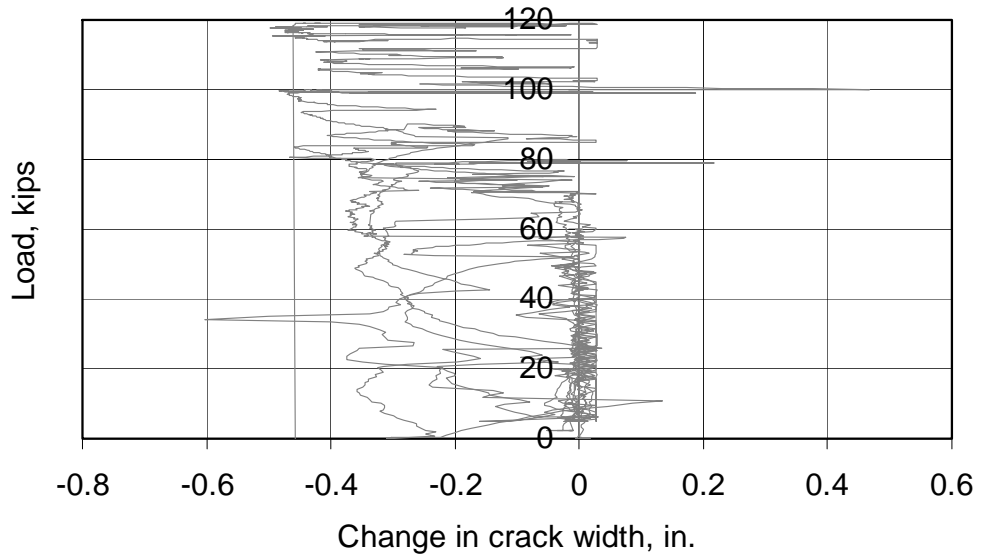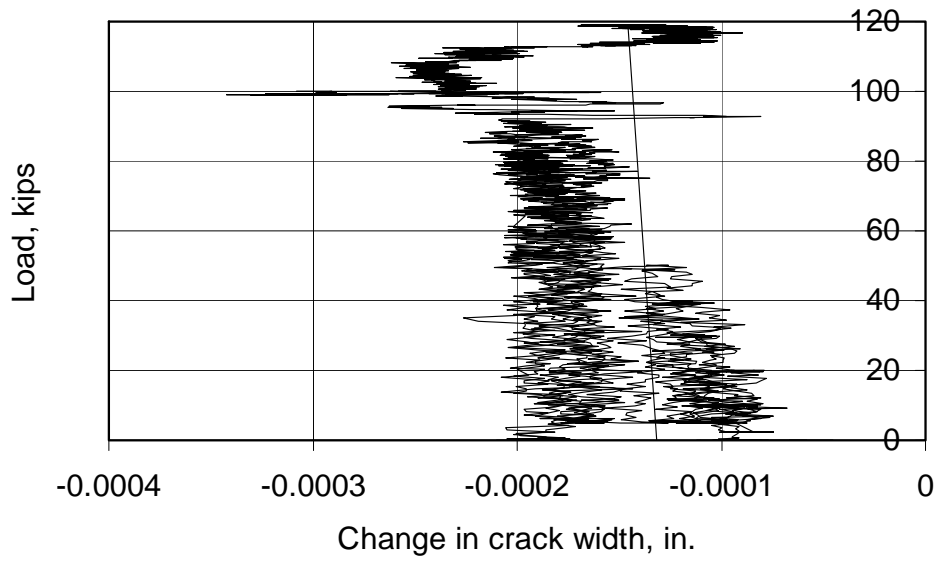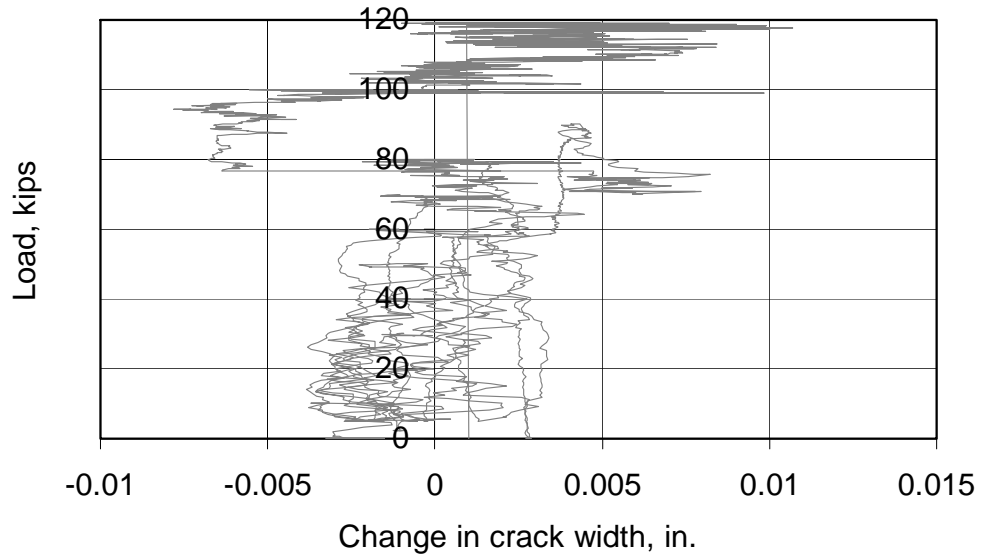
Appendix F: Data from Shear-dominated Tests
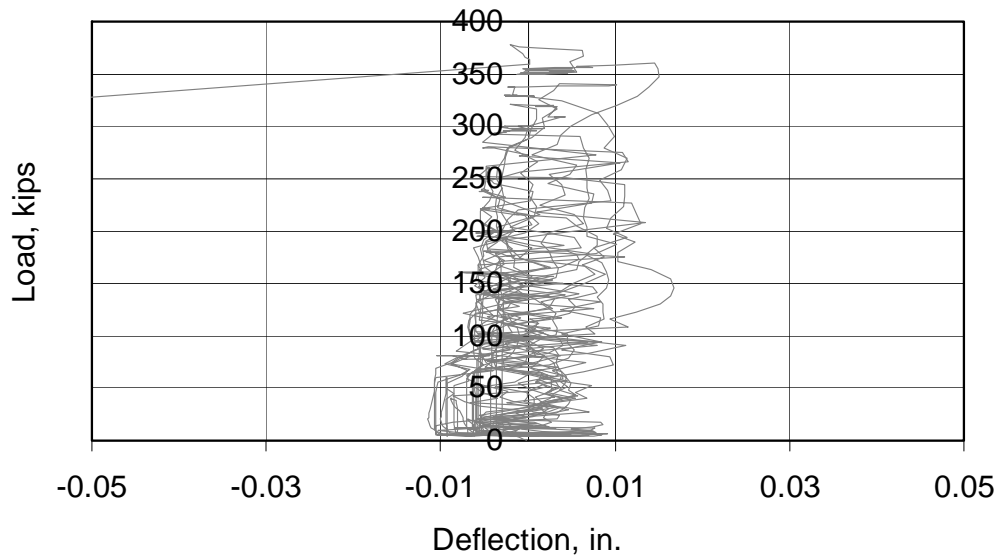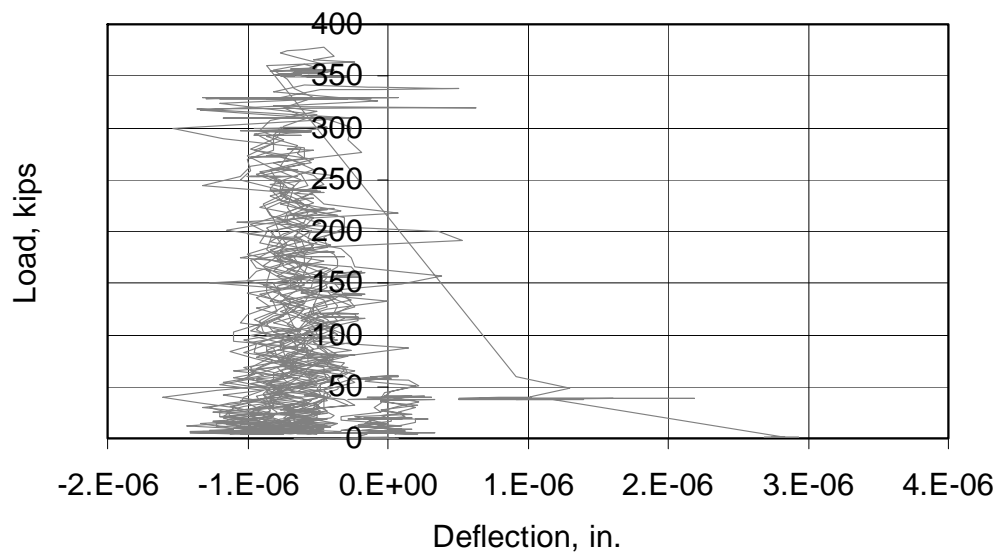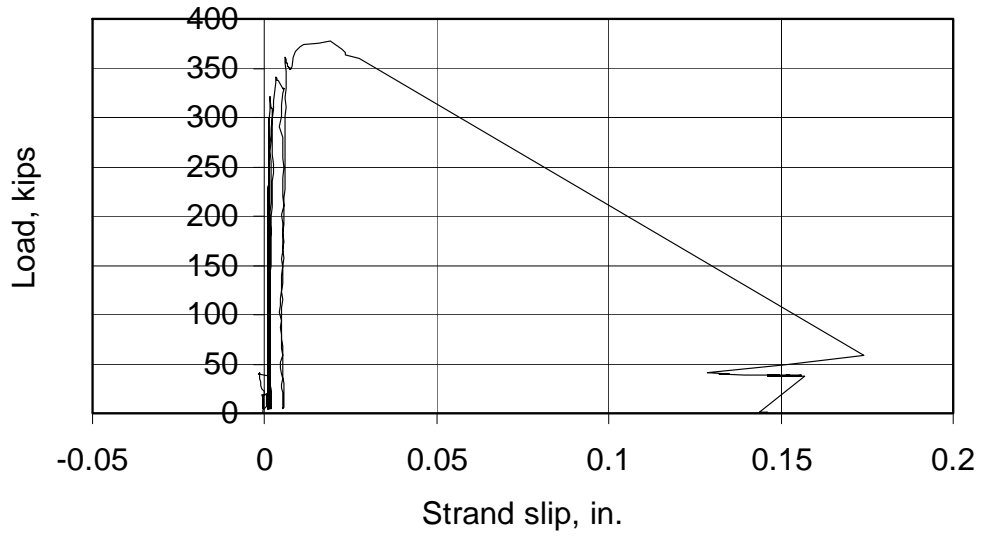
BG1S

BG1S - South Bearing Pad, West Face
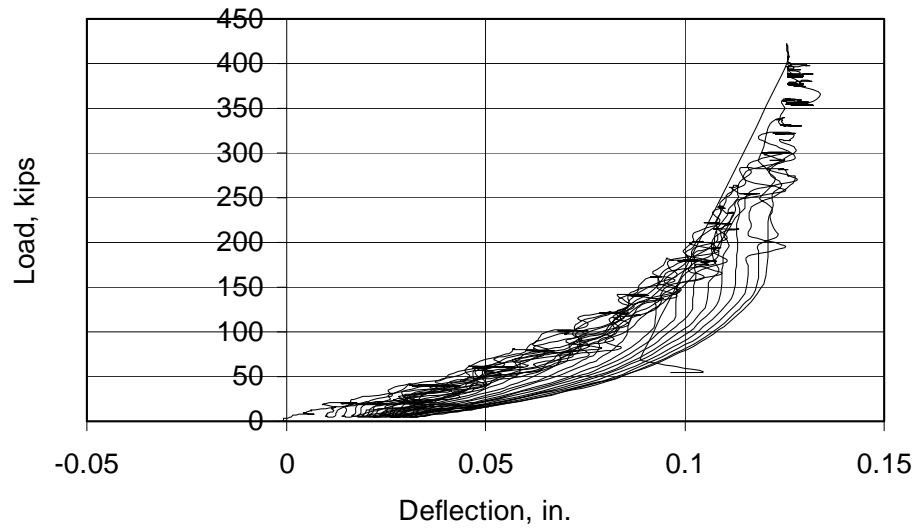
BG1S - South Bearing Pad, East Face
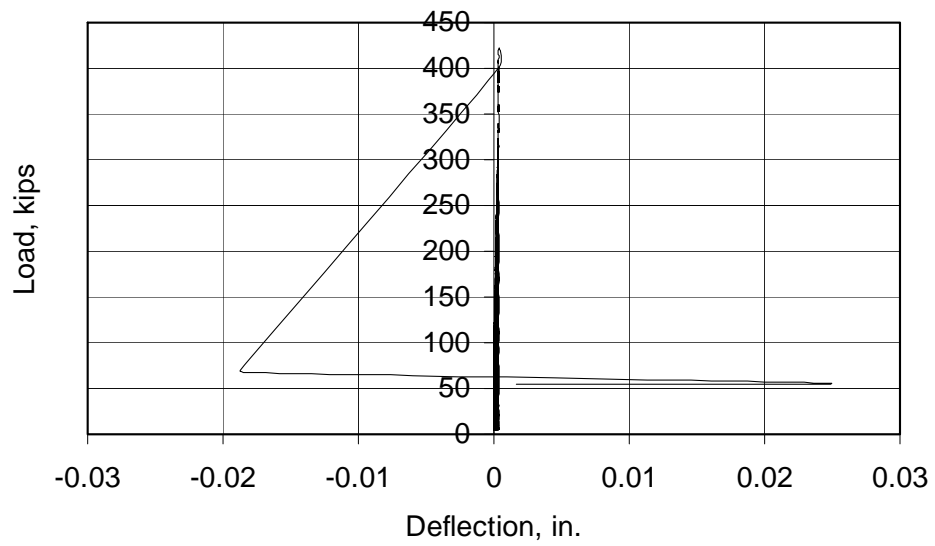
BG1S - P1
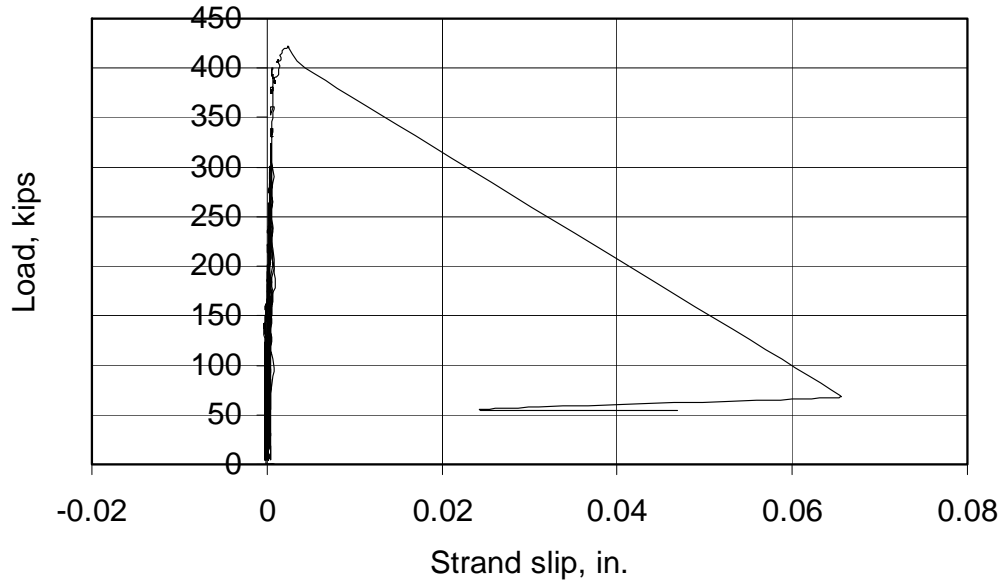
BG1S - P2

242
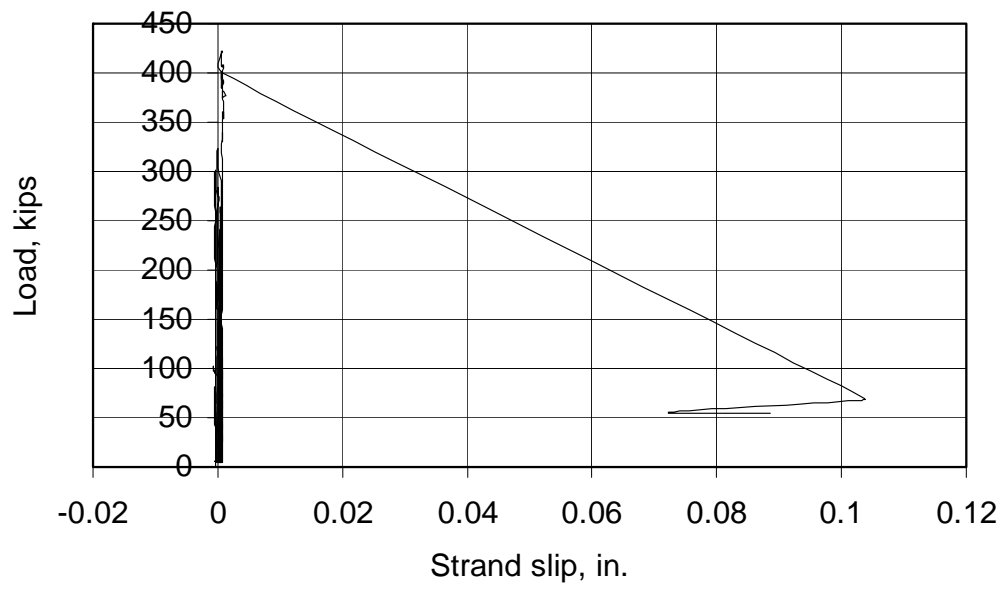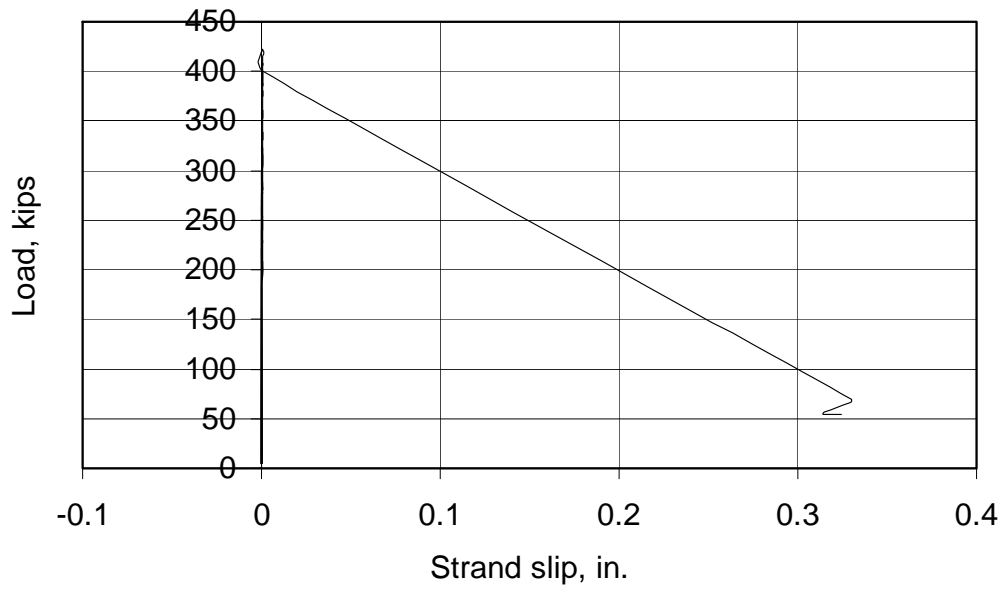
BG1S - P3

BG1S - P4

BG1S - P5

BG1S - P6

244
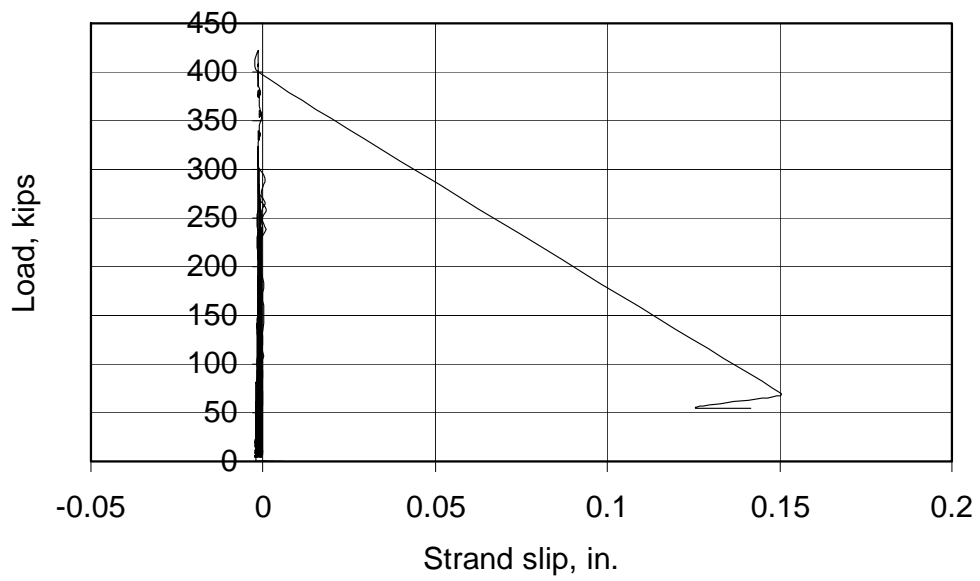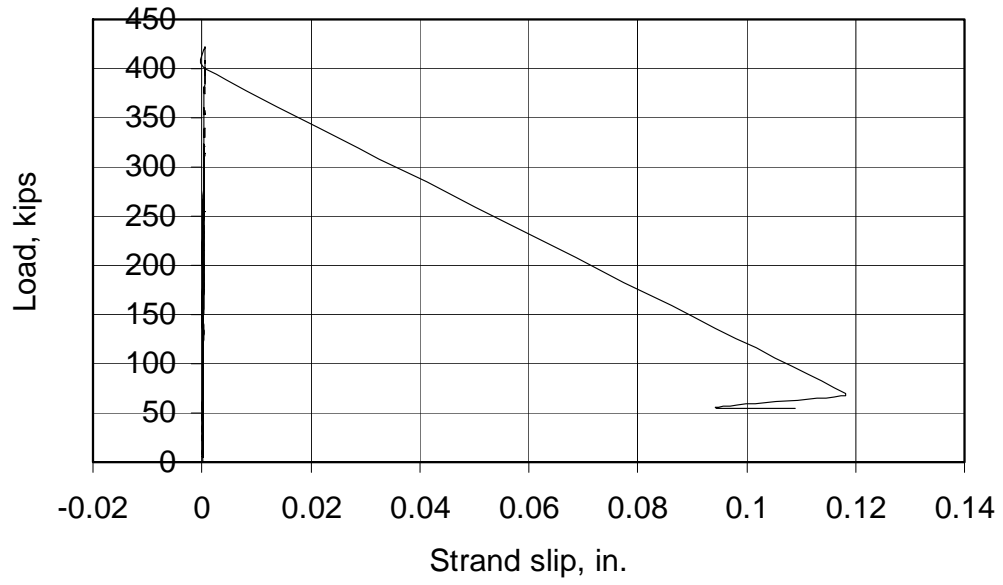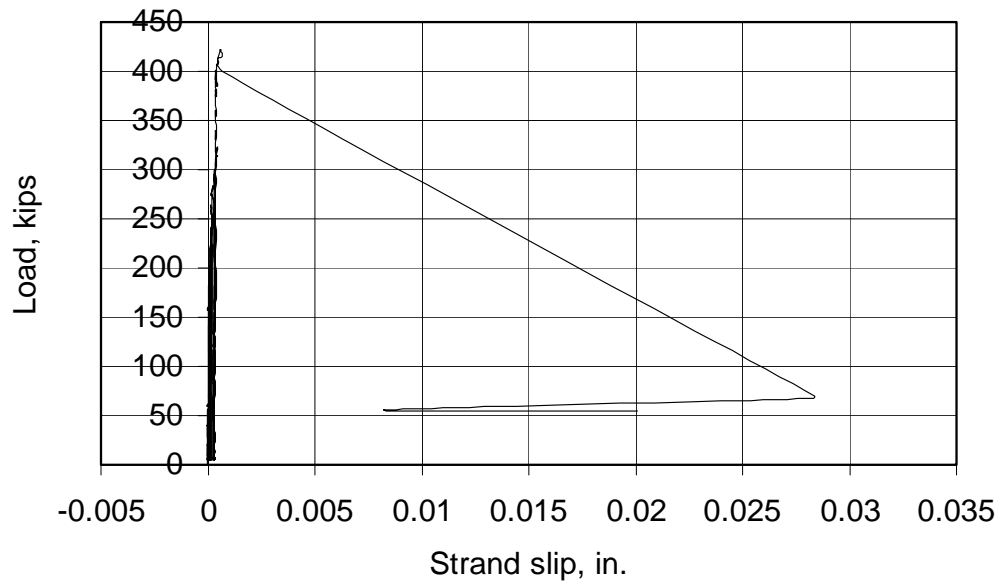
BG1S - P7

BG1S - P8

BG1S - L1

BG1S - L2

246

BG1S - L3

Load, kips (y-axis)

Extension, in. (x-axis)

BG1S - L4

Load, kips (y-axis)

Extension, in. (x-axis)
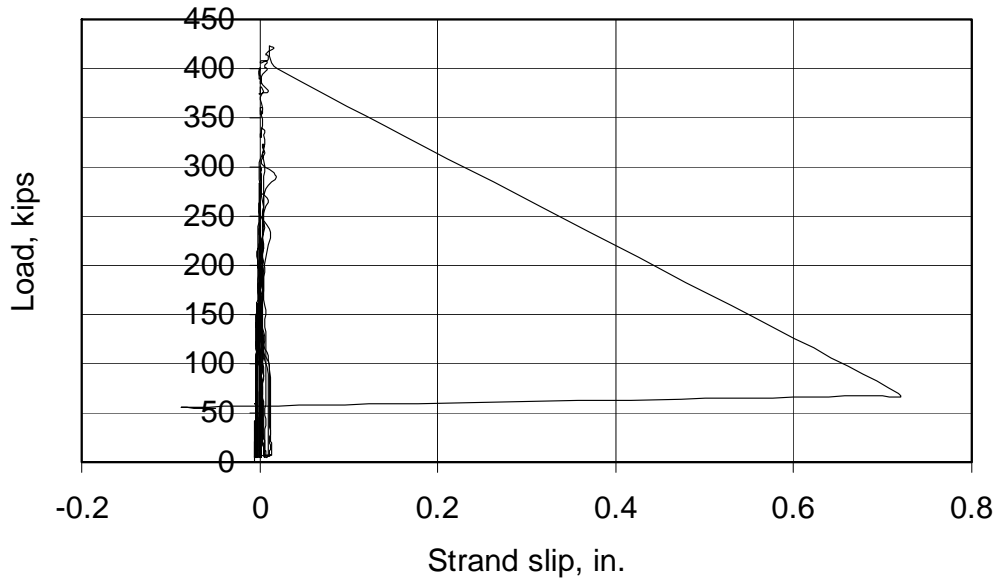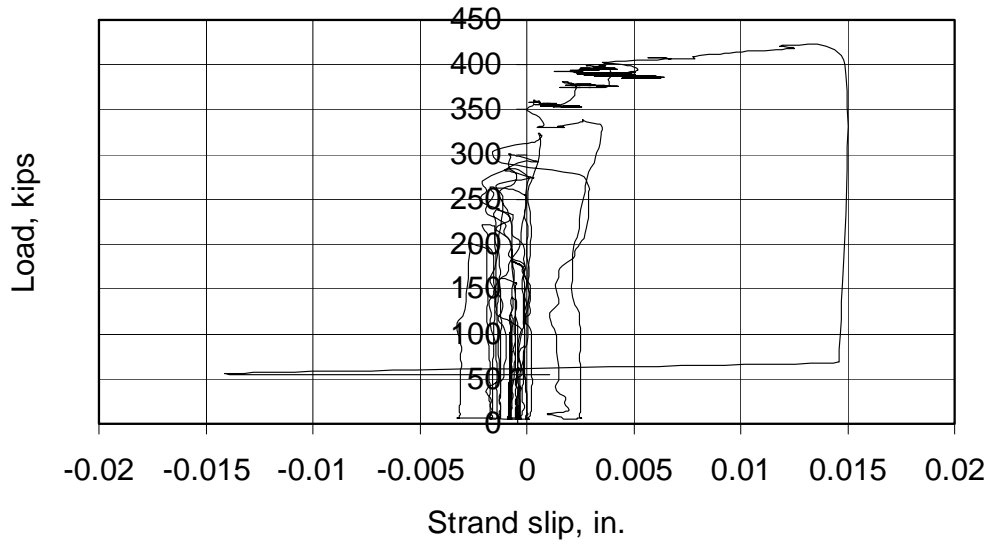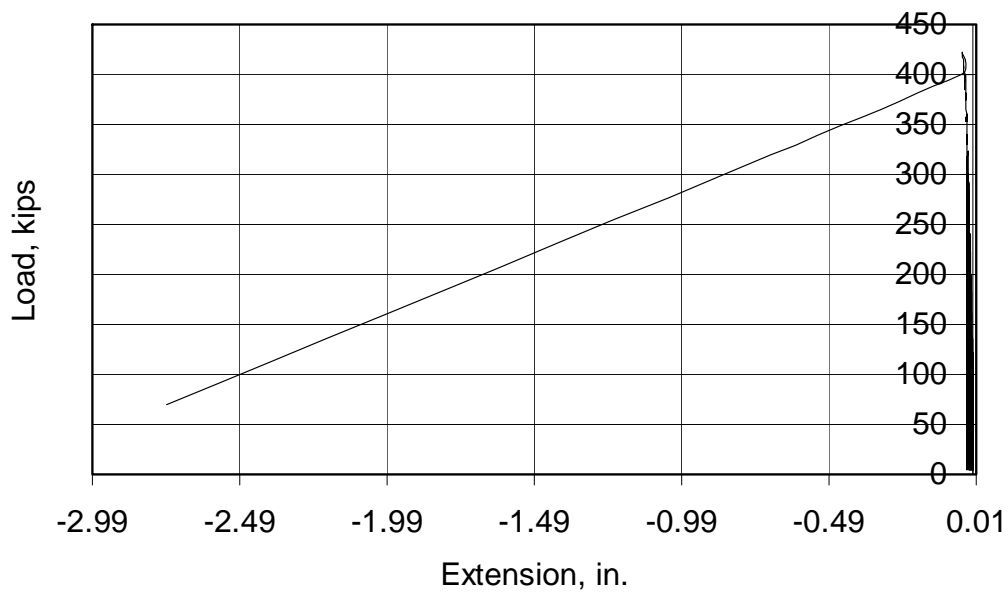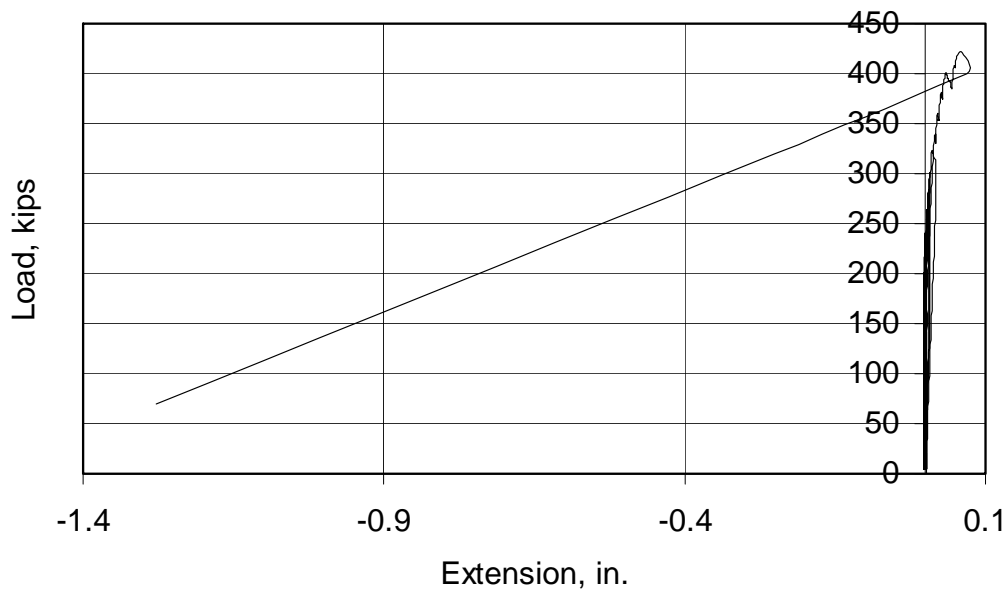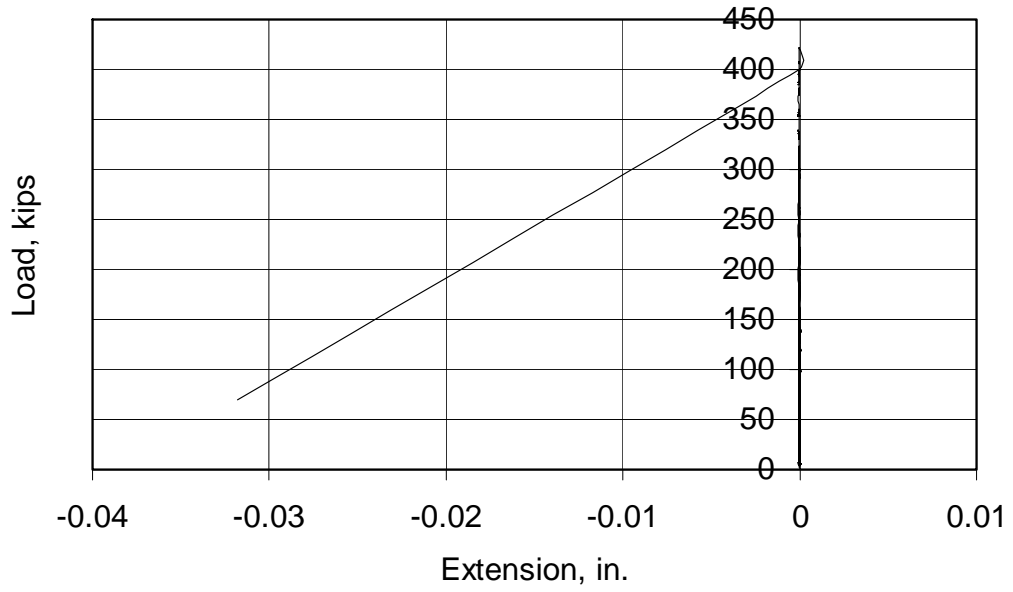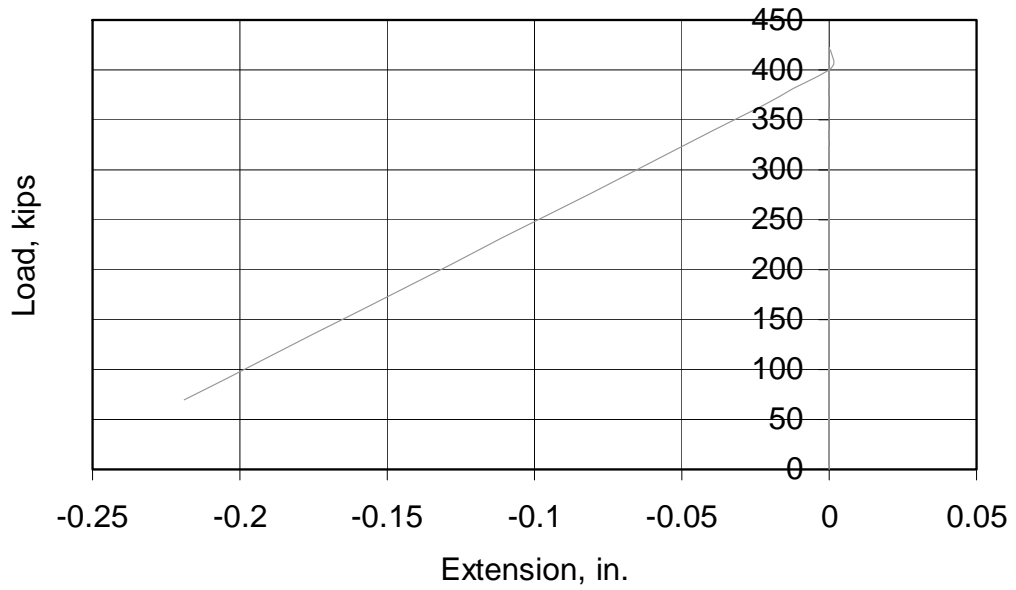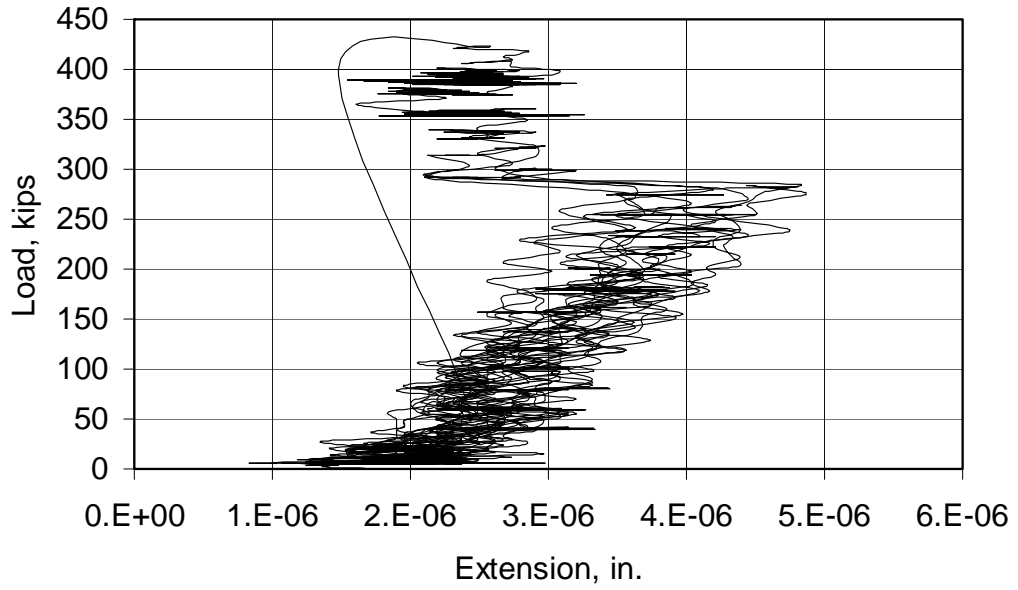
BG1S - L5

BG1S - L6

BG1S - L7

BG1S - L8

249
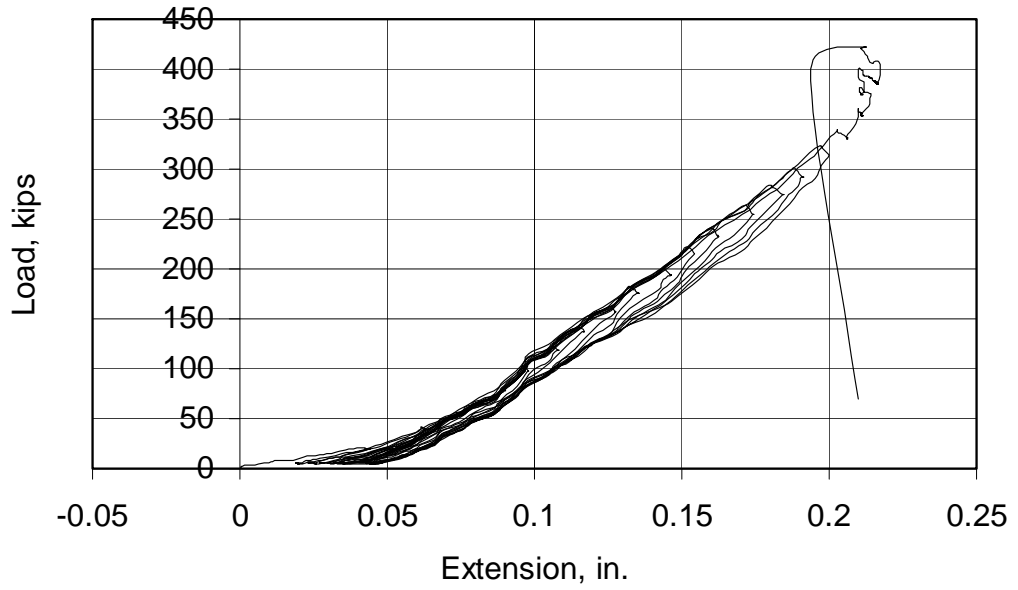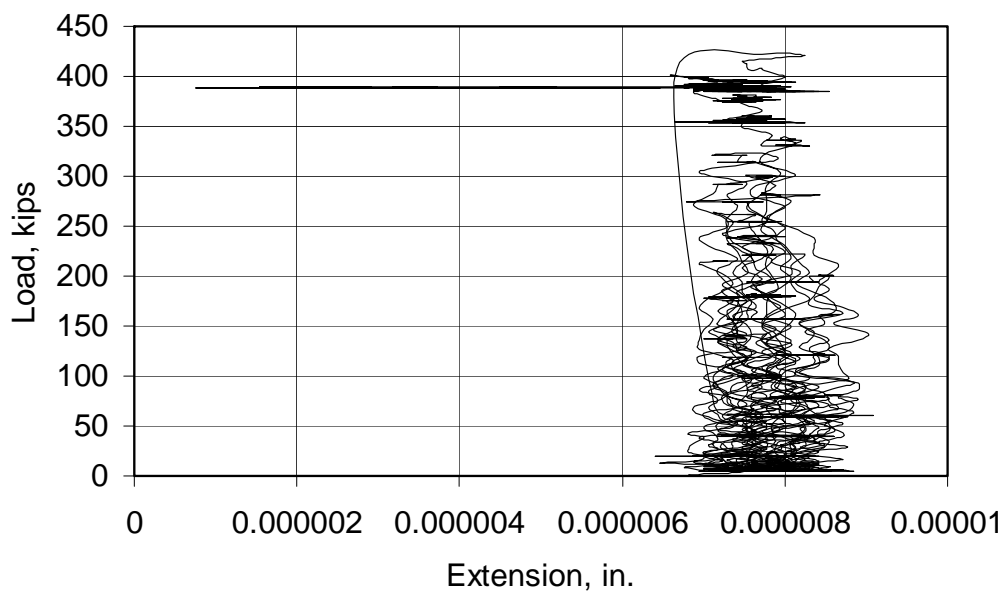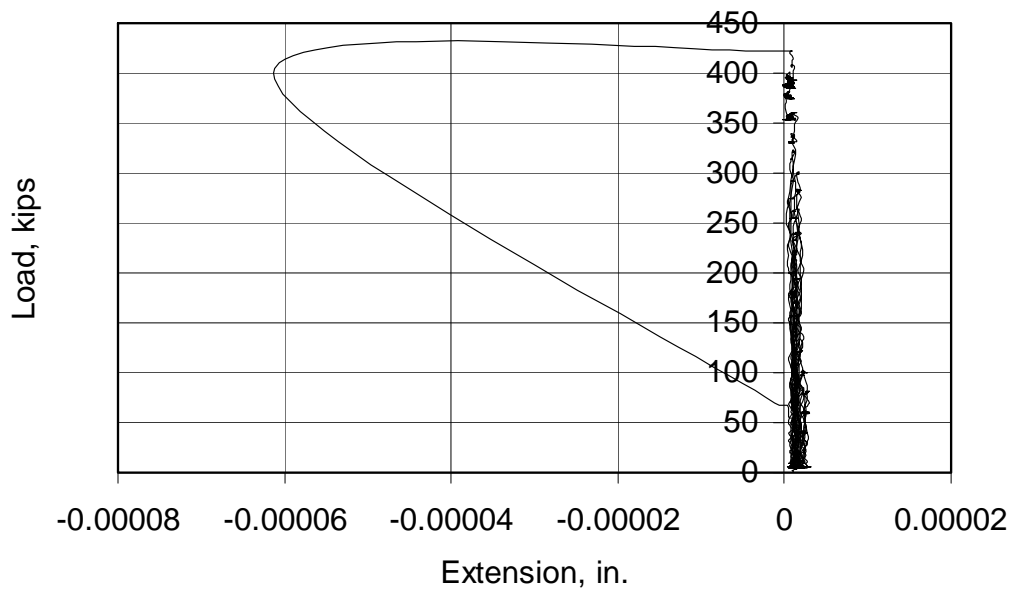
BG2S

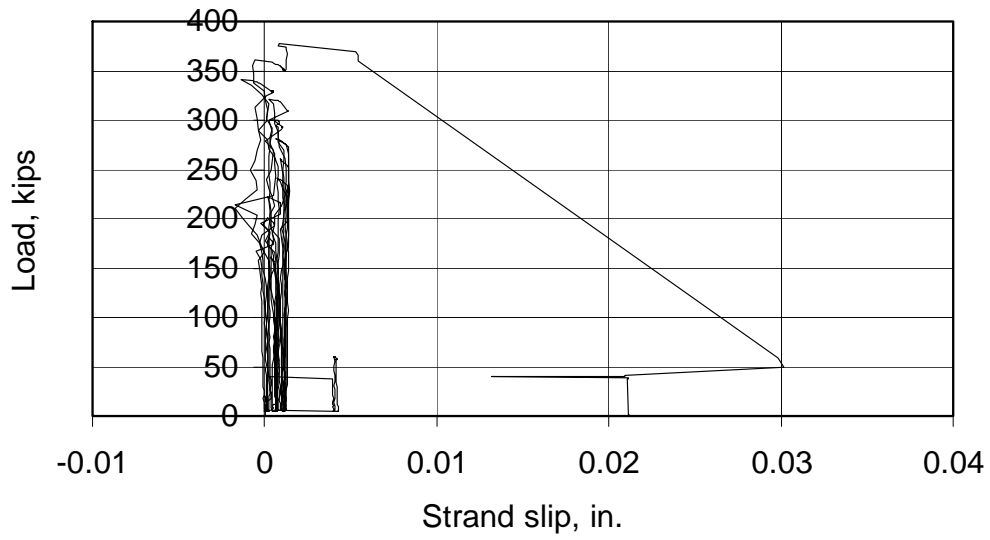## BG2S - South Bearing Pad, West Face
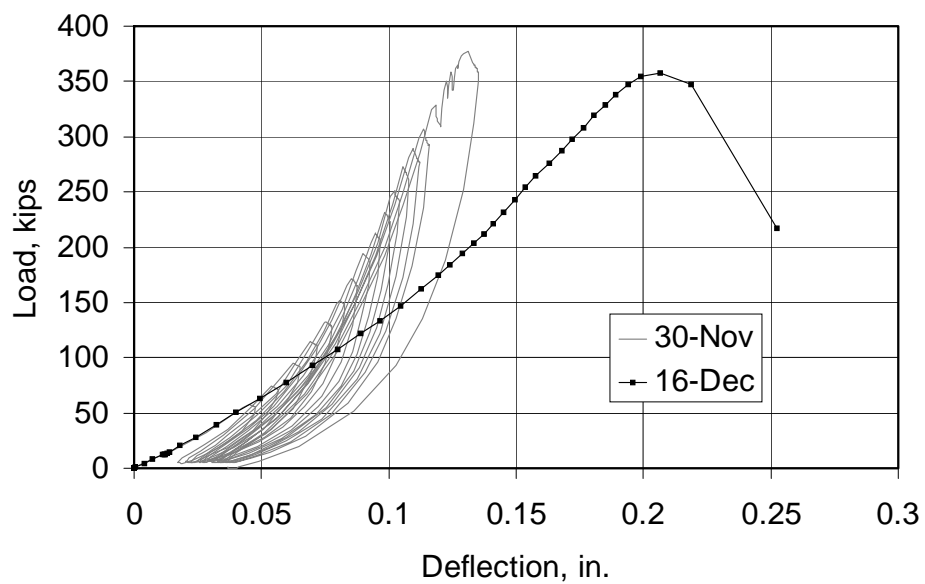
BG2S - South Bearing Pad, East Face

BG2S - P1

BG2S - P2

251

BG2S - P3

BG2S - P4

252
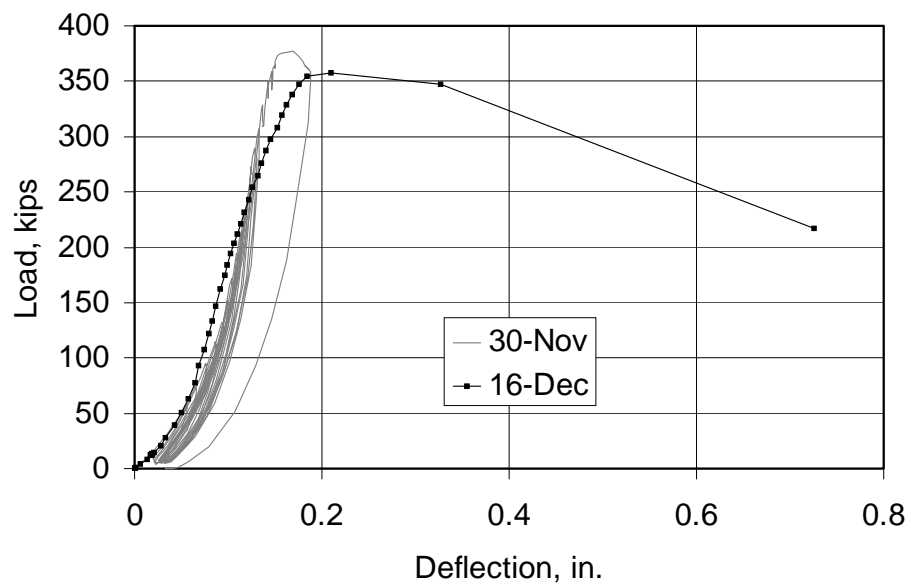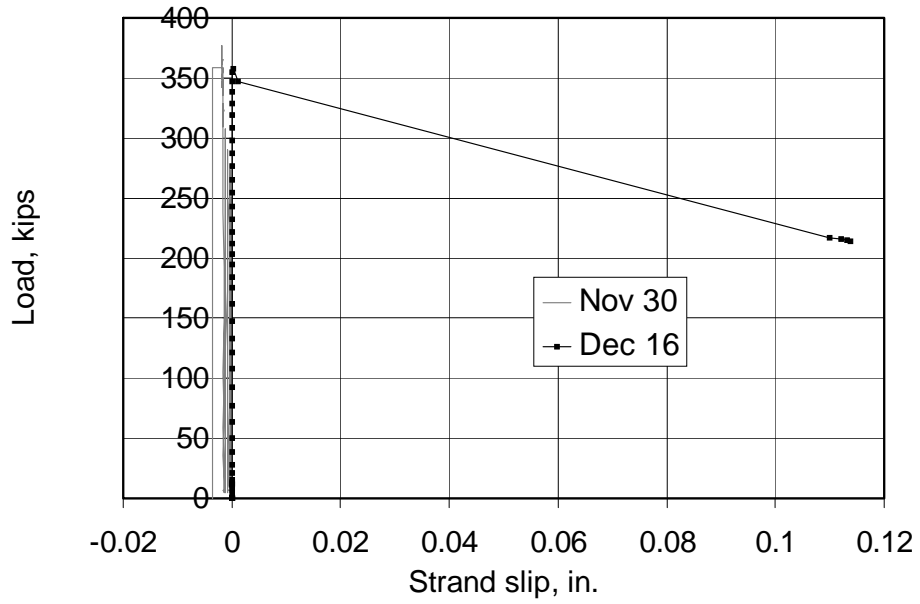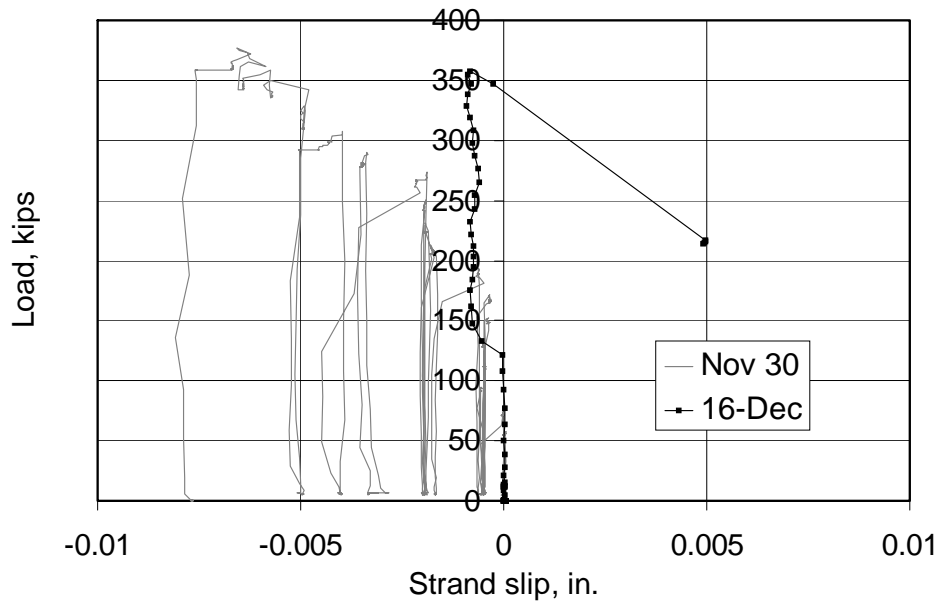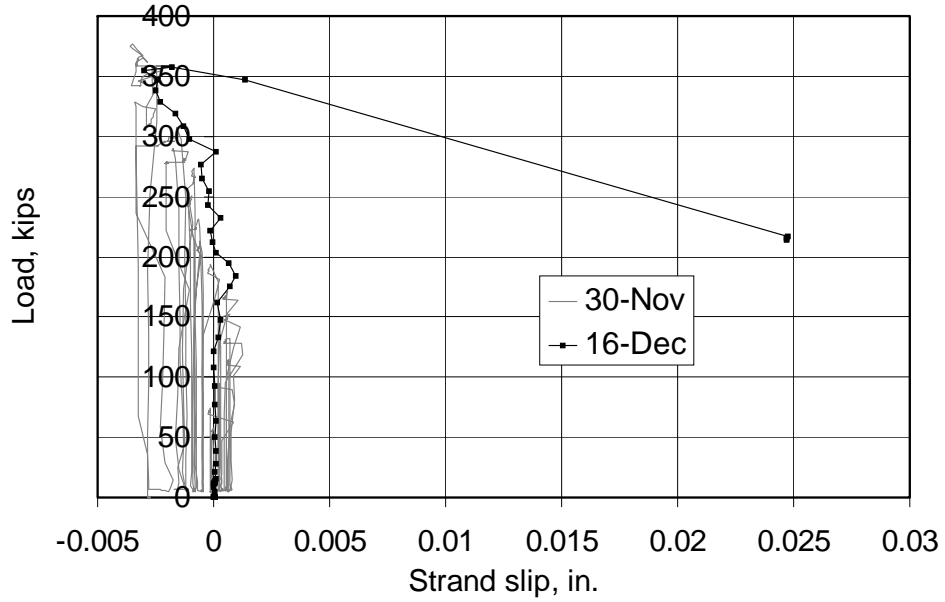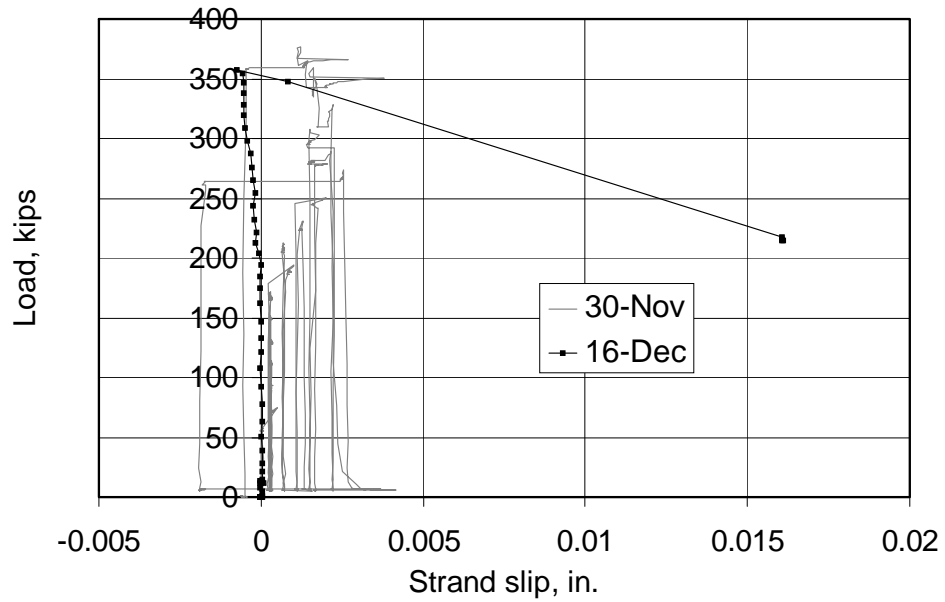
BG2S - P5

BG2S - P6

BG2S - P7

BG2S - P8

254

BG2S - L1

Load, kips

Legend:
30-Nov
16-Dec

Extension, in.

BG2S - L2

Load, kips

Legend:
30-Nov
16-Dec

Extension, in.

255
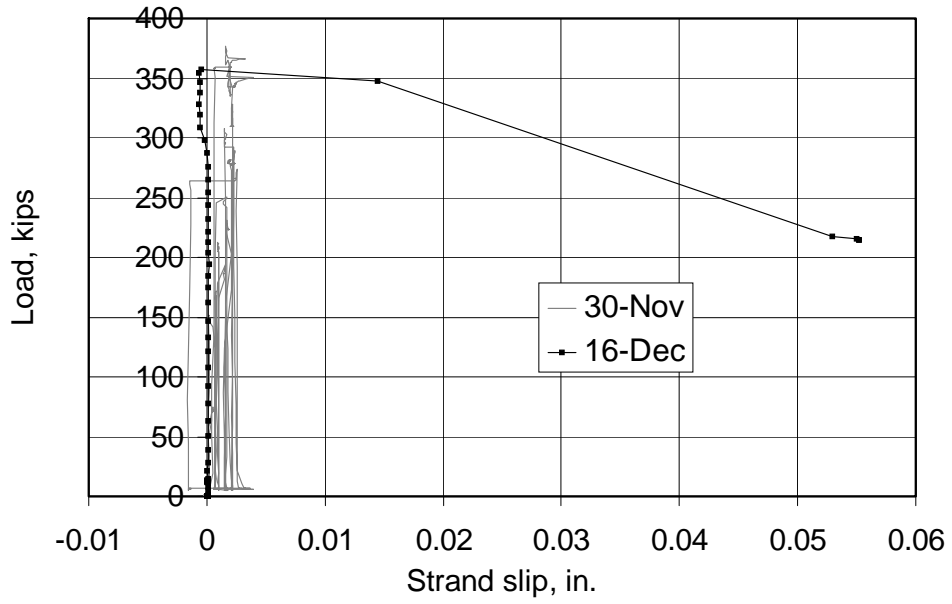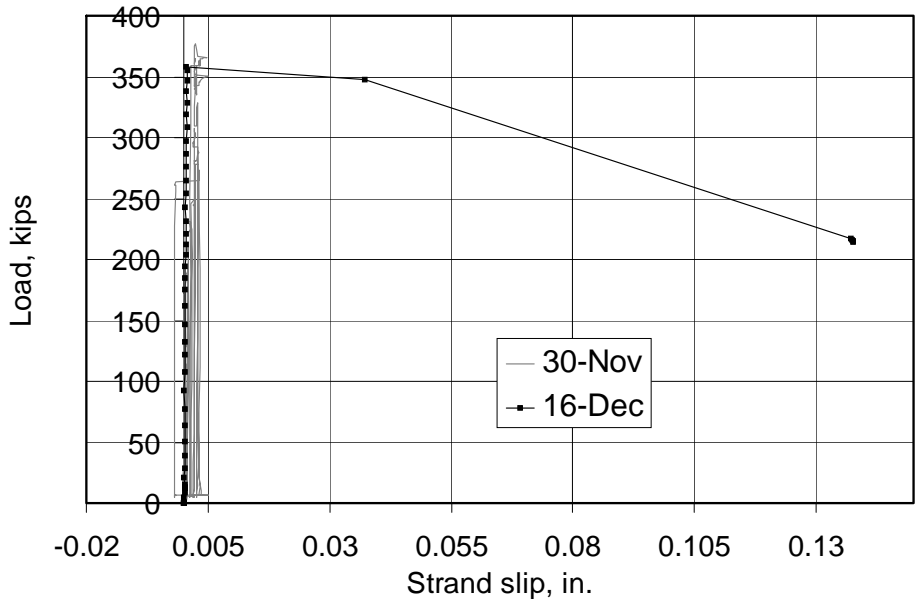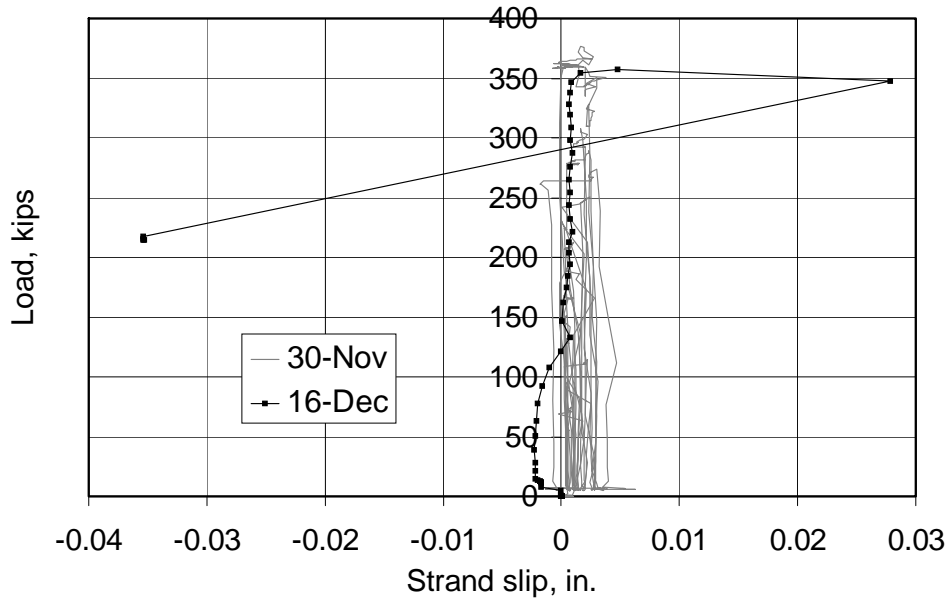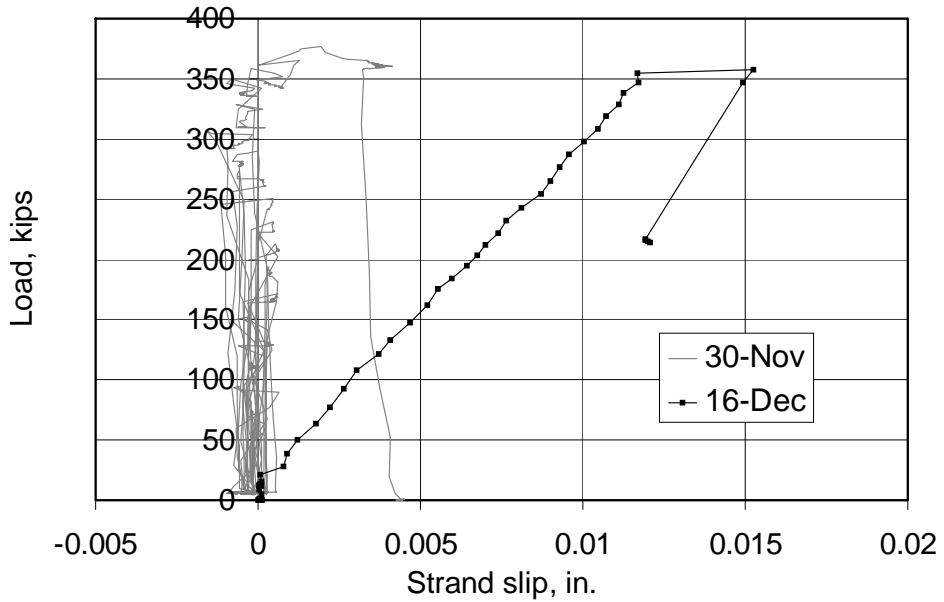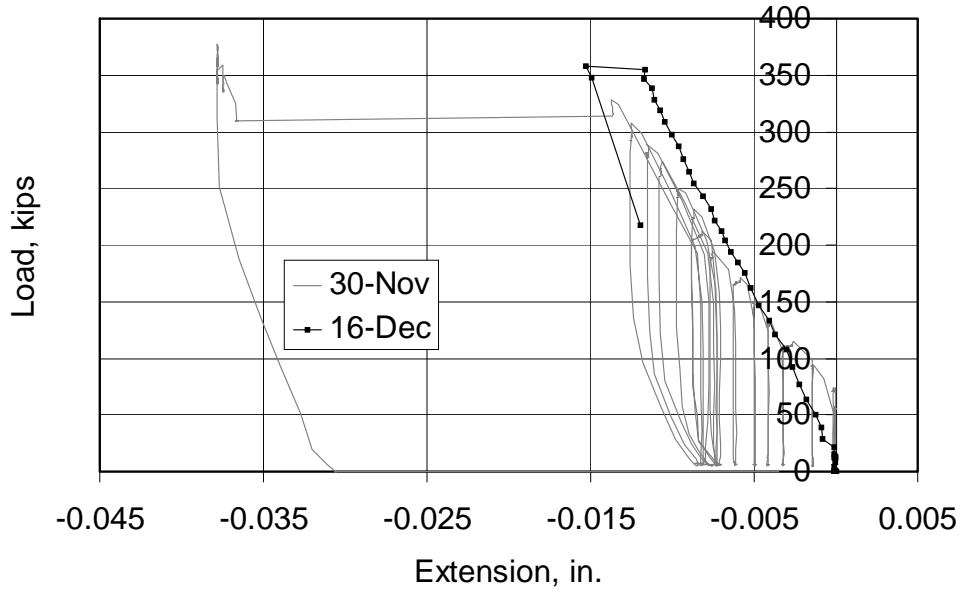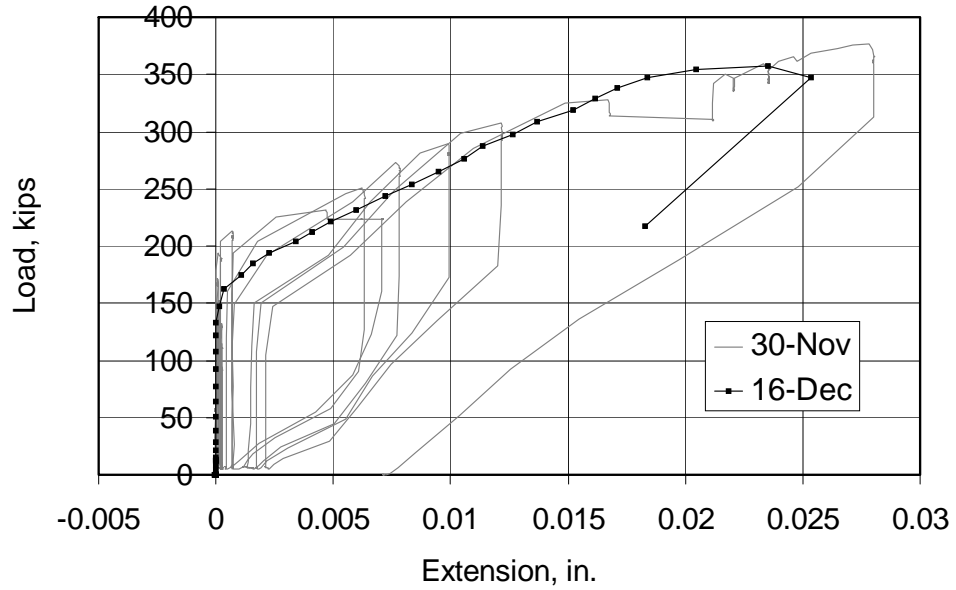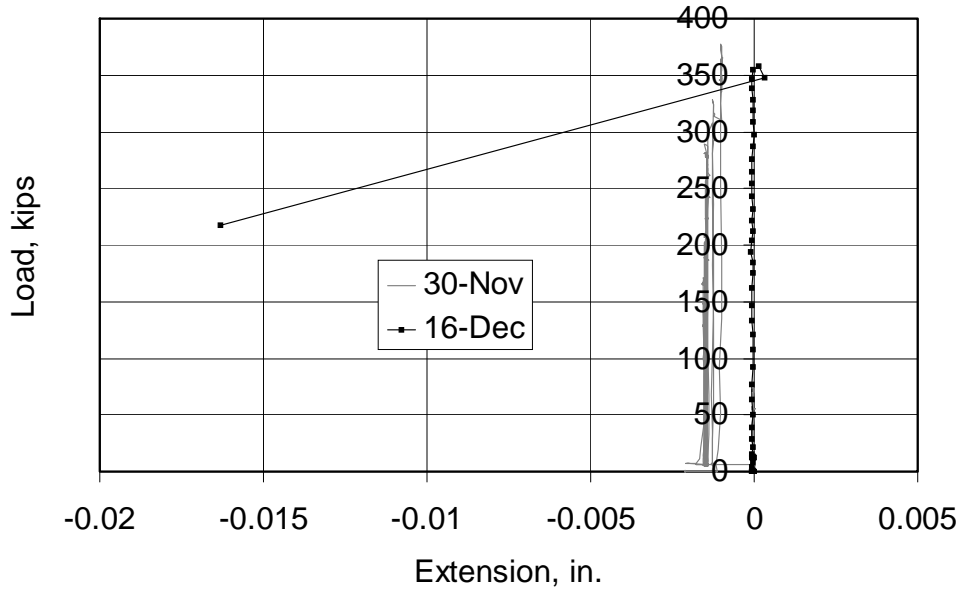
BG2S - L3

BG2S - L4

BG2S - L5

BG2S - L6

257
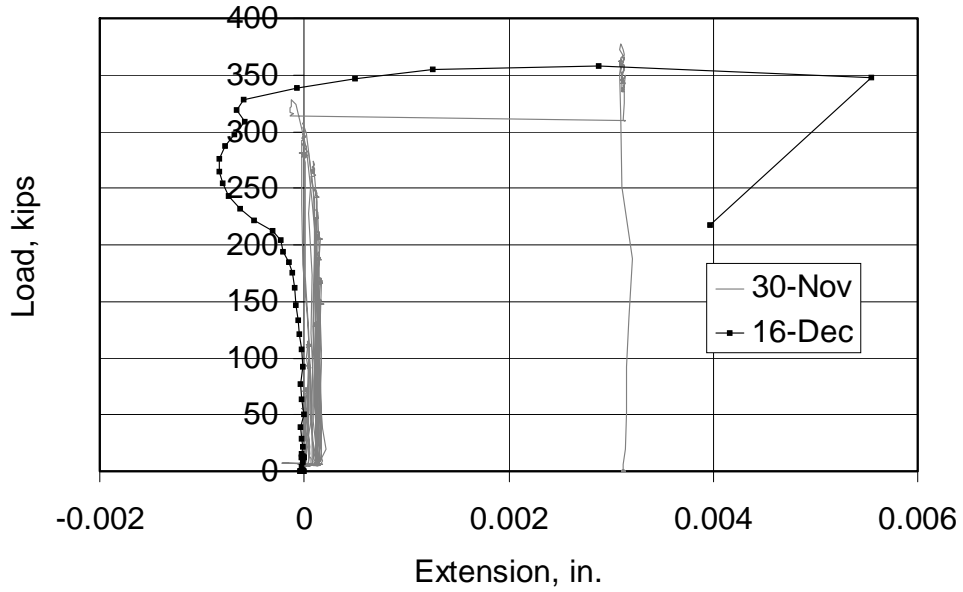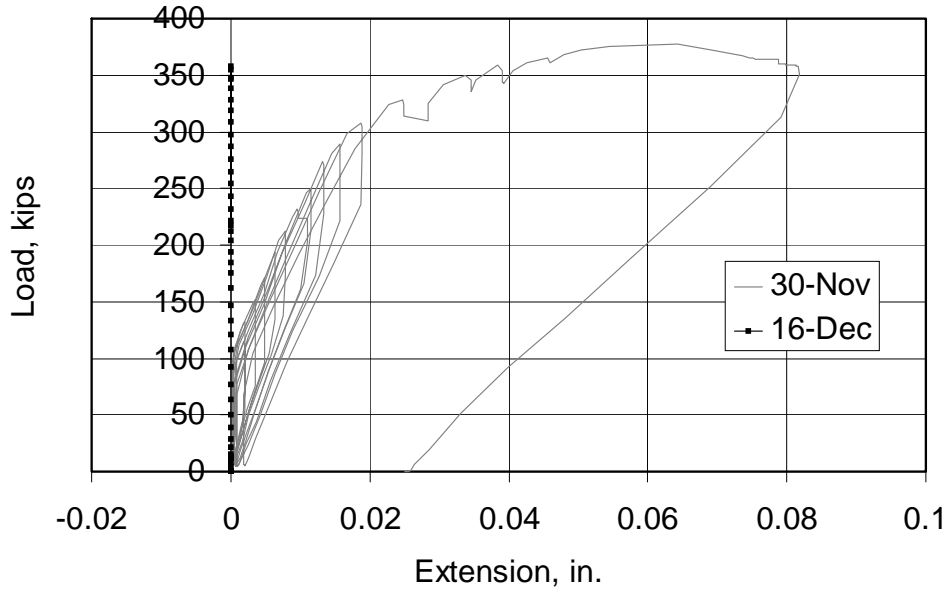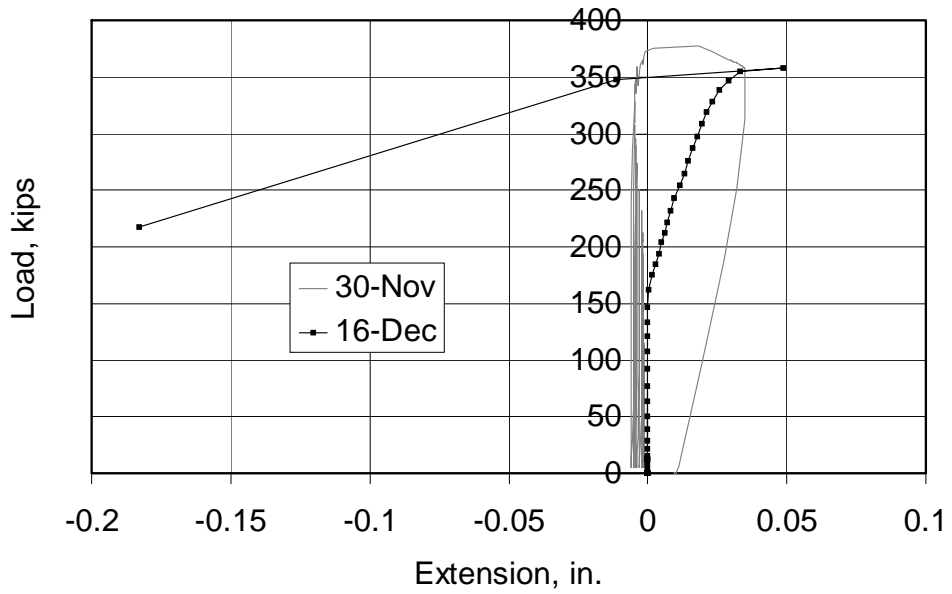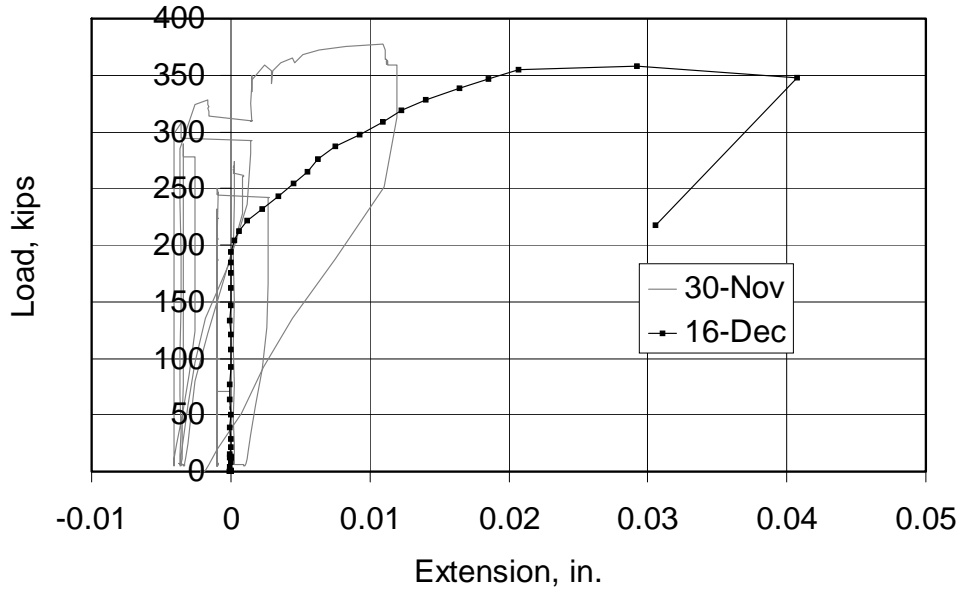
BG2S - L7

BG2S - L8

258
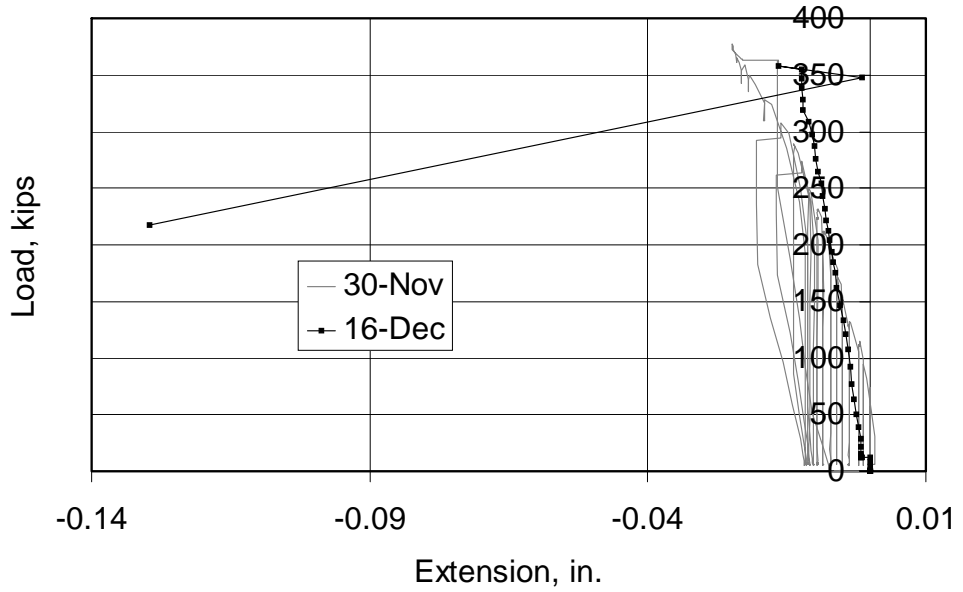
BG4S

BG4S - South Bearing Pad, West Face

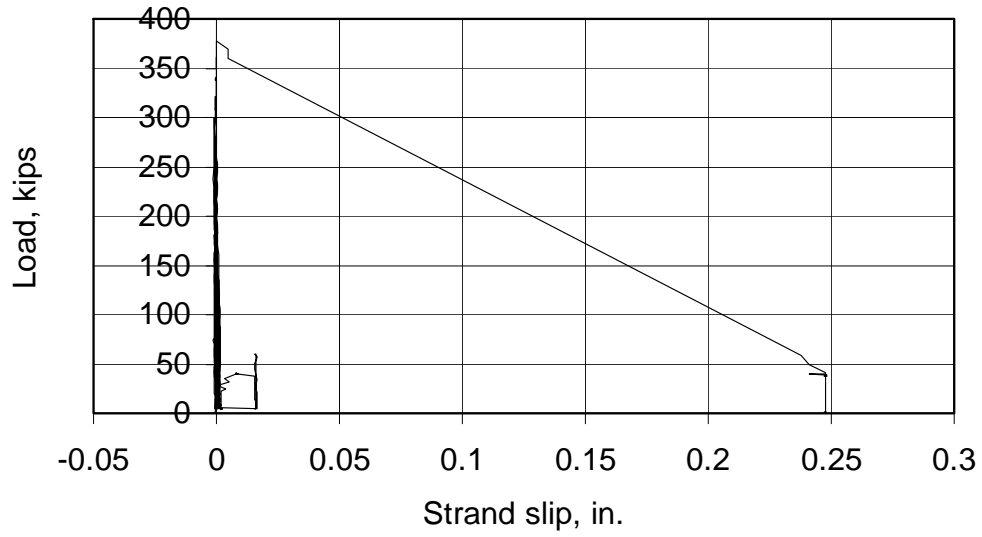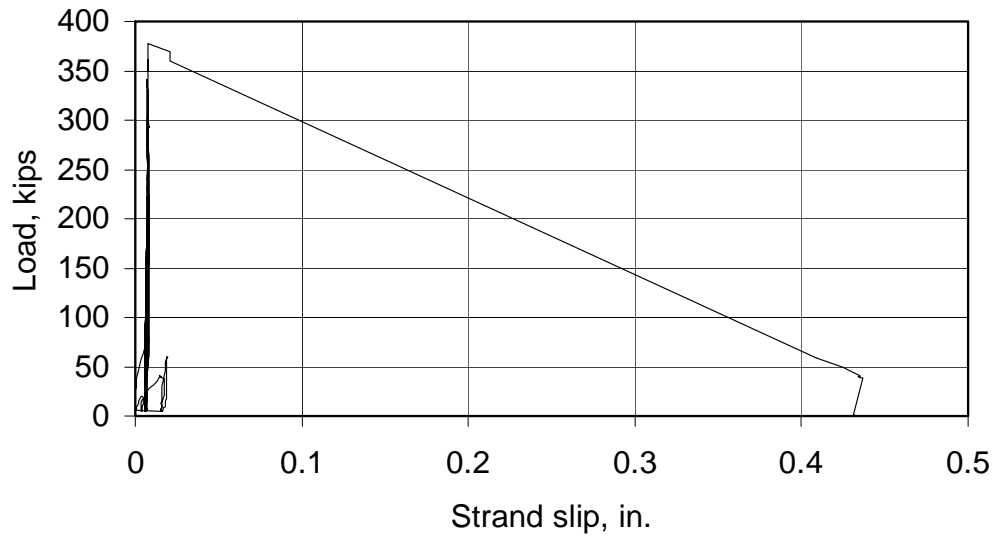
BG4S - South Bearing Pad, East Face

BG4S - P1

BG4S - P2

260

BG4S - P3

Load, kips (y-axis)
Strand slip, in. (x-axis)

BG4S - P4

Load, kips (y-axis)
Strand slip, in. (x-axis)
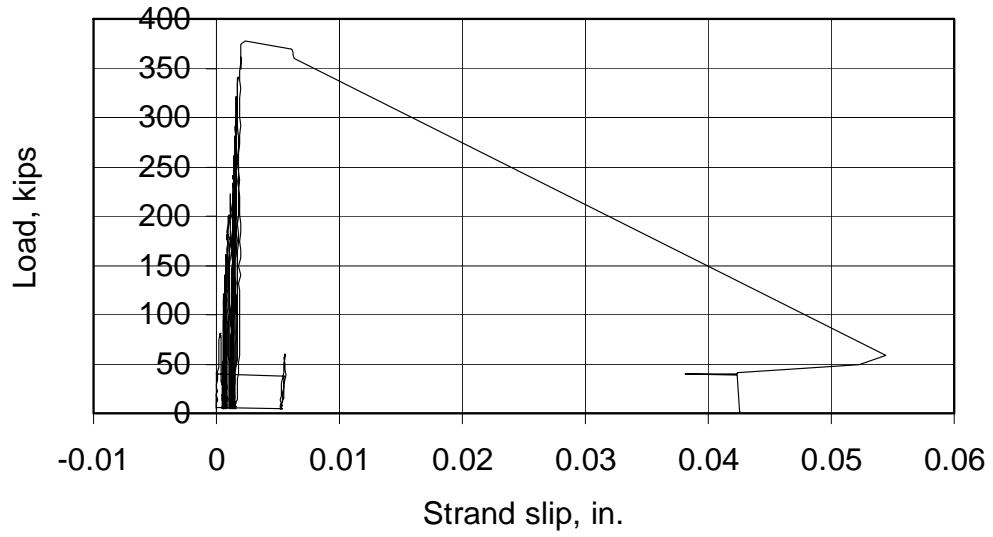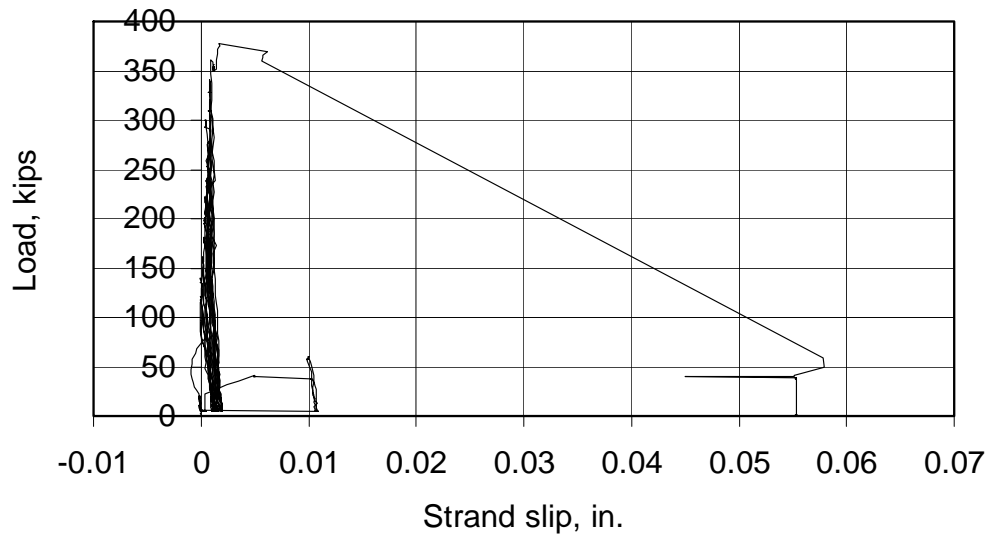
BG4S - P5
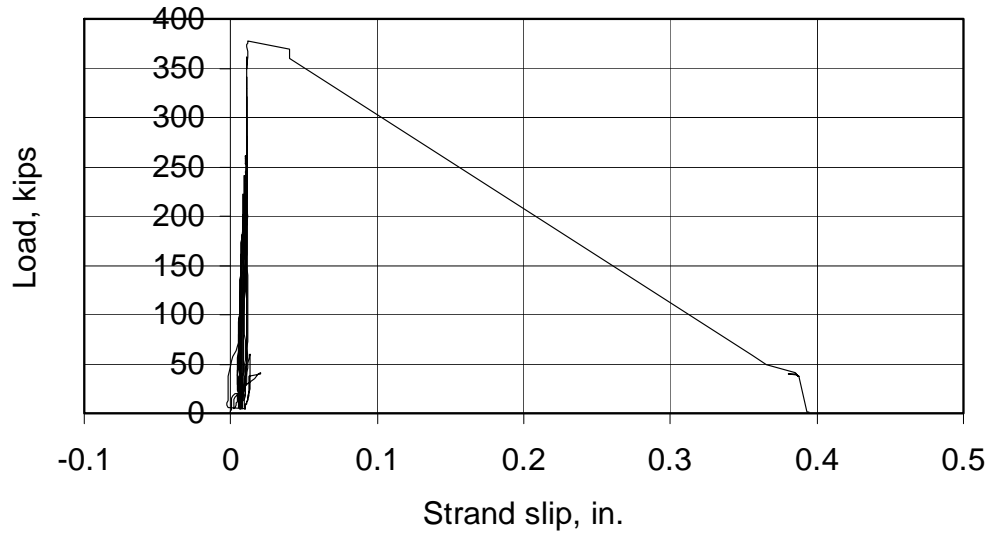
BG4S - P6

BG4S - P7

BG4S - P8

BG4S - L1

BG4S - L2

BG4S - L4

Load, kips

Extension, in.

BG4S - L5

Load, kips

Extension, in.

265

BG4S - L8

Extension, in.

266
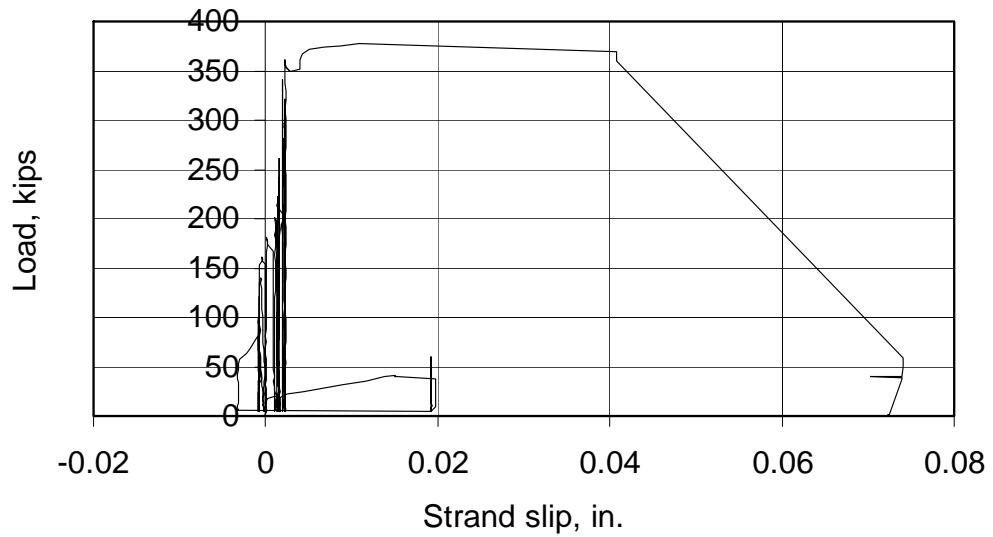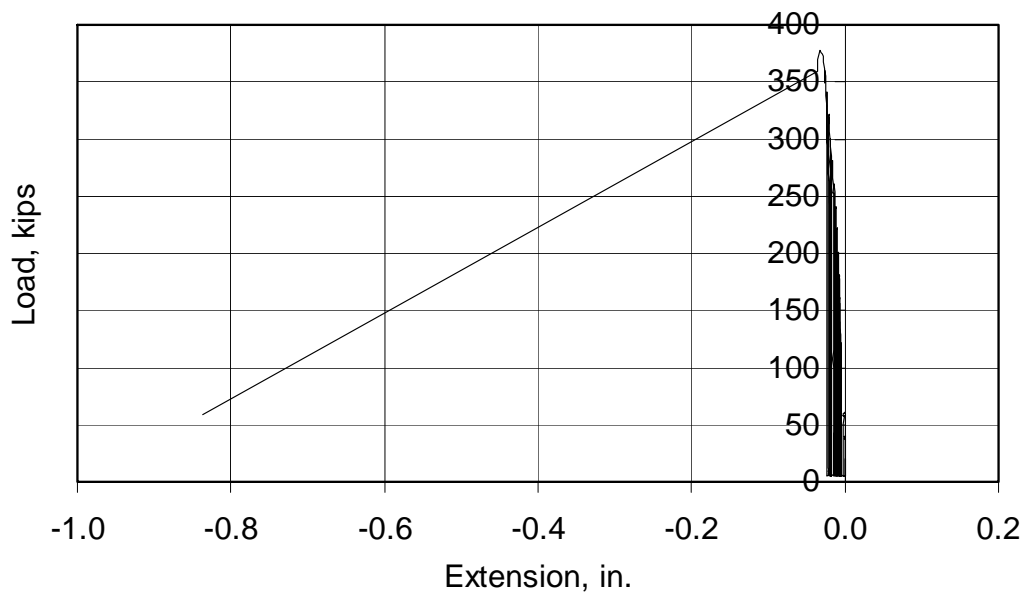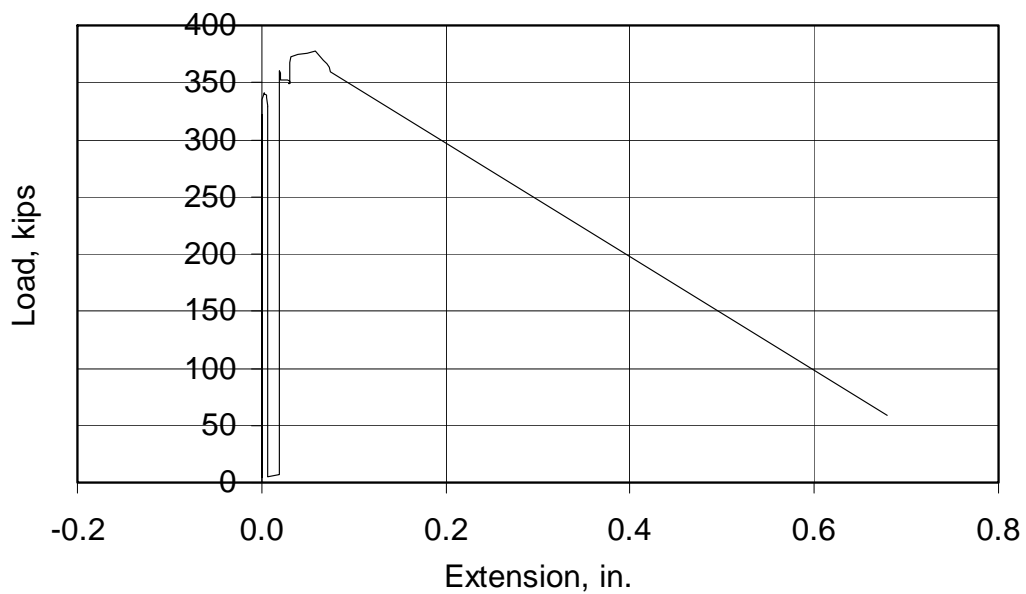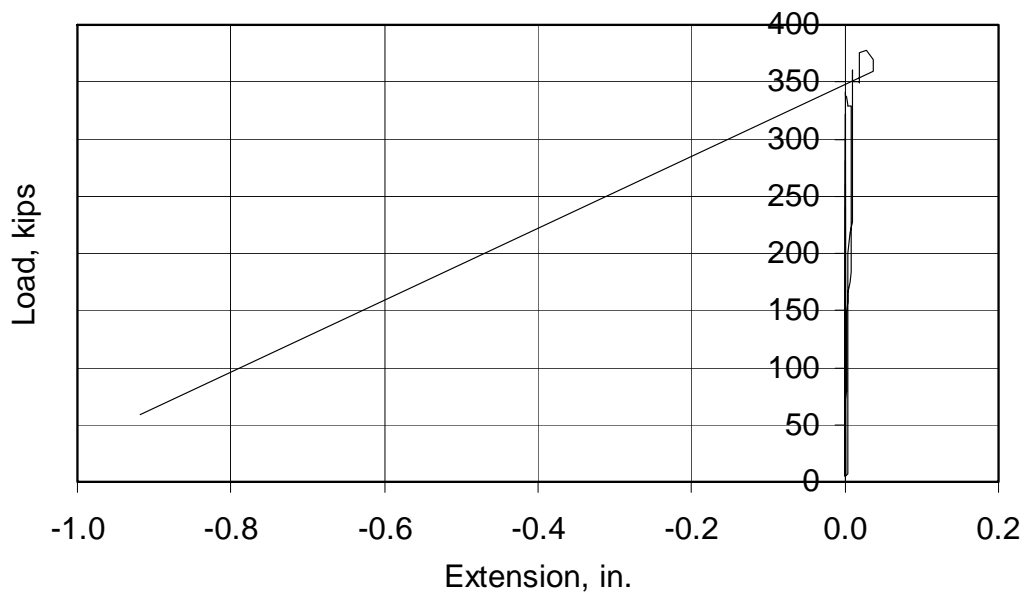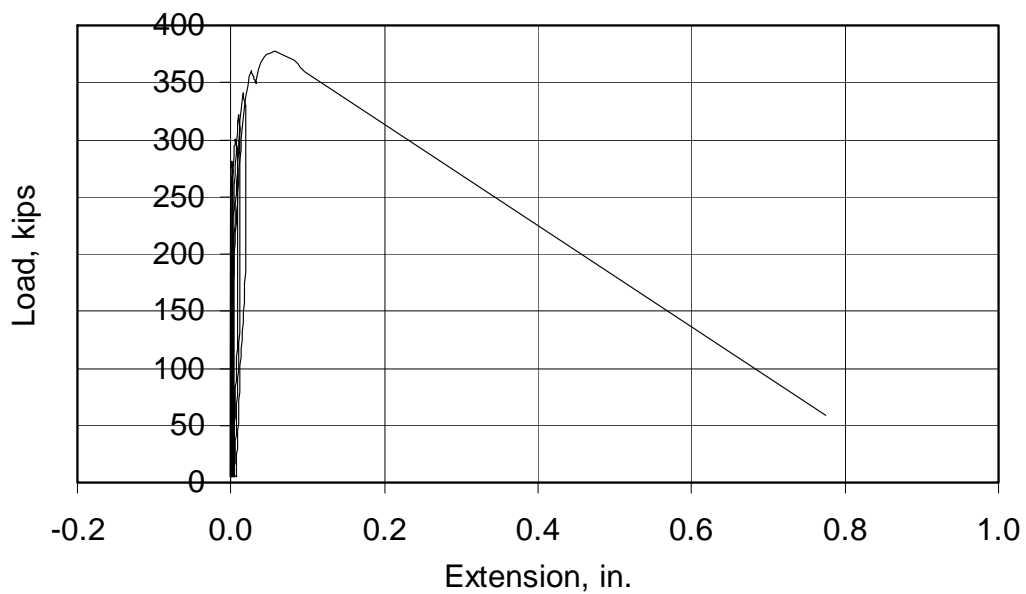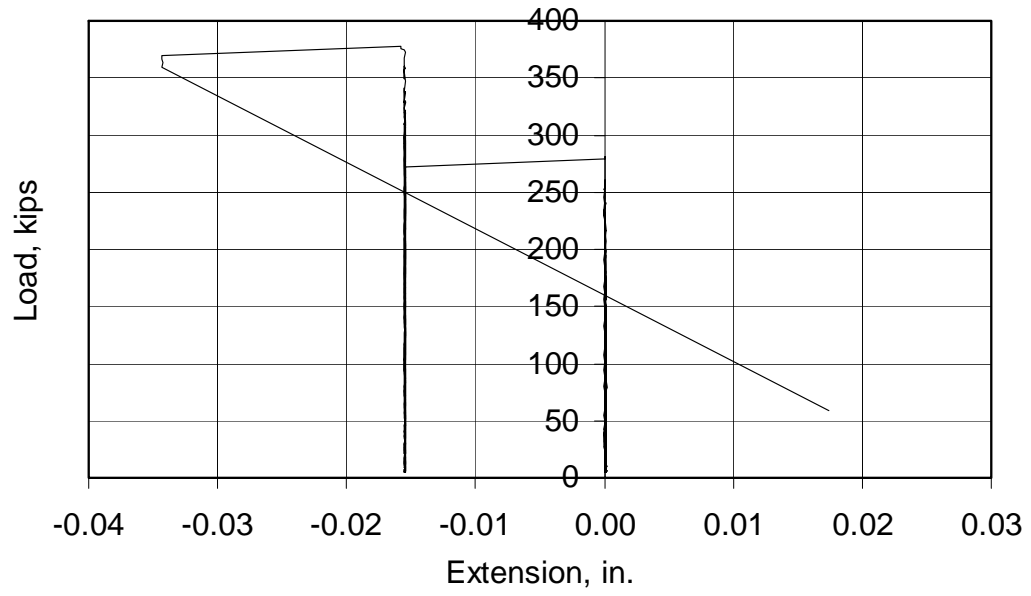
Appendix G: Data from Core Tests

| Core	date tested	L, in.	D1, in.	D2, in.	A, in.^{2}
BG1E-a	9/28/99	5.5	2.76	2.75	5.97
BG1E-b	9/28/99	5.5	2.76	2.75	5.97
BG1E-c	9/28/99	5.5	2.76	2.75	5.96
BG1E-d	9/28/99	5.5	2.75	2.76	5.97
BG1W-a	9/28/99	4.3	2.77	2.75	5.97
BG1W-b	9/28/99	4.1	2.76	2.77	6.00
BG1W-c	9/28/99	4.3	2.75	2.73	5.88
BG1E-1	2/22/00	5.8	2.76	2.76	5.98
BG1E-2	2/22/00	5.8	2.76	2.76	5.97
BG2E-1	2/22/00	6.2	2.69	2.69	5.67
BG2E-2	2/22/00	6.1	2.69	2.70	5.69
BG2W-1	2/22/00	5.2	2.69	2.70	5.70
BG2W-2	2/22/00	5.4	2.70	2.71	5.74
BG4E-1	4/15/00	5.6	2.71	2.71	5.75
BG4E-2	4/15/00	5.3	2.71	2.71	5.77
BG4E-3	4/15/00	6.0	2.71	2.71	5.78
BG4W-1	4/15/00	5.8	2.70	2.71	5.74
BG4W-2	4/15/00	5.8	2.70	2.70	5.71
BG4W-3	4/15/00	5.5	2.70	2.70	5.72

BG1E-1
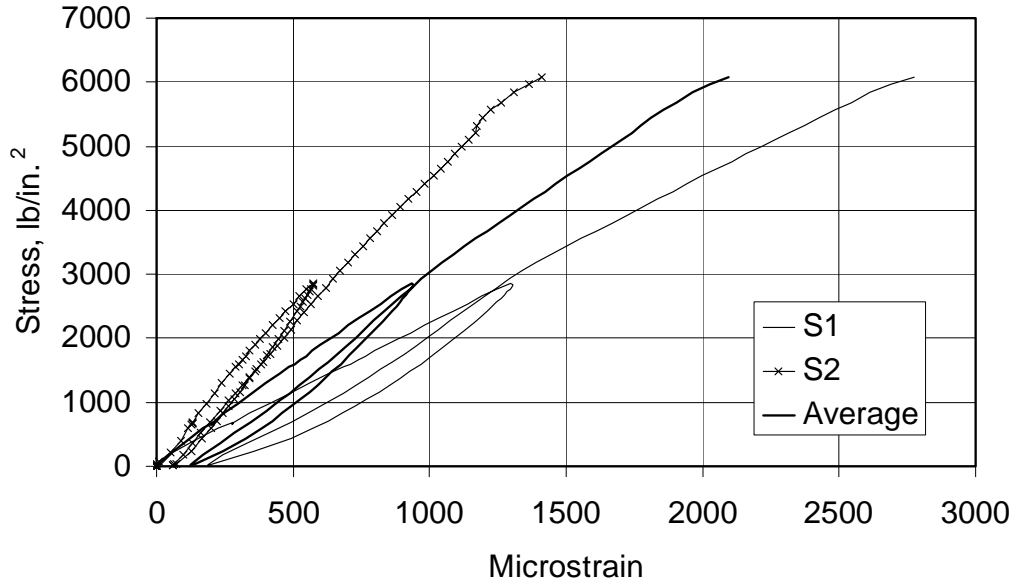
BG1E-2
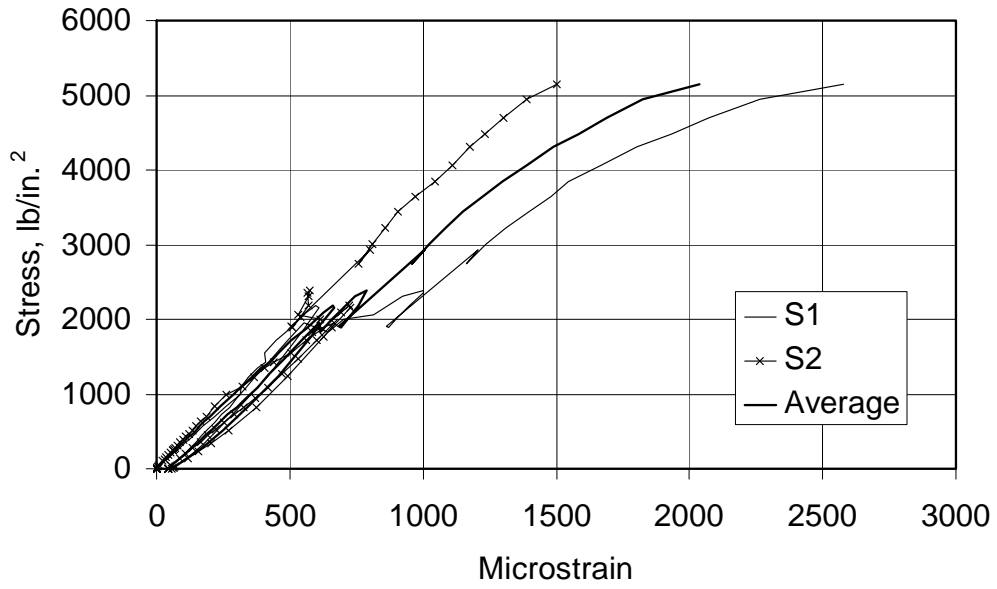
BG2E-1
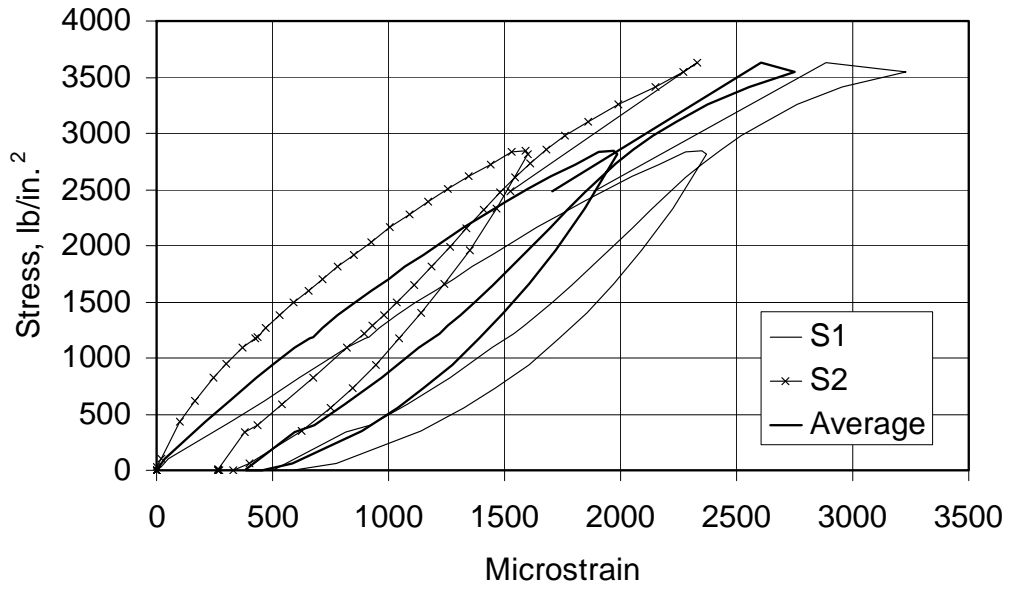
BG2E-2
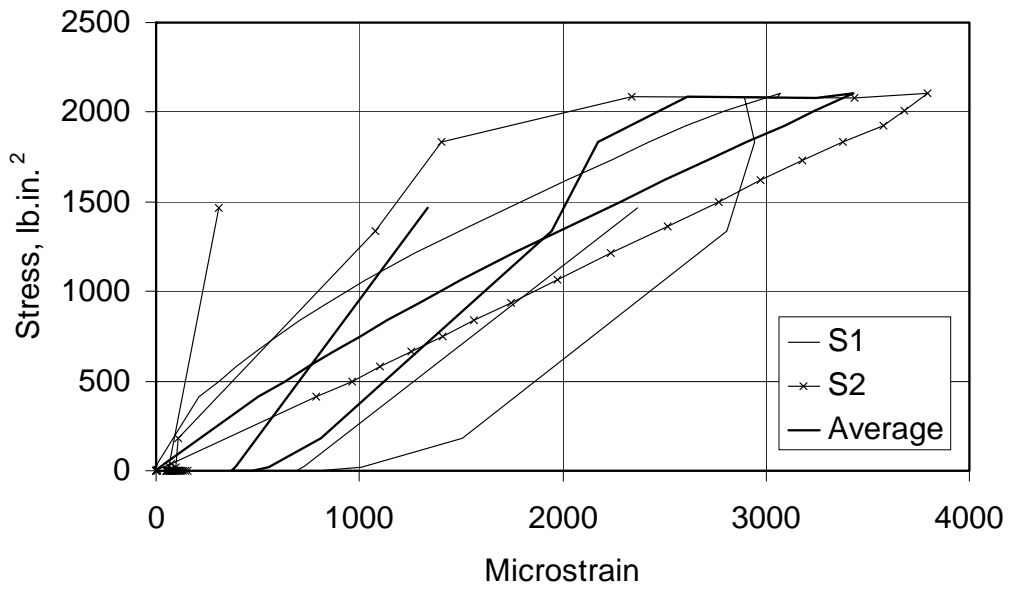
BG2W-1
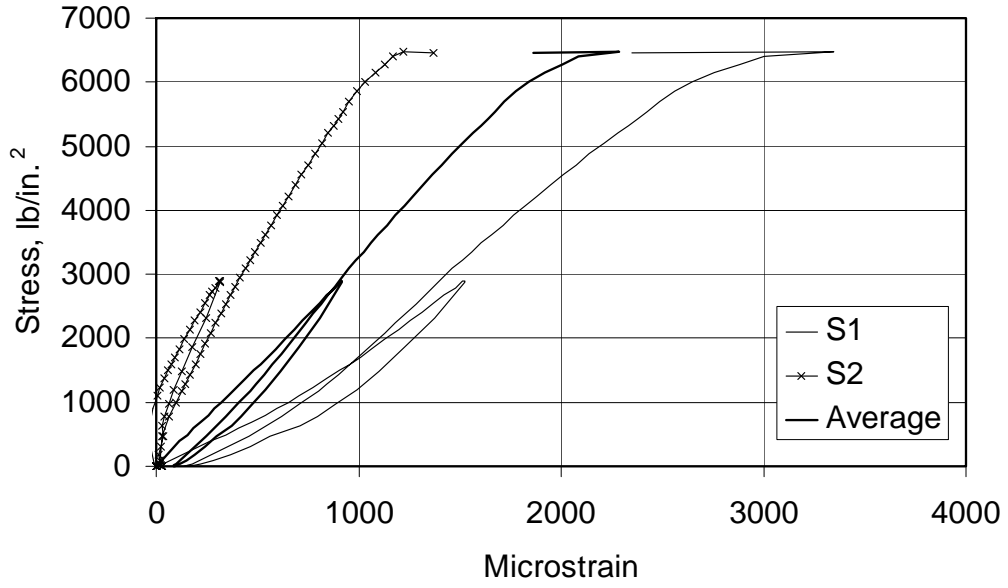
BG2W-2
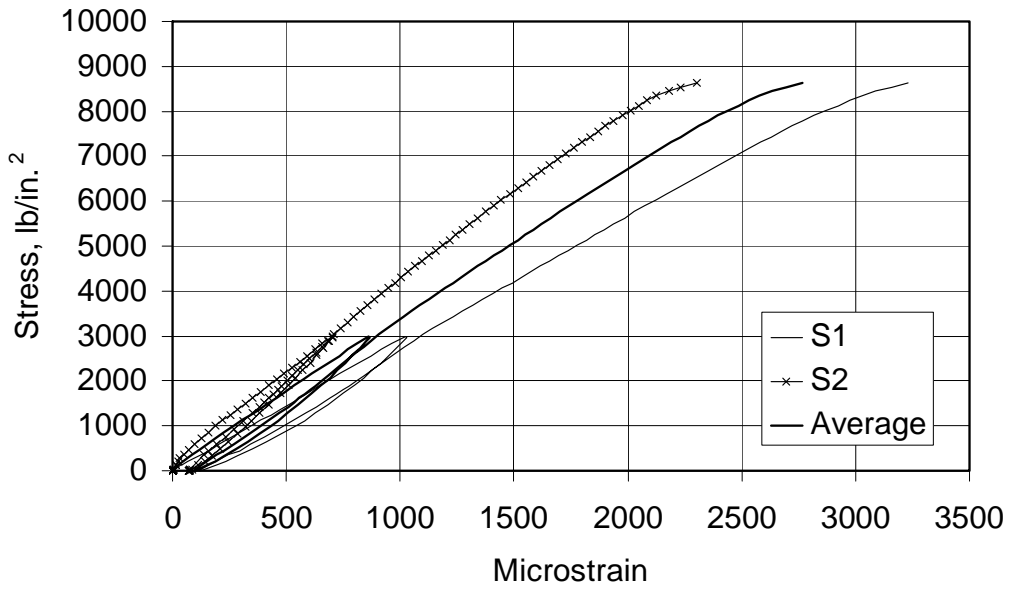
BG4E-1
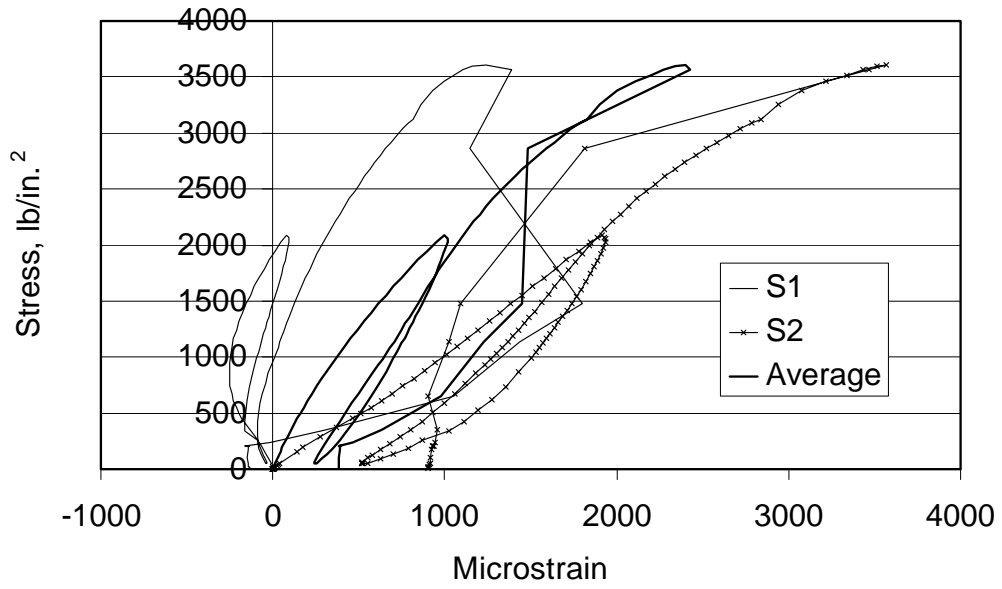
BG4E-2
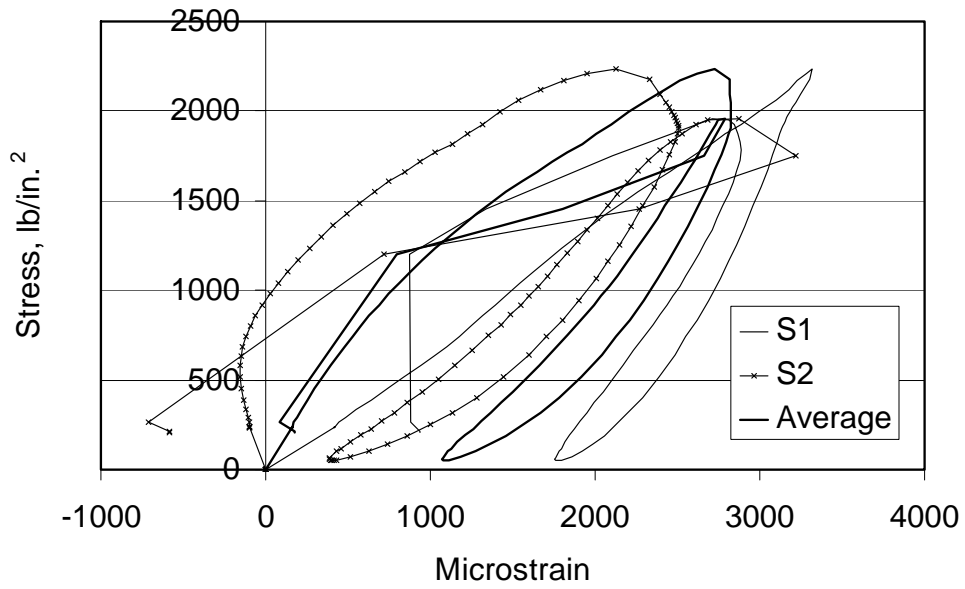
BG4E-3
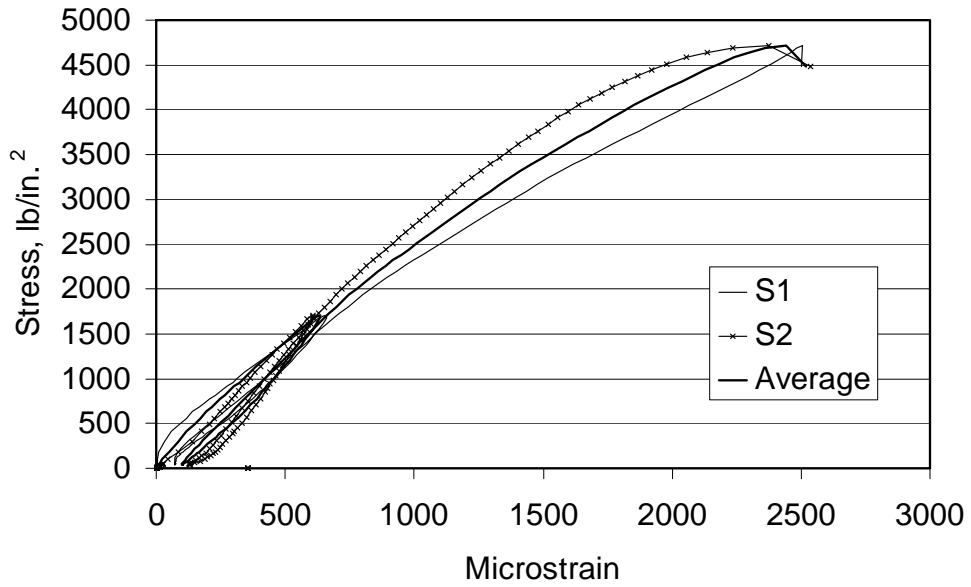
BG4W-1
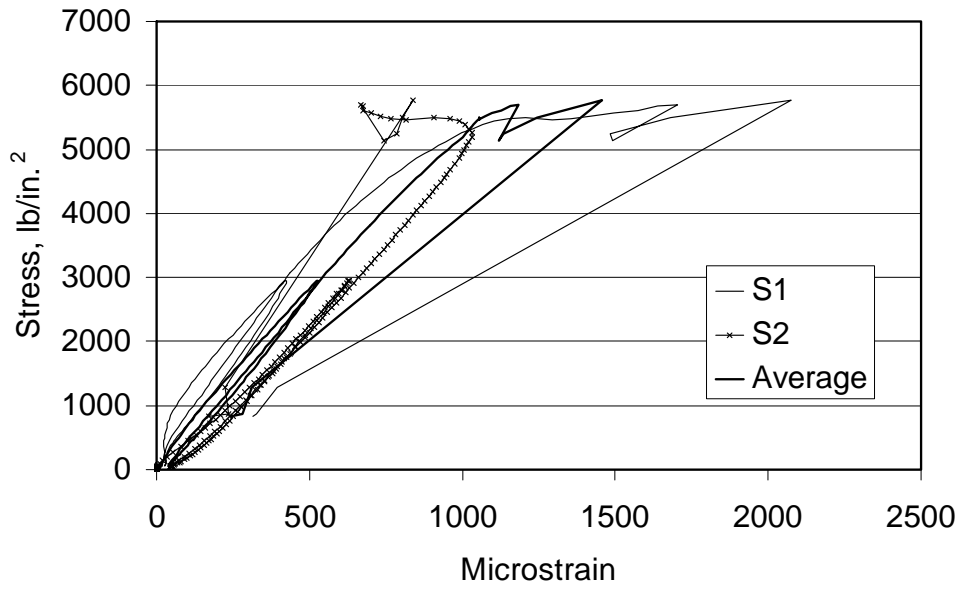
BG4W-2
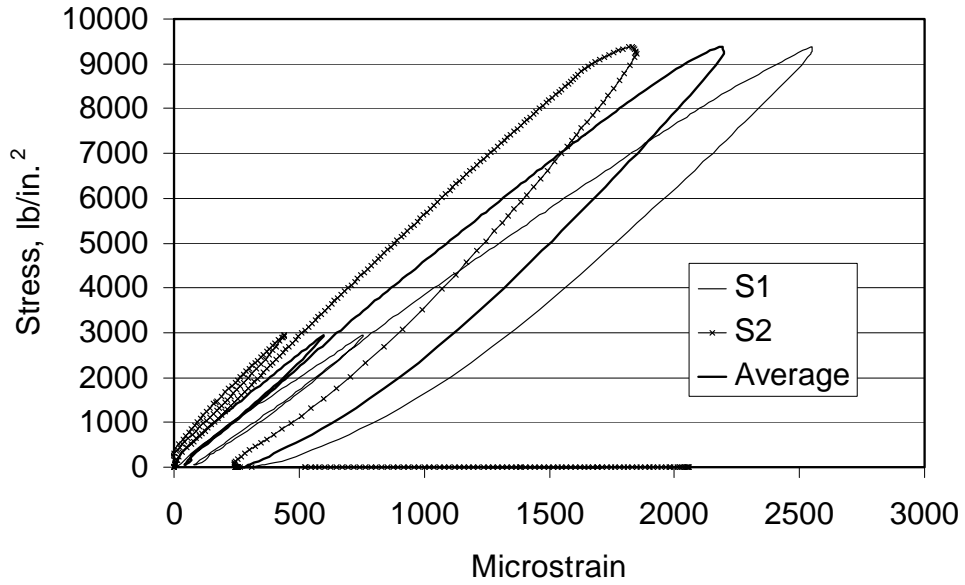
BG4W-3
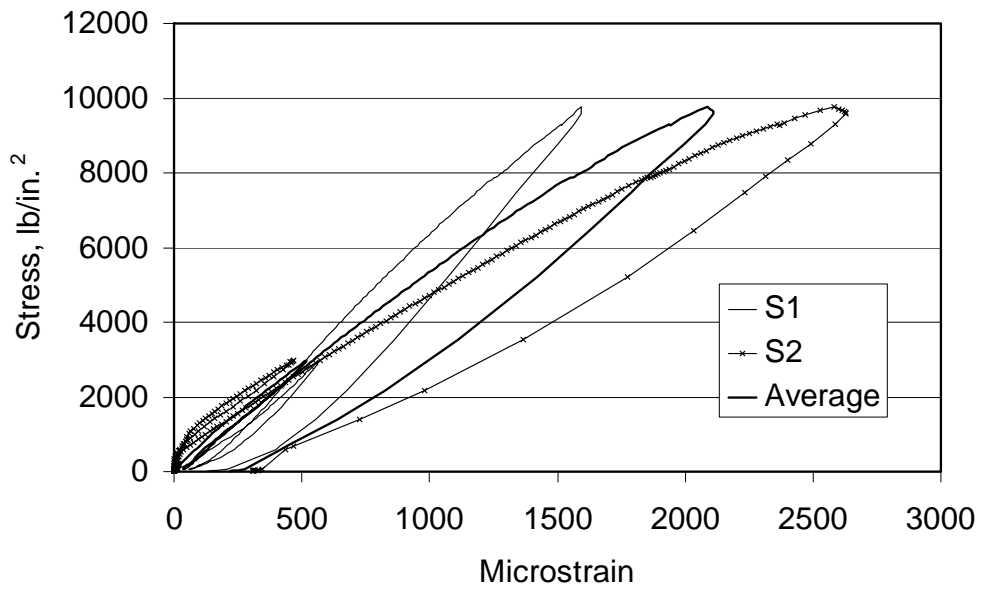
Appendix H: Locations of Points Monitored on Field Structures

I-10		
Point	Distance from end, in.	Distance from end, m
1	36	0.9144
2	63	1.6002
3	40	1.016
4	51	1.2954
5	66	1.6764
6	42	1.0668
7	31	0.7874
8	65	1.651
9	78	1.9812
10	90	2.286
11	21	0.5334
12	35	0.889

US-90		
Point	Distance from end, in.	Distance from end, m
1	24	0.6096
2	114	2.8956
3	53	1.3462
4	200	5.08
5	10	0.254
6	18	0.4572
7	34	0.8636
8	76	1.9304
9	183	4.6482
11	234	5.9436
12	17	0.4318
13	99	2.5146
14	161	4.0894
15	25	0.635
16	57	1.4478
17	179	4.5466

Robinson		
Point	Distance from end, in.	Distance from end, m
1	183	4.6482
4		
5		
6	64	1.6256
7	93	2.3622
8	70	1.778
9	92	2.3368
11	87	2.2098
12	167	4.2418
13	169	4.2926
14	253	6.4262
15	263	6.6802
16	31	0.7874
17	15	0.381
18	5	0.127
e	211	5.3594
f	243	6.1722

References

ACI Committee 301, "Specifications for Structural Concrete for Buildings," (ACI 301-66), ACI Manual of Concrete Practice, Part 2, Detroit, Michigan, 1967.

ACI Committee 318 "Building Code Requirements for Structural Concrete (318-99) and Commentary (318R-99)," Farmington Hills, Michigan, 1999.

ASTM C39-99 "Standard Test Method for Compressive Strength of Cylindrical Concrete Specimens," American Society for Testing and Materials, 1999.

ASTM C469-94 "Standard Test Method for Static Modulus of Elasticity and Poisson's Ratio of Concrete in Compression," American Society for Testing and Materials, 1994.

ASTM C617-98 "Standard Practice for Capping Cylindrical Concrete Specimens," American Society for Testing and Materials, 1998.

Collepardi, M., "Damage by Delayed Ettringite Formation," Concrete International, V. 21, No 1, January 1999, pp.69-74.

Fúnez, Luz Marina, "Field Observation of Bridges with Premature Concrete Deterioration: Structural Implications," MS Report, December 1999.

Hime, W. C., "Delayed Ettringite Formation—A Concern for Precast Concrete?" PCI Journal, July-August 1996, pp. 26-30.

Kesner, K. E., "Detection and Quantification of Distributed Damage in Concrete Using Transient Stress Waves," Master's Thesis prepared for Cornell University of Civil & Environmental Engineering, 1997.

Klingner, R. E., Fowler, T. J., and Kreger, M. E., "Mitigation Techniques for In-Service Structures with Premature Concrete Deterioration," Proposal prepared for Texas Department of Transportation, 2000.

Klingner, R. E. and Fowler, T. J., "Structural Assessment of In-Service Bridges with Premature Concrete Deterioration," Proposal prepared for Texas Department of Transportation, 1998.

Lin, T. Y. and Burns, N. H., Design of Prestressed Concrete Structures, 3rd ed. New York: John Wiley & Sons, 1981.

Mattock, A. H., Kriz, L. B., and Hognestad, E., "Rectangular Concrete Stress Distribution in Ultimate Strength Design," Journal of the American Concrete Institute, V. 32, No. 8, February 1961, pp. 875-928.

Mielenz, R. C., Marusin, S. L., Hime, W. G., and Jugovic, Z. T., "Investigation of Prestrestessed Concrete Railway Tie Distress," Concrete International, V. 17, No. 12, December 1995, pp. 62-68.

Tinkey, B. V., "Nondestructive Testing of Prestressed Bridge Girders with Distributed Damage," Master's Thesis prepared for the Graduate School of the University of Texas at Austin, May 2000.